COMPARISON OF DOWNSCALED RCM AND GCM DATA FOR HYDROLOGIC IMPACT ASSESSMENT

COMPARISON OF DOWNSCALED RCM AND GCM DATA FOR HYDROLOGIC IMPACT ASSESSMENT

By:

MANU SHARMA

B.Sc. (McMaster University)

A Thesis

Submitted to the School of Graduate Studies

in Partial Fulfillment of the Requirements

for the Degree

Master of Applied Science

McMaster University

Department of Civil Engineering

MASTER OF APPLIED SCIENCE — McMaster University

Civil Engineering — Hamilton, Ontario

TITLE: Comparison of Downscaled RCM and GCM data for Hydrologic Impact Assessment

AUTHOR: Manu Sharma

B.Sc. (McMaster University)

SUPERVISOR: Dr. Paulin Coulibaly

NUMBER OF PAGES: xvi, 103

Abstract

From observations of increases in global average air and oceanic temperatures, melting of polar ice and significant increases in net anthropogenic radiative forcing, it is clear our global climate system is undergoing substantial warming (IPCC, 2007). A key area of concern for hydrologists and engineers alike is to determine how this warming will affect various hydrologic processes. To date, climate change impact studies have generally involved the downscaling of large-scale atmospheric predictors with the result then being input into a hydrological model to see how flow in a river/basin will change under various future climate change scenarios. Although many studies have been completed using large scale global climate model (GCM) data, few studies have shown the strength of regional climate models (RCM). In this work, a comparison between the effectiveness of using CRCM4.2 vs. CGCM3.1 data in a climate change impact study (climate forcing under the SRES A2 climate scenario) is considered. The study area is the Chute-du-Diable sub-basin located within the Saguenay-Lac-Saint-Jean Watershed in Quebec, Canada. Downscaled results are compared with observed meteorological data for the years 1961-1990 at the Chute-des-Passes (CDP) and Chute-du-Diable (CDD) weather stations; and flow is simulated in the Mistassibi River and the Chute-du-Diable reservoir. A regression technique (SDSM) and a dynamic artificial neural network model (Time lagged feed-forward neural network (TLFN)) are used for downscaling the CRCM4.2 and CGCM3.1 data, and the HBV2005 hydrological modeling system is used for simulating flows in the watershed. For the current period (1961-1990), downscaling results reveal that downscaled CRCM4.2 is closer to observed meteorological data at both CDD and CDP stations than downscaled CGCM3.1 is. The Wilcoxon Rank-Sum test and Levene test reveal that regardless of the climate model, both TLFN and SDSM are capable of capturing the monthly means and variance of precipitation and temperature. Statistical results reveal that TLFN is best for downscaling temperature and SDSM is best for downscaling precipitation. With respect to the future climate scenario, regardless of the climate model or the downscaling method, a 1 to 3˚C increase in annual mean maximum temperature and a 1 to 4˚C increase in annual mean minimum

temperature are predicted for the 2050s future period. In the case for precipitation, the CRCM4.2 model shows increases in annual precipitation will vary from 1 to 7% in the 2050s regardless of the downscaling method used. The CGCM3.1 model on the other hand, shows increases in annual precipitation ranging from 15 to 23% regardless of the downscaling method employed. Additionally, simulations of river flows and reservoir inflows reveals significant changes in mean flow will occur as a result of the warming trend. Simulations show that for both SDSM and TLFN, CRCM4.2 and CGCM3.1 show an increase in river flow and reservoir flows throughout all seasons except for the summer where reduction of flow is observed. Annually, at the Chute-du-Diable reservoir mean flow changes vary from a 16-28% increase in the 2050s and at the Mistassibi River annual mean flow changes vary from a 12-62% increase. In all cases CGCM3.1 model shows a larger increasing trend than the CRCM4.2 model.

Acknowledgement

I would like to thank my supervisor Dr. Paulin Coulibaly for his help and guidance over the last several years.

Thank you to Dr. Yonas Dibike, ALCAN and Environment Canada for providing the experiment data.

To my friends in the lab, thank you for keeping things cheerful.

Lastly, to my family, thank you for your support and patience.

Table of Contents

List of Tables

List of Figures

List of Symbols

m	The size of the hidden layer
n	Time step
wj	The weight vector for the connection between the hidden and output layers
wji	The weight matrix for the connection between the input and hidden layers
$\varphi 1$	Transfer function at the output layer
$\varphi 2$	Transfer function at the hidden layer
k	Memory depth
bj, bo	Bias Values
G	Large scale predictor
L	Local scale predictand
z	Normalized Value
x	Raw predictor value
μ	Mean of x for the baseline period
σ	Standard deviation of x for the baseline period
P	Precipitation
ET	Evapotranspiration
ΔS	Change in Storage
Q	Runoff

Chapter 1: Introduction

1.1 Background

From observations of increases in global average air and ocean temperatures, melting of polar ice and significant increases in net anthropogenic radiative forcing, it is clear our global climate system is undergoing substantial warming (IPCC, 2007). It is well known that changes in global temperature will have a significant effect on the climate system and all of the five major components (the atmosphere, hydrosphere, cryosphere, lithosphere, and biosphere) which make up this system. Arguably, the hydrosphere, which is concerned with the distribution, occurrence and circulation of all water within the climate system, will be one of the most affected components; and as such, understanding the impacts of climate change on these processes through the use of hydrological models has become a very important area of study. Hydrological modeling not only provides details into how exchange processes, water quantities and flows will change as result of climate change, but also provides clues as to what measures will need to be implemented to help protect and sustain one of the earth's most precious resources.

To date a large diversity of climate change impact studies, covering a variety of geographic areas have been completed. For example, Mareuil et al., 2007 showed that for the 2050s (2040-2060) under the doubling of atmospheric carbon dioxide climate scenario, spring and summer-fall peak flows will be reduced by 12-30%. Similarly, Dibike & Coulibaly, 2005 showed that under a more conservative climate change scenario, an overall increasing trend in mean annual river flow and reservoir inflow as well as earlier spring peak flows could be observed for the 2050s and 2080s future period. Jyrkama & Sykes, 2007 on the other hand focused on groundwater recharge and showed that under climate change, groundwater recharge would increase and that warmer winter temperatures will reduce the extent of ground frost and shift spring melt from spring towards winter. For more examples see (Minville et al., 2008; Simonovic & Li, 2004; Prudhomme & Davies, 2009; Dibike & Coulibaly, 2006; Arora, 2001; Brissette et al., 2006)

Generally speaking, climate change impact studies involve the use of two types of models: global climate models (GCM) and some conceptual or statistical based hydrological model. The large scale 3-dimensional global climate models provide both current estimates of various atmospheric predictors (eg. precipitation, near surface maximum temperature, specific humidity, air pressure etc.) and future projections of how these predictors will change under various climate change scenarios. Each climate scenario assumes a distinctly different direction for future developments and is based on key characteristics of population growth, economic development and technological change (CCCma, 2009). These climate models divide the earth into a grid of 2-4 deg resolution with 10-31 vertical layers and solve a variety of physical equations which represent the complex network of physical processes that link the radiation balance of Earth to the general circulation of the atmosphere, the oceans and the hydrological cycle (Arora, 2001). Hydrological models use current and future global climate model data as input and simulate flow along with other processes and how they change throughout a catchment. However, a major difficulty in successfully coupling these two models stems from the fact that the spatial resolution of GCMs is quite coarse, in the order of 300 x 300 km, and at that scale, spatial heterogeneities of the physiography are lost, making it very difficult for accurate modeling of the land phase (Dibike & Coulibaly, 2005). Thus, although GCMs are accurate at hemispheric or even continental scales, the data is far too coarse for accurate hydrologic modeling at the watershed scale and as such it is necessary to downscale the GCM data to the appropriate site scale if accurate hydrological modeling is to be carried out. Regional climate models can be used in place of GCMs as they operate on a smaller grid size (approx. 45 x 45 km), but these models also suffer from similar systematic biases and have trouble capturing certain climatic elements (e.g. convective precipitation) over complex terrains.

Downscaling techniques generally fall into two categories: empirical (statistical) downscaling and dynamical downscaling (using regional climate models). Several types of empirical downscaling which include, but are not limited to, regression based techniques (Karl et al., 1990; Nieto & Wilby, 2005; Dibike & Coulibaly, 2005) and

artificial neural networks (Hewitson & Crane, 1996; Coulibaly et al., 2005; Haylock et al., 2006) have been implemented in the past. However, although many studies have compared various downscaling techniques (Wilby & Wigley, 1997; Xu, 1999; Dibike & Coulibaly 2005) few have considered the effectiveness of empirically downscaling a dynamical downscaling approach in a climate change impact study (or in other words, using an empirical downscaling technique to downscale regional climate model data). The importance of further statistically downscaling regional climate model data has been noted in several studies (Osborn & Hulme, 1997 and Murphy, 2000).

1.2 Research Objectives

To date, several hydrological modeling studies have been completed on the Saguenay-Lac-Saint-Jean Watershed located in Northern Quebec, Canada (see Dibike & Coulibaly, 2005; Coulibaly et al., 2005; Khan et al., 2006a and Khan et al., 2006b). As an extension to some of the above work, a study is being proposed to compare the effectiveness of using large scale global climate data downscaled via the conventional statistical methods in practice (Statistical downscaling model (SDSM) and Time-lagged feedforward neural network (TLFN)) versus the application of a more dynamical downscaling approach, the use of regional climate models (RCMs). However, unlike in most previous studies of this nature, the goal is not to just compare downscaled GCM data with regional climate model data; but to further statistically downscale the RCM data, to assess if any improvements can be achieved. Specifically, there are four major objectives for this study:

(1) Conduct a comparison of the ability of two well known empirical downscaling techniques (SDSM, TLFN) to downscale both GCM and RCM data.
(2) Compare downscaled precipitation, maximum temperature and minimum temperature results with observed measurements to assess if improvements can be achieved from further downscaling the RCM data.
(3) Perform a comparison of downscaled GCM data versus downscaled RCM data, as input into a hydrological model to provide insights as to if the use of downscaled

regional climate model data is more effective in hydrological studies then the use of conventional downscaled GCM data.

(4) Investigate the effects of climate change in the study area through the incorporation of various future climate projection scenarios.

Chapter 2: Study Area and Data

2.1 Study Area

The selected study area for this research is the Chute-du-Diable sub-basin (located at approximately 50°N, 71°W), an area of approximately 9,700 km^2 located within the Saguenay-Lac-Saint-Jean Watershed (Coulibaly et al., 2001). The downscaling experiments are conducted with 30 years (1961-1990) of meteorological data (daily total precipitation, maximum temperature and minimum temperature) obtained from the ALCAN hydro-meteorological network at the Chute-Des-Passes (CDP) (located at 49.5°N, 71.15°W) and Chute-Du-Diable (CDD) (located at 48.5°N, 71.42 °W) weather stations. From the 30 years of observed data representing the current climate, the first 20 years (1961-1980) is used for calibrating the downscaling models, while the remaining ten years of data is used for model validation. Hydrological modelling will be completed for the Chute-du-Diable reservoir and Mistassibi River located in the vicinity of the CDD and CDP weather stations. Observed reservoir and river flows for 1961-1990 have been provided by ALCAN. Figure 1 provides a geographical map of the study area.

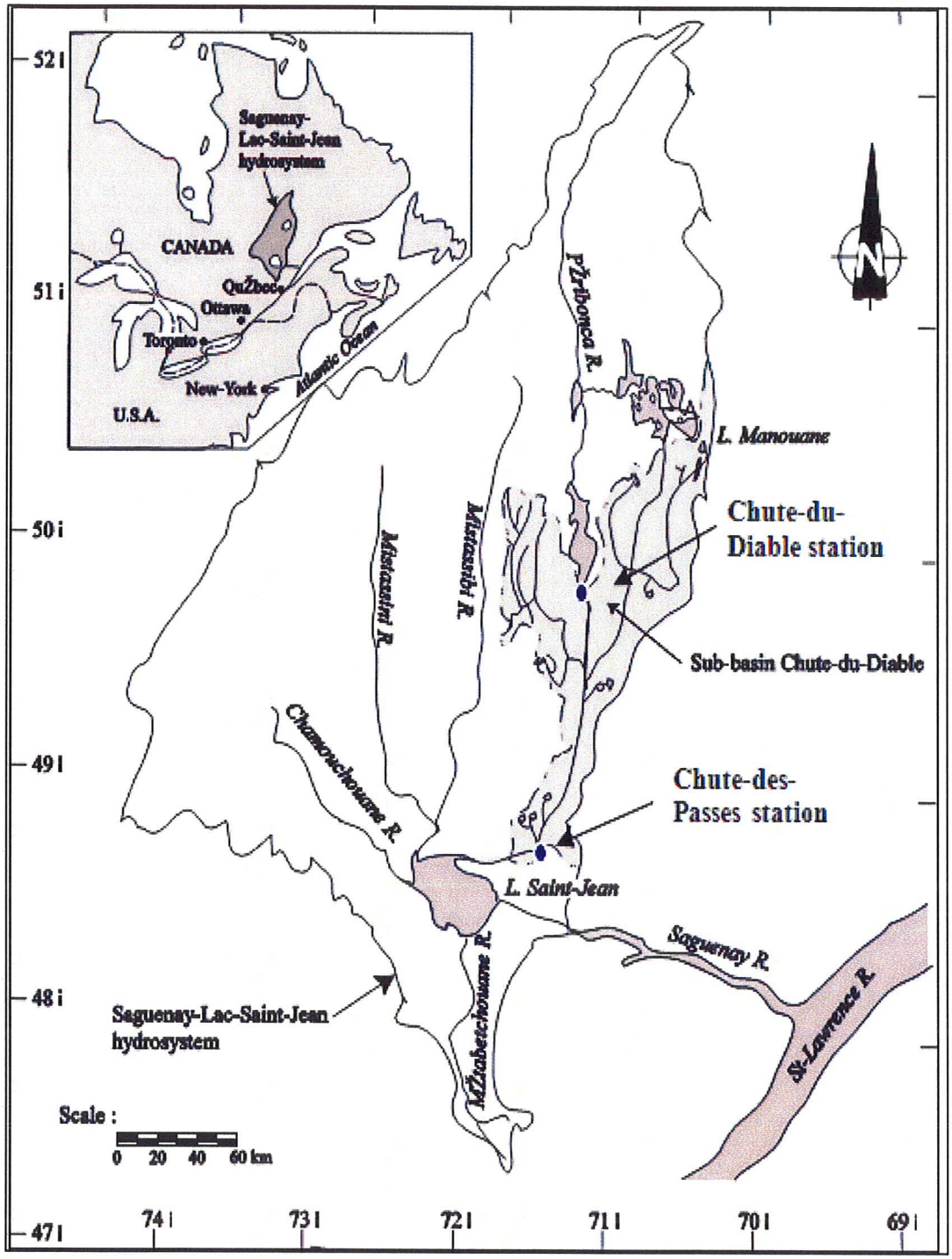

Figure 1: Location of Study Area in Northeastern Canada (taken from Coulibaly et al., 2001)

2.2 Data Collection

Global climate data is extracted from the latest (currently) third generation Canadian coupled global climate model CGCM3.1. The CGCM3.1 model is run at two different resolutions: the T47 version has a surface grid whose spatial resolution is roughly 3.75 degrees lat/lon and 31 levels in the vertical and the T63 version, which has a surface grid whose spatial resolution is roughly 2.8 degrees lat/lon and 31 levels in the vertical (CCCma, 2009). Aside from spatial resolution the largest difference between the two versions stems from the number of oceanic grids underlying every atmospheric grid cell. The T47 version has four grid cells, while the T63 version has six grid cells (CCCma, 2009). Thus the T63 version provides slightly better resolution of zonal currents in the Tropics, more nearly isotropic resolution at mid latitudes, and somewhat reduced problems with converging meridians in the Arctic (CCCma, 2009); see McFarlane et al. 2005, Scinocca et al., 2008, Flato & Boer 2001, Kim et al., 2002, 2003 for more information on the specifics of the CGCM model description. In this study the CGCM3.1 version T63 model was used with data being extracted from the Canadian Centre for Climate Modelling and Analysis website.

As in previous Canadian global climate models, along with the current period, data is available for four future climate scenarios (SRES A1B, SRES B1, SRES A2 and COMMIT). Each future climate scenarios assumes a distinctly different direction for future developments and cover a wide range of key "future" characteristics such as population growth, economic development, and technological change (CCCma, 2009). Figure 2 below shows how greenhouse gas concentrations and aerosol loadings vary for the four future climate scenarios.

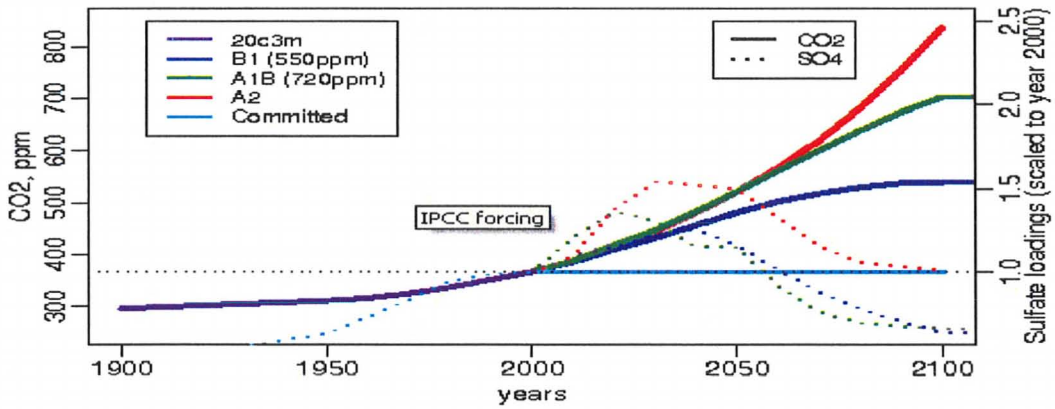

Figure 2: Future climate change scenarios (taken from CCCma, 2009)

All the 2D and 3D predictors available on the CCCma website were downloaded for the grid point (104, 50) closest to both CDP and CDD stations. SRES A2 future climate scenario was selected for the climate change impact analysis. The A2 scenario describes a very heterogeneous world, where population growth is high and economic development, per capita growth and technological change are more fragmented and slower than in other storylines (CCCma, 2009). Daily data was extracted for both the current (1960-1990) and 2050s (2046-2065) future period.

Canadian regional climate model (CRCM) data was made available by Environment Canada. The CRCM which can be set up to run on a domain covering any part of the globe, first emerged from combining the semi-Lagrangian semi-implicit MC2 (Compressible community mesoscale model) dynamical kernel with the CCCma atmospheric GCM physics parameterization package (CCCma, 2009). Briefly, the MC2 is based on fully elastic, non-hydrostatic Euler field equations solved with a state-of-the-art semi-implicit and semi-Lagrangian (SISL) numerical integration scheme (Bergeron et al., 1994 and Laprise et al., 1997). The first part of the nesting procedure consists of driving the CRCM with a time series of atmospheric fields from the driving model (e.g., CGCM2) (namely pressure, temperature, water vapor and horizontal wind components) at the external lateral boundaries exactly. Towards the interior of the domain, through an external sponge belt ("sponge zone"), the driving atmospheric fields (e.g., CGCM3)

(generally only the winds) are gradually blended with corresponding CRCM fields (CCCma, 2009). The second part of the nesting consists in specifying fixed geophysical (i.e. soil and vegetation properties including orography) and time-dependant fields (i.e., sea-surface and sea-ice temperature) adapted to the CRCM grid (CCCma, 2009). More details on the numerical formulation of the CRCM can be found in Caya & Laprise, 1999.

RCM data was extracted from the latest version CRCM4.2 model. A description of CRCM4.2 and its validation can be found in Music & Caya, 2007. Data was downloaded for the grid points 49.6°N, 71.2°W and 48.8°N, 71.6°W closest to the CDP and CDD stations, for both the current period (1961-1990) and the 2050s future period (2046-2065). As with the CGCM3.1 model, the SRES A2 climate scenario was selected.

Chapter 3: Review of Downscaling Methods

Although much progress has been made in developing global climate models, the spatial resolution remains quite coarse: typically, the cells are about 3 to 4 degrees in latitude and from 4 to 10 degrees in longitude (Prudhomme et al., 2002). At this resolution details about the local climate are lost and accurate hydrological simulations are difficult to produce. Downscaling techniques are thus implemented to convert GCM outputs into local or station scale meteorological variables which are a necessity for the reliable modelling of the hydrosphere as shown in Figure 3.

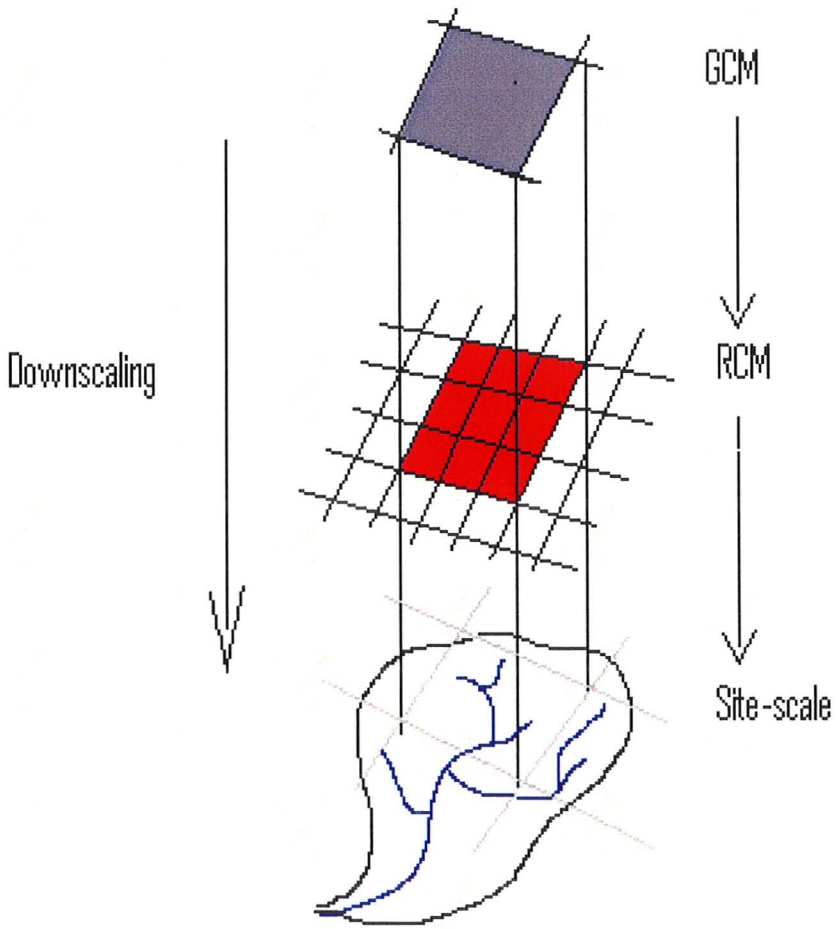

Figure 3: Schematic illustrating the general approach to downscaling (adapted after Wilby & Dawson, 2007)

Generally there are two broad downscaling methods, dynamic downscaling and empirical (statistical) downscaling. Dynamic downscaling involves extracting local-scale information by developing and using regional climate models (RCMs) with the coarse GCM data used as boundary conditions (Coulibaly et al., 2004). Empirical downscaling, on the other hand, derives local scale information from the larger scale through inference (Coulibaly et al., 2004). This approach involves developing statistical relationships between the large scale atmospheric GCM predictors (e.g. specific humidity, geopotential heights, and sea level pressure) and locally observed climate data (e.g. temperature and precipitation). As outlined in Xu (1999), the statistical downscaling procedure generally follows four steps: (1) identify a large-scale predictor G which controls the local parameter L; (2) find a statistical relationship between L and G; (3) validate the relationship with independent data; (4) if the relationship is confirmed, G can be derived from GCM experiments to estimate L.

The general practice of downscaling and its limitations are well documented (see, for example, Kattenberg et al., 1996; Wilby, 1994, 1997; Wilby & Wigley, 1997; Xu, 1999; Dibike & Coulibaly 2005; Prudhomme et al., 2006; Grotch & MacCracken, 1991; Von Storch et al., 1993; Giorgi & Mearns, 1991)

3.1 Dynamical Downscaling

Dynamic downscaling models involve creating limited area models (LAMs) or regional climate models (RCM) that are nested from data contained within GCMs (Murphy, 2000). Nesting an RCM within the 'driving' global climate model enables simulations of climate features and physical processes to be in much greater detail for a limited area of the globe, whilst drawing information about initial conditions, time-dependent lateral meteorological conditions and surface boundary conditions from the larger scale GCM (CICS, 2009). Subsequently, the global model simulates the response of the global circulation to large-scale forcings, whilst the RCM accounts for sub-GCM grid scale forcings, such as complex topographical features and land cover inhomogeneity, in a physically-based way and thus enhances the simulations of

atmospheric and climatic variables at finer spatial scales (CICS, 2009). Here the assumption is that predictions based explicitly on relevant physical processes will be better than those in which the underlying physics is only represented implicitly, via empirical relationships (Murphy, 2000).

Dynamic models, because of their uniqueness to a particular study region have several advantages and disadvantages. Regional climate models can resolve smaller-scale atmospheric features such as orographic precipitation or low-level jets better than the host GCM (Wilby, 2002). As such dynamic downscaling is well suited to areas that have a high degree of topographic, or land cover variation. However, although RCMs have recently been developed that can attain horizontal resolutions in the order of tens of kilometers or less over a selected area of interest; the models are computationally demanding (Coulibaly et al., 2005). RCMs are as computationally demanding as GCMs: placing constraints on the feasible domain size, number of experiments and duration of simulations (Wilby et al., 2002; Hewitson and Crane, 1996). Furthermore, the scenarios are very sensitive to the choice of boundary conditions (such as soil moisture) (Wilby et al., 2002). The models also suffer from similar bias problems as the larger scale global climate models (Hay & Clark, 2003). Compared with statistical downscaling, the spatial patterns produced by RCMs are more homogeneous, but not necessarily more realistic (Cubash et al., 1996; Mearns et al., 1999). Finally, dynamical downscaling operates on some (high-resolution) grid-point scales and thus the results will be in the form of spatial averages. These models still cannot meet the needs of spatially explicit models of ecosystems or hydrological systems, and there will remain the need to downscale the results from such models to individual sites or localities for impact studies (Xu 1999; Osborn and Hulme, 1997; Murphy 2000).

3.2 Empirical (Statistical) Downscaling

The second general method for downscaling global climate data is through the use of empirical techniques. In situations where a low-cost, rapid assessment of highly localized climate change impacts is required, statistical downscaling (currently)

represents the more promising option (Wilby et al., 2002). Several types of empirical downscaling which include, but are not limited to, regression based techniques (Karl et al., 1990; Nieto & Wilby, 2005; Dibike & Coulibaly, 2005) and artificial neural networks (Hewitson and Crane, 1996; Coulibaly et al., 2005) have been implemented to date. Notably, mathematically, in all empirical cases a predictor-predictand relationship needs to be defined [Predictand = f (predictors)] where the *predictor* variables provide daily information concerning the large-scale state of the atmosphere and the *predictand* describes conditions at the site scale (Dibike & Coulibaly, 2005). The transfer function (f) then represents the variety of modeling tools ranging from linear regression to neural networks that can be used to fulfill the inequality. To date, linear and non–linear regression, artificial neural networks, canonical correlation and principal components analyses have all been used to derive predictor–predictand relationships (Wilby & Dawson, 2007). The underlying assumption of this technique is that there are certain physical relationships underlying the statistical relationships developed, and that these physical relationships hold regardless of whether the model simulation is a control (stationary) experiment or an experiment incorporating a changed climate (Easterling, 1999). Xu, 1999 summarize the common assumptions of statistical downscaling with three points: (1) local-scale parameters are a function of synoptic forcing; (2) the GCM used to derive the downscaled relationships is valid at the scale used and; (3) the relationship derived remains valid under greenhouse gasing. In the context of climate change, it is difficult to guarantee this assumption, and it remains a main weakness of the methodology (Hewitson & Crane, 1996; Prudhomme et al., 2002).

3.2.1 Regression based downscaling technique

Among types of regression based downscaling, a technique widely used, and focused on in this study is the statistical downscaling method (SDSM) (Wilby et. al, 2002, Dibike & Coulibaly 2005). SDSM is best described as a hybrid of the stochastic weather generator and transfer function methods as large–scale circulation patterns and atmospheric moisture variables are used to condition local–scale weather generator

parameters (Wilby and Dawson, 2007). The task of statistically downscaling daily weather series can be broken into several discrete processes (denoted in Fig. 4 by the heavy boxes): (1) quality control and data transformation; (2) screening of predictor variables; (3) model calibration; (4) weather generation (using observed predictors); (5) generation of climate change scenarios; (6) diagnostic testing and statistical analyses. SDSM uses multiple linear regression to model the relationship between a dependant variable (the predictand) and the independent variables (the predictors). Since regression-based downscaling methods rely on empirical relationships between local-scale predictands and regional-scale predictor(s), predictor selection is a very involved process in this method if accurate results are to be attained (Wilby et al., 2002). Predictor variables are selected by using correlation analysis, partial correlation analysis and scatter plots, and also considering physical sensitivity between selected predictors and predictand for the site in question (Coulibaly et al., 2005).

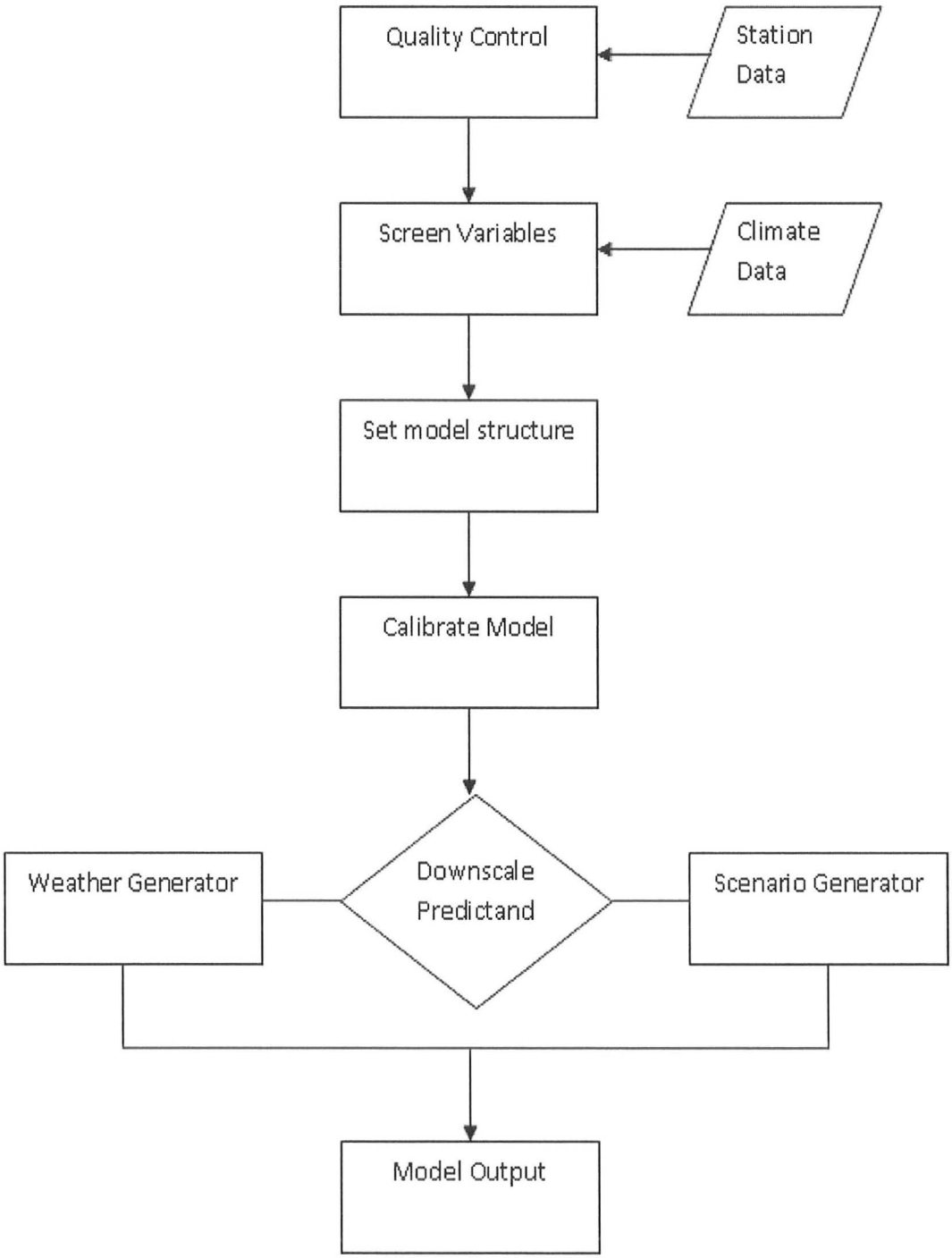

Figure 4: SDSM downscaling procedure (adapted after Wilby and Dawson, 2007)

Three implicit assumptions are made when using this downscaling technique: 1) the predictors are variables of relevance and are realistically modeled by the GCM; 2) the predictors employed full represent the climate change signal; 3) the relationship is also valid under altered climate conditions (Von Storch et al., 2000). The main strength of regression methods is the relative ease of application; once the method has been established and tested it can be applied effectively to other regions and parameters (Haylock et al., 2006). Unfortunately, these models often explain only a fraction of the observed climate variability (especially when the predictand is precipitation) (Dibike & Coulibaly, 2005). Regression methods also assume stationarity of model parameters under future climate conditions and scenarios are known to be highly sensitive to the choice of predictor variables and statistical transfer function (Winkler et al., 1997). Furthermore, downscaling future extreme events using regression methods is problematic since these phenomena, by definition, often lie at the margins or beyond the range of the calibration data set (Haylock et al., 2006, Dibike & Coulibaly 2005). Robust estimates are strongly dependent on the quality and the length of the data series used for the calibration (Wilby and Wigley, 1997) and on the performance of the regression models in capturing the variability of the observed data (Barrow et al., 1996)

3.2.2 Time-lagged-feedforward Neural Networks

An Artificial Neural Network (ANN) is a very sophisticated information processing paradigm that is inspired by the way biological nervous systems, such as the brain, process information. In order to achieve good performance, neural networks employ a massive interconnection of simple computing cells referred to as "neurons" (or processing elements) that perform useful computations through a process of learning (Haykin, 1999). Generally, the development of ANN is based on the following rules: (i). Information processing occurs at neurons or nodes; (ii). Signals are passed between nodes through connection links; (iii). Every connection link has an associated weight that represents its connection strength; (iv). Each node typically applies a nonlinear

transformation called an activation function to its net input to determine its output signal (Haykin, 1999).

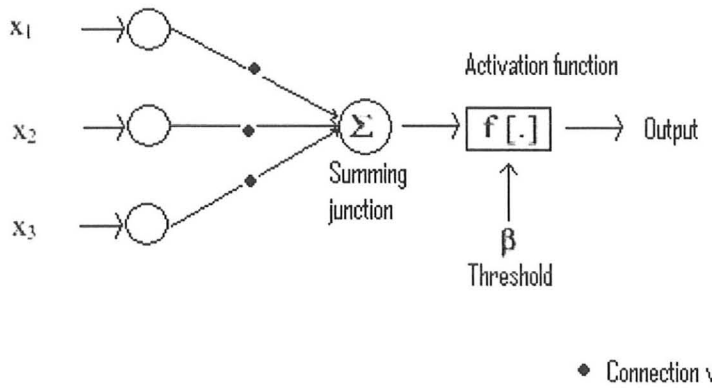

Figure 5: Nonlinear structure of an artificial neuron (adapted after Haykin, 1999)

In other words, a neural network is characterized by its architecture that represents the pattern of connection between nodes, its method of determining the connection weights, and the activation function (Khan et al., 2006). Without getting into too many details, it is important to note that neural networks are further classified by the number of layers they posses (single-Hopfield nets; bi-layer- Carpenter/Grossberg adaptive resonance networks; and multilayer perceptrons (MLP)) and the direction of flow and processing (feed-forward or recurrent). Multilayer perceptrons (MLP) combined with a back propagation algorithm are the most widely used in hydrological studies and such will be the main focus here (Coulibaly et al., 2001).

Time lagged feed-forward neural network (TLFN) is a neural network that can be formulated by replacing the neurons in the input layer of an MLP with a memory structure, which is sometimes called a tap delay-line (Coulibaly et al., 2005). The size of the memory layer (the tap delay) depends on the number of past samples that are needed to describe the input characteristics in time and it has to be determined on a case-by-case basis. A major assumption in the use of TLFN is that the local weather is not only conditioned by the present large-scale atmospheric state, but also the past states

(Coulibaly et al., 2005). TLFN uses delay-line processing elements which implement memory by delay as shown in Figure 6.

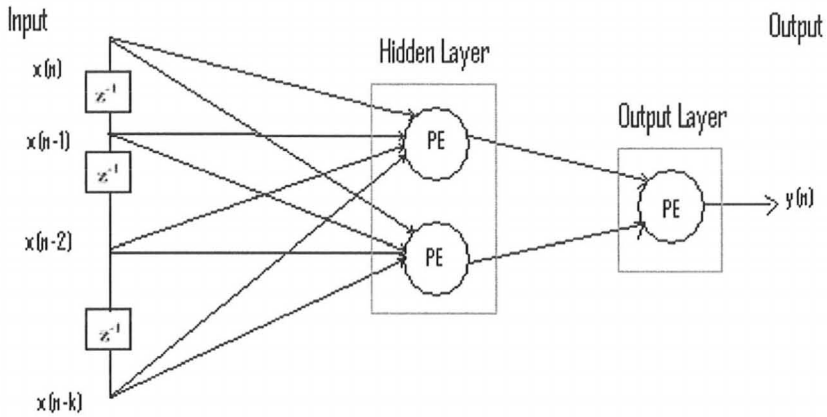

Figure 6: TLFN with one hidden layer, two processing elements and a tap-delay line with k+1 taps (z^{-1} is an operator that delays the input by one sample (adapted after Coulibaly et al., 2005)

In a feed-forward network, the nodes are generally arranged in layers, starting from a first input layer and ending at the final output layer with network computations proceeding in the forward direction only (Coulibaly et al., 2005). There can be several hidden layers, with each layer having one or more nodes. Information passes from the input to the output side. The nodes in one layer are connected to those in the next, but not to those in the same layer. Thus, the output of a node in a layer is only a dependent on the inputs it receives from previous layers and the corresponding weights. The output (y) of such a network with one hidden layer is given by (1):

$$y(n) = \varphi_1\left(\sum_{j-1}^{m} w_j y_j(n) + b_0\right)$$

$$y(n) = \varphi_1\{\textstyle\sum_{j-1}^{m} w_j \varphi_2\left[\sum_{i=0}^{k} w_{ji} x(n-1) + b_j\right] + b_0\} \quad (1)$$

where m is the size of the hidden layer, n is the time step, w_j is the weight vector for the connection between the hidden and output layers, w_{ji} is the weight matrix for the

connection between the input and hidden layers φ_1 and φ_2 are transfer functions at the output and hidden layers and b_j and b_o are bias values to be determined during training (Coulibaly et al., 2005).

The ability of neural networks to model both linear and nonlinear processes as well as their ability to adapt weights within the structure to correspond with changes to the surrounding environments making them adaptable to many regions makes these models effective downscaling instruments (Coulibaly et al., 2005). However, the user must also have a good understanding of network architecture and transformations that are present within the network. Without such knowledge there is an increased risk of errors associated within the structure of potentially complex networks (Coulibaly et. al., 2005). Further neural networks generally have difficulty downscaling precipitation owing to the inability of ANNs to reproduce two key features of high-resolution precipitation time series: intermittency and variability (Liu, 2007). ANNs tend to generate small trace precipitation amounts on actual dry days and therefore tend to underestimate dry spell length. To date, several studies have been completed where ANNs are used in downscaling large scale global model output (see for example, Schoof & Pryor 2001; Khan et al., 2006; Dibike & Coulibaly, 2006; Haylock et al., 2006; Tripathi et al., 2006; Tolika et al., 2008; Coulibaly et al., 2005)

Chapter 4: Exploratory Raw Data Analysis

4.1 Raw CGCM3.1 vs. Raw CRCM4.2

In order to establish the importance of downscaling, a good place to begin is by comparing the raw CGCM3.1 and raw CRCM4.2 outputs of daily precipitation, maximum temperature and minimum temperature with observed records at the Chute-du-diable (CDD) and Chute-des-Passes (CDP) weather stations. In all cases, the residual plots in Figures 7-12 represent the difference between the statistics (mean and variance) of the observed daily data and those of the raw output from the CGCM3.1 and CRCM4.2 climate models (or simply, the observed-simulated). Residual plots for station CDP can be found in the Appendix (A1-A6).

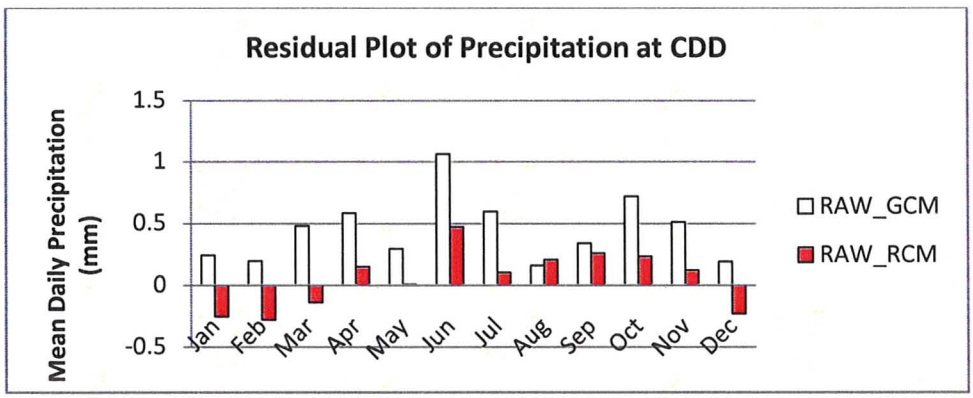

Figure 7: Residual plot of mean precipitation at CDD: Raw GCM & Raw RCM output

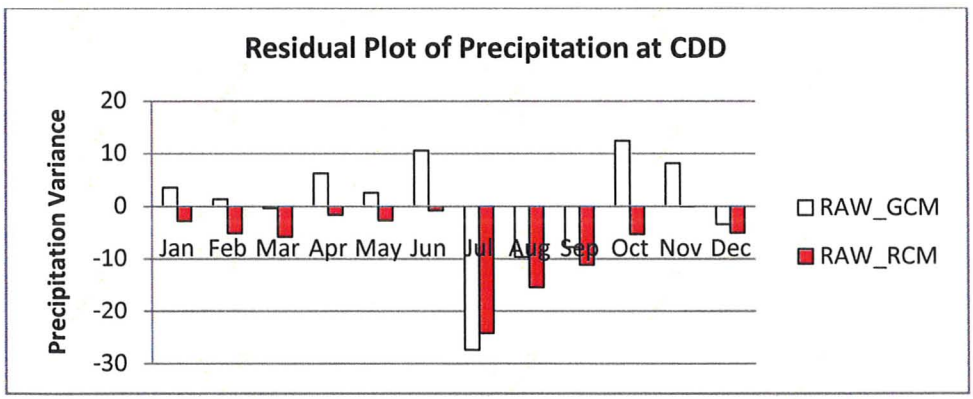

Figure 8: Residual plot of precipitation variance at CDD: Raw GCM & Raw RCM output

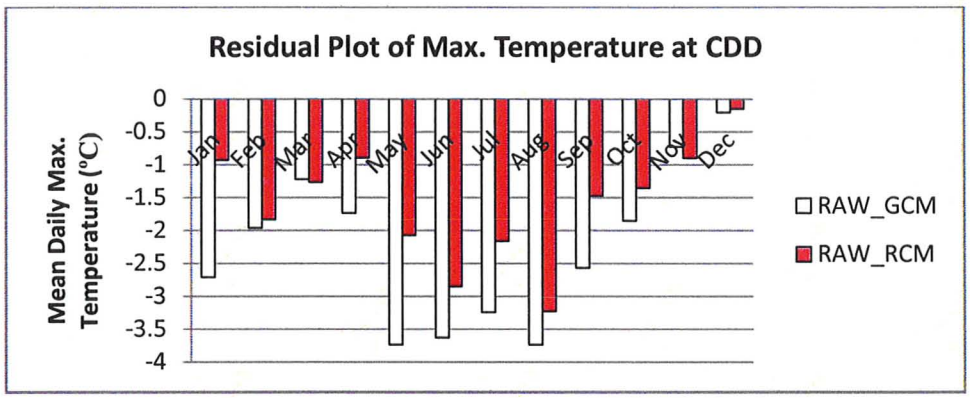

Figure 9: Residual plot of mean max. temp. at CDD: Raw GCM & Raw RCM output

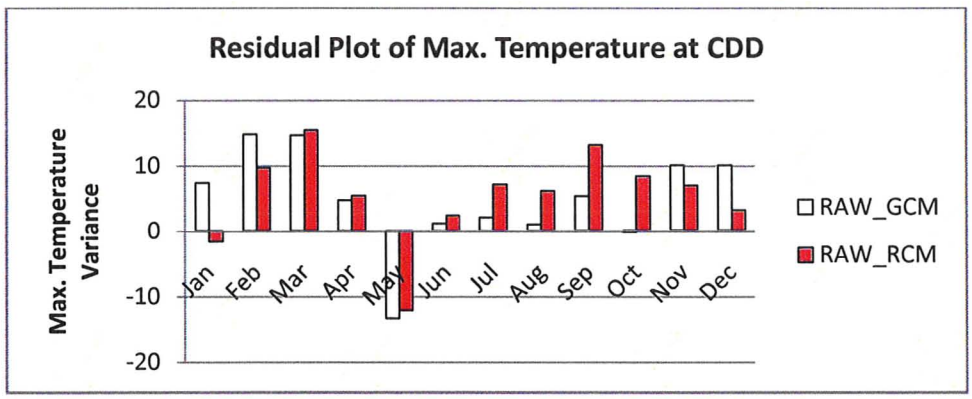

Figure 10: Residual plot of max. temp. variance at CDD: Raw GCM & Raw RCM output

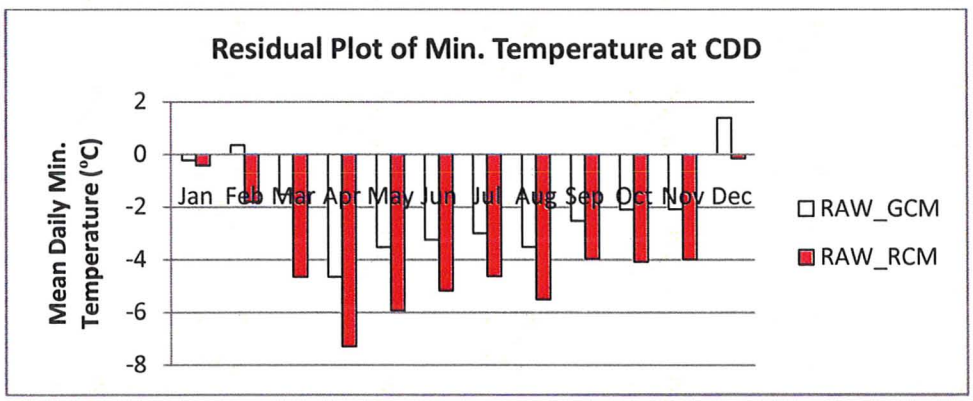

Figure 11: Residual plot of mean min. temp. at CDD: Raw GCM & Raw RCM output

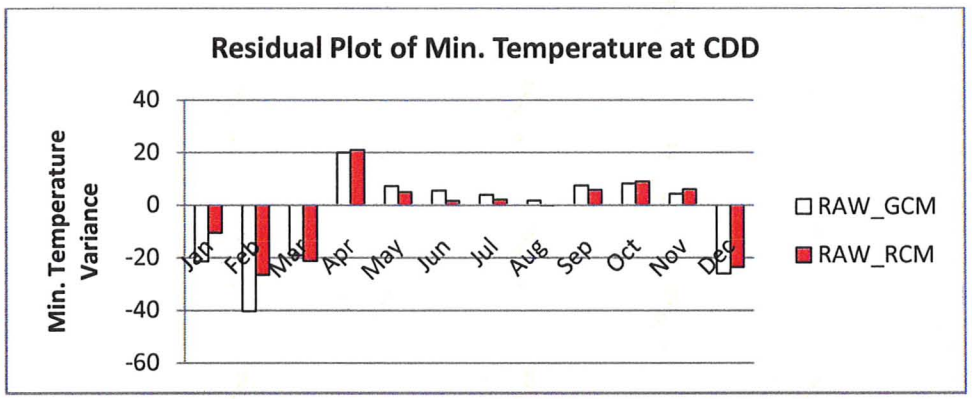

Figure 12: Residual plot of min. temp variance at CDD: Raw GCM & Raw RCM output

From Figures 7, 8 above and Figures 1A and 2A in the Appendix, it appears that for precipitation the CGCM3.1 model overestimates the mean for all months at both CDD and CDP stations. The CRCM4.2 model on the other hand underestimates mean precipitation during the winter season and over estimates the remainder of the year. Further, it appears that the raw CRCM4.2 precipitation is more accurate at representing the observed mean precipitation than the raw CGCM3.1 output as the residual values are smaller. When comparing the variance we see at both CDD and CDP stations, the raw CRCM4.2 output is better than the CGCM3.1 model at representing the observed variability for precipitation.

For maximum temperature, Figures 9, 10 and Figures 3A and 4A in the Appendix shows that the raw CRCM4.2 output is more accurate than the raw CGCM3.1 output at representing the mean maximum temperature throughout the entire year for both CDD and CDP stations. Both models generally underestimate the mean maximum temperature, except for the October, November and December months at CDP where the CGCM3.1 model overestimates the mean. In terms of variability, both models overestimate the mean maximum temperature in all months. In general, the raw CRCM4.2 model output is better at representing the maximum temperature variability.

Similarly for minimum temperature, Figures 11, 12 and Figures 5A and 6A in the Appendix shows that both the CRCM4.2 and CGCM3.1 models generally underestimate

the mean minimum temperature at both CDD and CDP stations. The residual values reveal that in this case, the raw CGCM3.1 output is more accurate than the raw CRCM4.2 output at representing the mean minimum temperature. At representing the variability, it can be seen that both models, at both stations, underestimate the minimum temperature variability for the winter months and overestimate the variability for the rest of the year. In terms of overall accuracy, there is no clear distinction between the two models as in some months the raw CRCM4.2 residual values are smaller and in others the raw CGCM3.1 residuals are smaller.

From the above residual plots and their respective analysis, it appears overall that the raw CRCM4.2 is more accurate than the CGCM3.1 at representing the observed conditions at both CDD and CDP stations. However, the CRCM4.2 residuals are still fairly significant and the goal in the next section will be to see if further downscaling the raw CRCM4.2 data will bring improved results.

Chapter 5: SDSM and TLFN Downscaling

5.1 Predictor Selection and Model Setup

As mentioned in Chapter 3, since regression-based downscaling methods rely on empirical relationships between local-scale predictands and regional-scale predictor(s), predictor selection is a very involved process if accurate results are to be attained (Wilby et al., 2002). Predictor variables are selected by using correlation analysis and also considering the physical sensitivity between selected predictors and predictand for the site in question (Coulibaly et al., 2005). Table A1 and A2 in the Appendix outline the predictors selected for downscaling the CRCM4.2 and CGCM3.1 data at CDD and CDP stations using the SDSM and TLFN downscaling methods respectively.

Prior to downscaling all predictors were normalized using equation (2) with mean and standard deviation for the baseline period 1961-1990 (Wilby et al., 2002):

$$z = \frac{x-\mu}{\sigma} \qquad (2)$$

Where z is the normalized value, x is the raw predictor value, μ is the mean of x for the baseline period and σ is the standard deviation of x for the baseline period.

Table A4 in Appendix A provides an example of the model parameters used in the setup of the SDSM and TLFN downscaling models for the case of precipitation at Station CDD. For Tmax and Tmin both SDSM and TLFN are very effective at modeling these predictands and much model parameter manipulation is not required.

5.2 Downscaling with SDSM

The results of downscaling daily precipitation, maximum temperature and minimum temperature are explained via bias plots, bias statistics tables, statistical tests, and a line plot comparing observed and simulated means. Analysis is divided into two sections, one for the CDD station and the other for the CDP station. In each section a comparison of downscaled CRCM4.2 and downscaled CGCM3.1 will be established.

Statistical analysis of the downscaled results is carried out by computing the root mean square error (RMSE), the mean absolute error (MAE) and the mean relative error (RE).

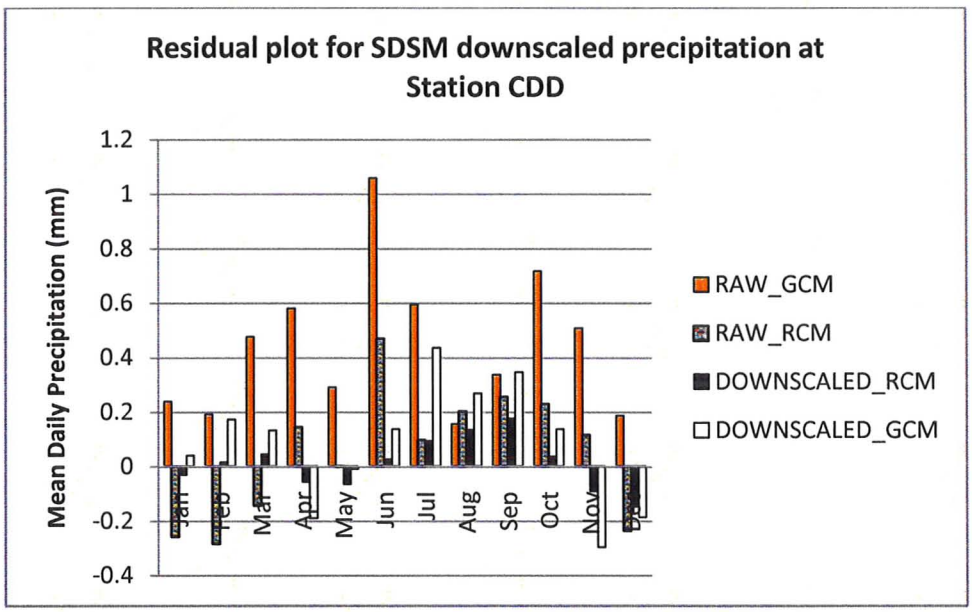

Figure 13: Residual plot for SDSM downscaled precipitation (comparing mean) at CDD

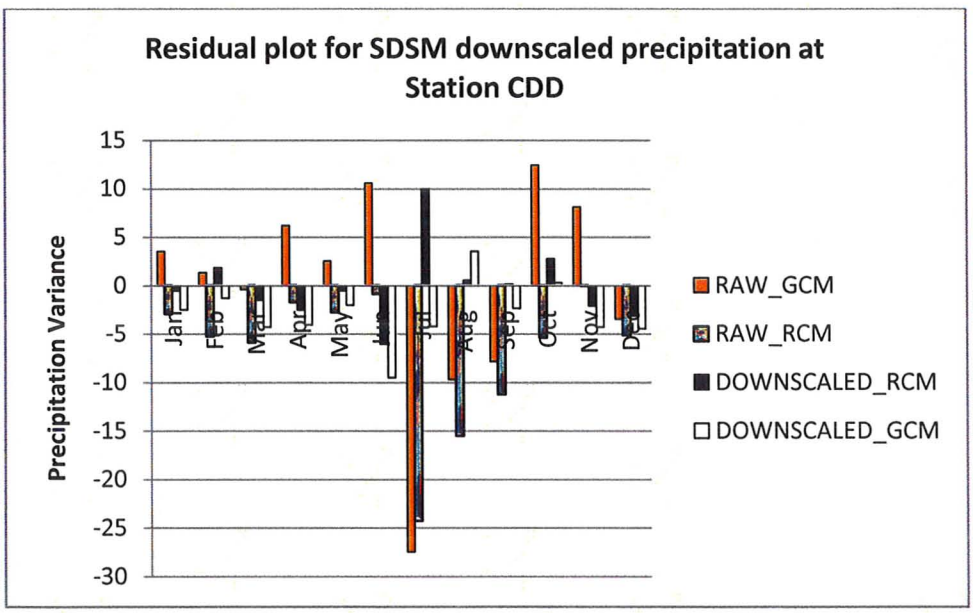

Figure 14: Residual plot for SDSM downscaled precipitation (comparing variance) at CDD

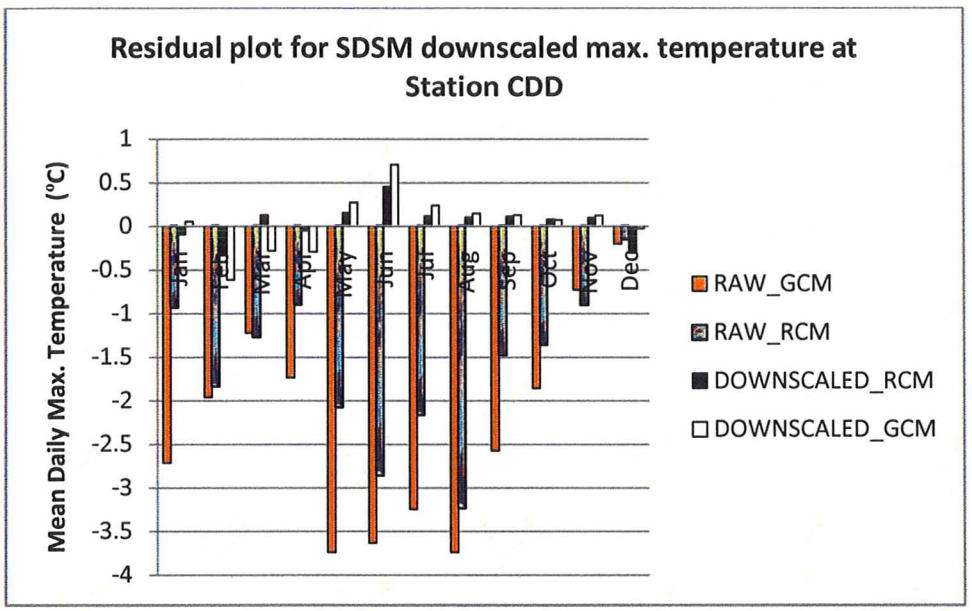

Figure 15: Residual plot for SDSM downscaled maximum temperature (comparing mean) at CDD

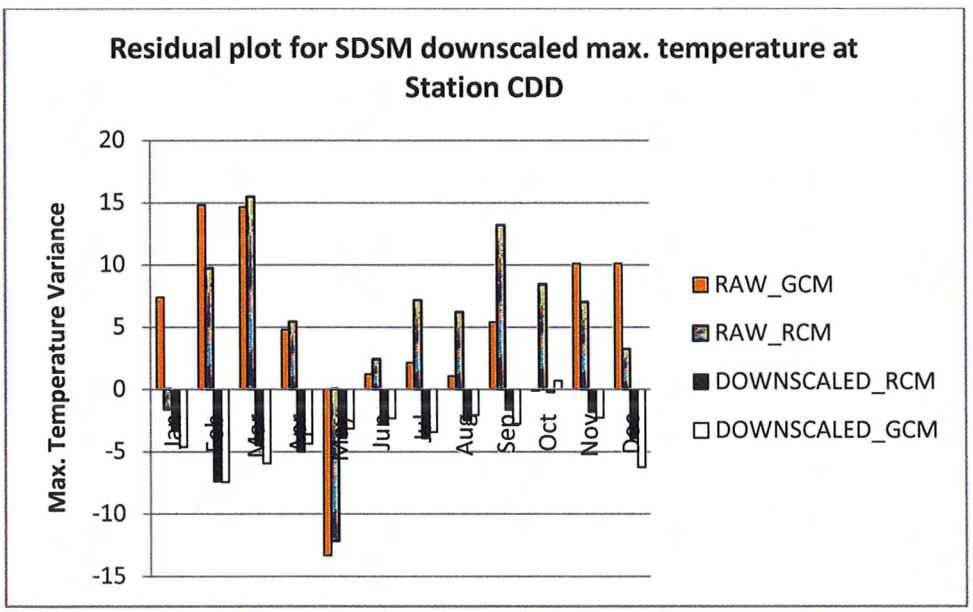

Figure 16: Residual plot for SDSM downscaled maximum. temperature (comparing variance) at CDD

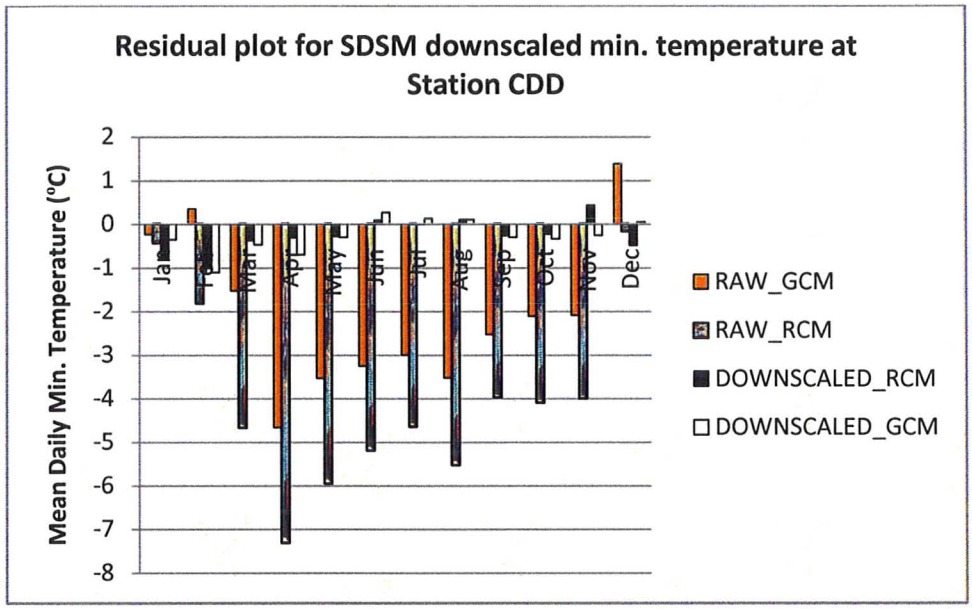

Figure 17: Residual plot for SDSM downscaled minimum temperature (comparing mean) at CDD

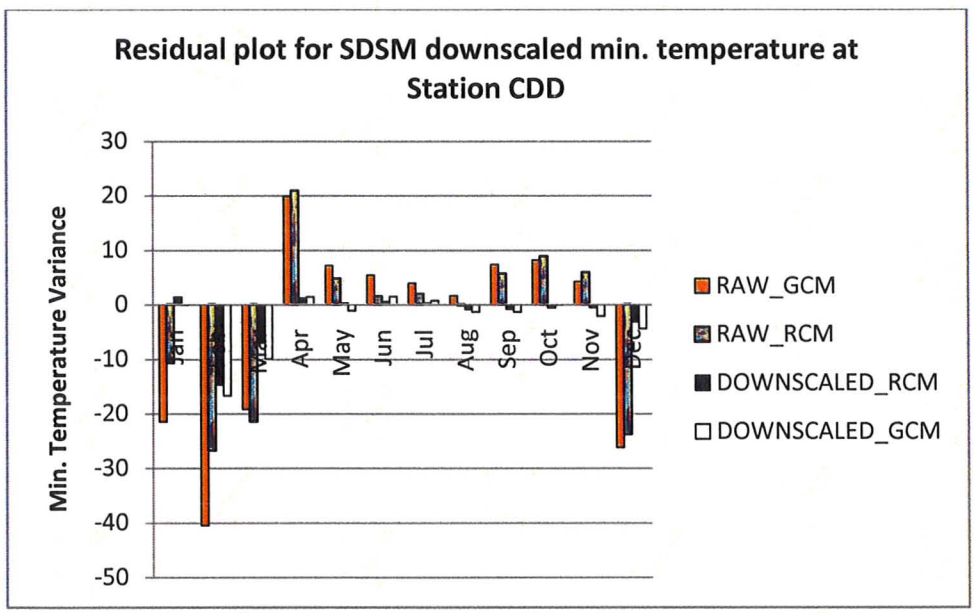

Figure 18: Residual plot for SDSM downscaled minimum temperature (comparing variance) at CDD

5.3 Downscaling with TLFN

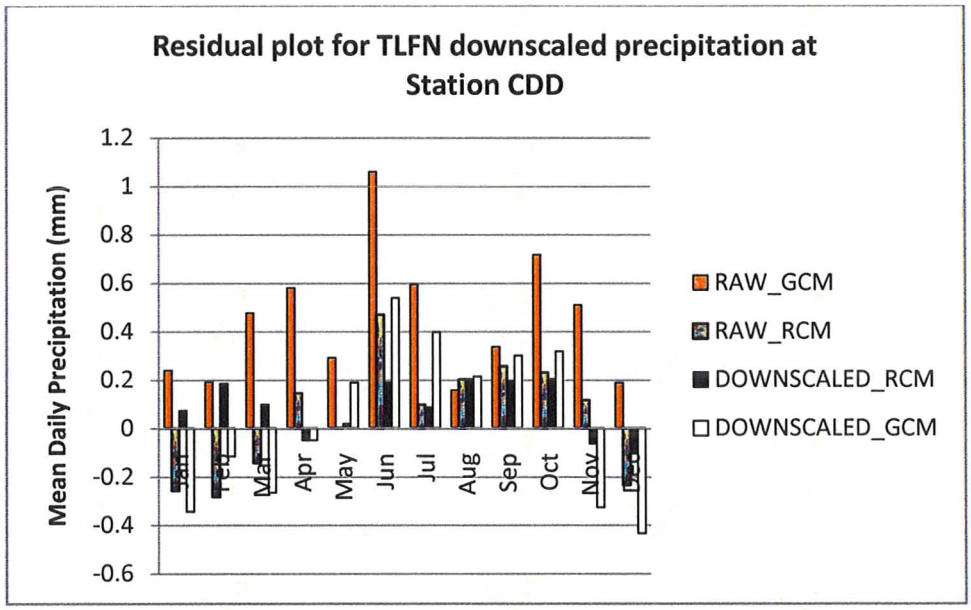

Figure 19: Residual plot for TLFN downscaled precipitation (comparing mean) at CDD

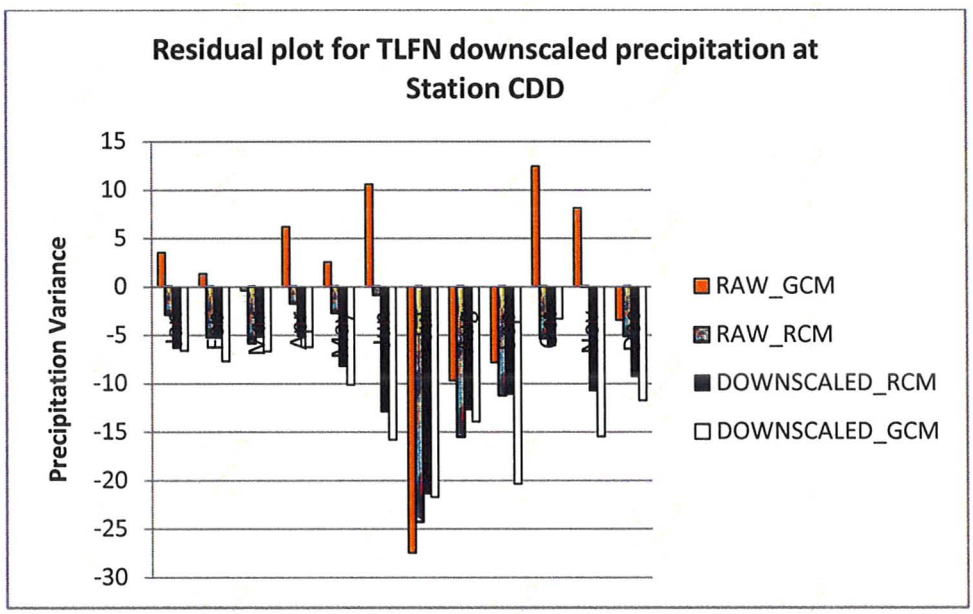

Figure 20: Residual plot for TLFN downscaled precipitation (comparing variance) at CDD

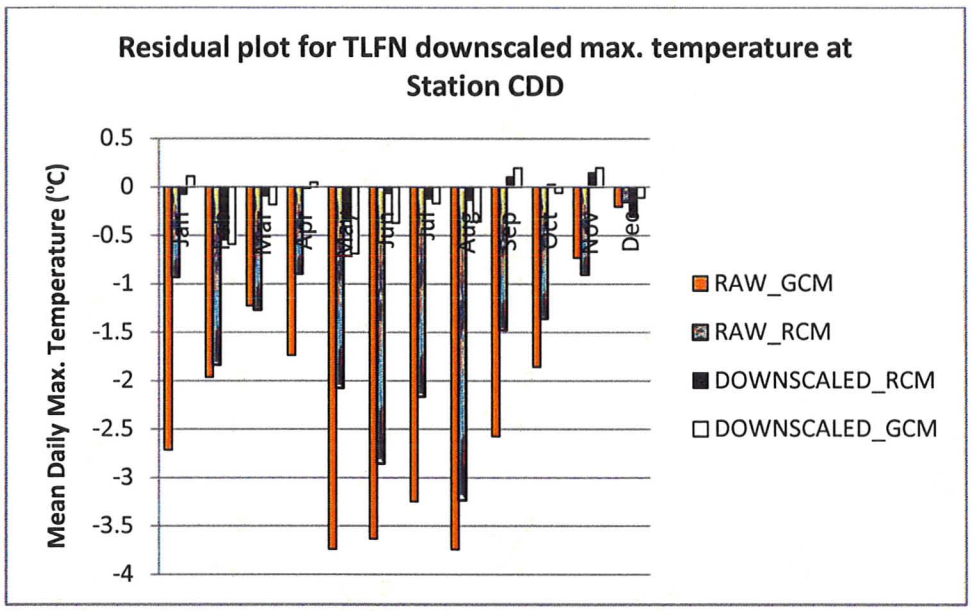

Figure 21: Residual plot for TLFN downscaled maximum temperature (comparing mean) at CDD

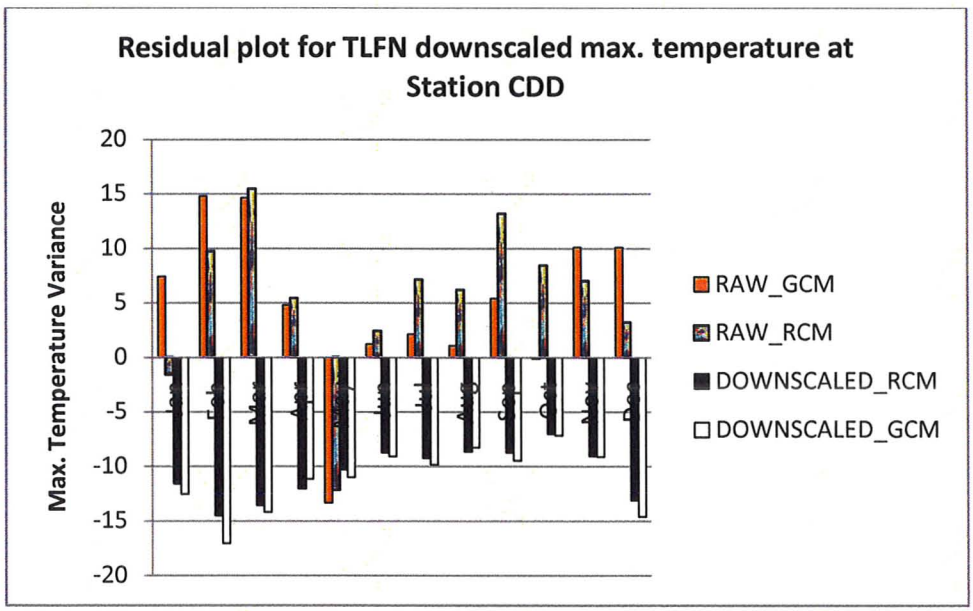

Figure 22: Residual plot for TLFN downscaled maximum temperature (comparing variance) at CDD

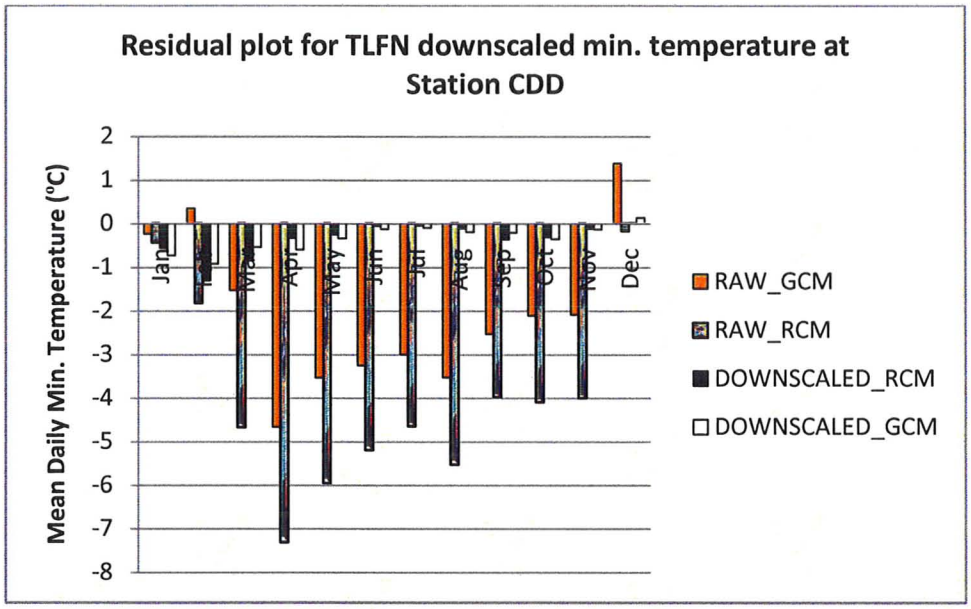

Figure 23: Residual plot for TLFN downscaled minimum temperature (comparing mean) at CDD

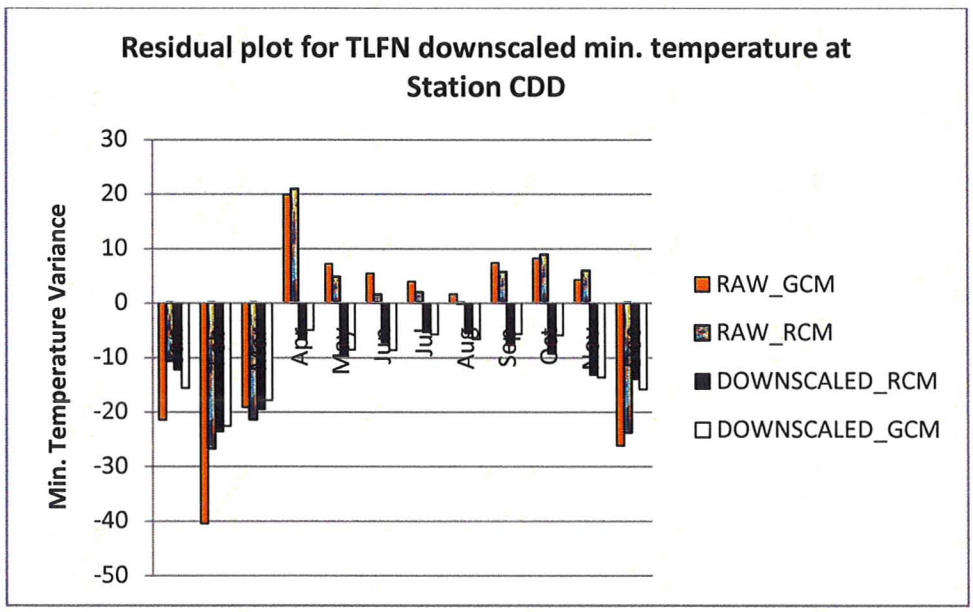

Figure 24: Residual plot for TLFN downscaled minimum temperature (comparing variance) at CDD

5.4 Comparison of CRCM4.2 and CGCM3.1 Downscaling Results

For downscaling daily precipitation, from the bias plots in the figures above, aswell as those in the Appendix, it is shown that for both SDSM and TLFN downscaling methods, CRCM4.2 downscaling results are better than CGCM3.1 downscaling results as the monthly mean and variance bias values are smaller. In other words, the downscaled CRCM4.2 results are closer to the observed values than the downscaled CGCM3.1 results at both CDD and CDP stations. Both CRCM4.2 and CGCM3.1 models, at both CDD and CDP stations over estimate the mean precipitation in the summer to early fall months and underestimate the mean precipitation during the November and December months. In terms of variance, the TLFN downscaling method, drastically underestimates the variance at both stations with both CRCM4.2 and CGCM3.1 data throughout all months. The TLFN downscaled bias values are particularily large in the summer months. The SDSM downscaling procedure is much better at capturing the degree of variance, but is consistent with TLFN in showing that the largest variance bias values are in the month of July. Additionally, Figures 25 and 26 below reveal that regardless of the downscaling method, significant improvement is achieved by downscaling the CRCM4.2 as the downscaled CRCM4.2 results are closer to the observed mean precipitation readings than the raw CRCM4.2 data at CDD. The same is found for the CDP station as shown in the Appendix. From Table 1, it is clear that regardless of the downscaling technique, the downscaled CRCM4.2 generally has a lower root mean square error (RMSE) and mean absolute error (MAE) then the downscaled CGCM3.1. The mean absolute error is calculated such that the cumulative difference between the simulated and observed precipitation values is considered. In comparing SDSM and TLFN, TLFN has larger MAE values due to the inability of TLFN to properly account for days with no precipitation. The bias values are thus larger for the TLFN model as compared to SDSM. The relative error (RE) statistics reveal that regardless of climate data type (CRCM4.2 or CGCM3.1), both downscaling techniques over estimate the mean annual cumulative precipitation.

For downscaling maximum daily temperature, from the bias plots in the previous sections, regardless of the climate data type, both SDSM and TLFN downscaling methods are capable of effectively capturing the mean maximum temperature. In some months CRCM4.2 downscaling mean bias values are smaller and in other CGCM3.1 bias values are smaller, but overall there is no observed trend in the downscaling results for the mean maximum temperature. More importantly however, Figures 27 and 28 below reveal that regardless of the downscaling method, a notable improvement results by downscaling the CRCM4.2 data as the downscaled results are much closer to the observed mean maximum temperature records (particularily through late spring – early fall) than the raw CRCM4.2 output. In terms of variability, we see the TLFN downscaling procedure once again drastically underestimates the variablity in all months at both CDD and CDP stations, regardless of the type of climate data being downscaled. In this case, the largest bias values for the TLFN procedure are observed in the winter months and the smallest bias values throughout the summer months. There is no clear trend with the SDSM downscaling procedure as at the CDD station the model understimates the variabilty throughout all months, but at the CDP station in some months there is no trend at all. For both methods, we see SDSM downscaling at station CDP is the best at capturing the observed variance. From Table 1, overall the downscaled CRCM4.2 has a lower RMSE and MAE than the downscaled CGCM3.1. For temperature the MAE is computed based on the average of the monthly differences in mean between the observed and simulated values. TLFN is the better downscaling technique as it has the lowest RMSE and MAE values. The RE values tell us that, TLFN underestimates the annual mean maximum temperature, whereas SDSM overestimates.

For downscaling minimum temperature, from the bias plots above and those in the Appendix, it is clear that regardless of the climate data type or the downscaling method, the downscaled results are very good as the mean is captured very well at both the CDD and CDP stations. In terms of the mean, both downscaled CRCM4.2 and downscaled CGCM3.1 results at both stations are improved with no clear trend in the results to justify one downscaling technique to be more accurate than the other. In terms

of variabilty, TLFN once again undersestimates the degree of variance in all months, with the largest bias values in the winter months and smallest in the summer months. SDSM is much better at capturing the variance as the bias values are small throughout all months for both downscaled CRCM4.2 and CGCM3.1 at both stations. More importantly however, Figures 29 and 30 below reveal that regardless of the downscaling method, a significant improvement (most notably throughout the entire spring, summer and fall seasons) results by downscaling the CRCM4.2 at both CDD and CDP. From table 1, the downscaled CRCM4.2 has a lower RMSE and MAE then the downscaled CGCM3.1, with TLFN once again outperforming SDSM as it has lower RMSE and MAE values. From the RE values, in this case regardless of the downscaling technique, the downscaled CRCM4.2 underestimates the mean minimum temperature and the downscaled CGCM3.1 overestimates.

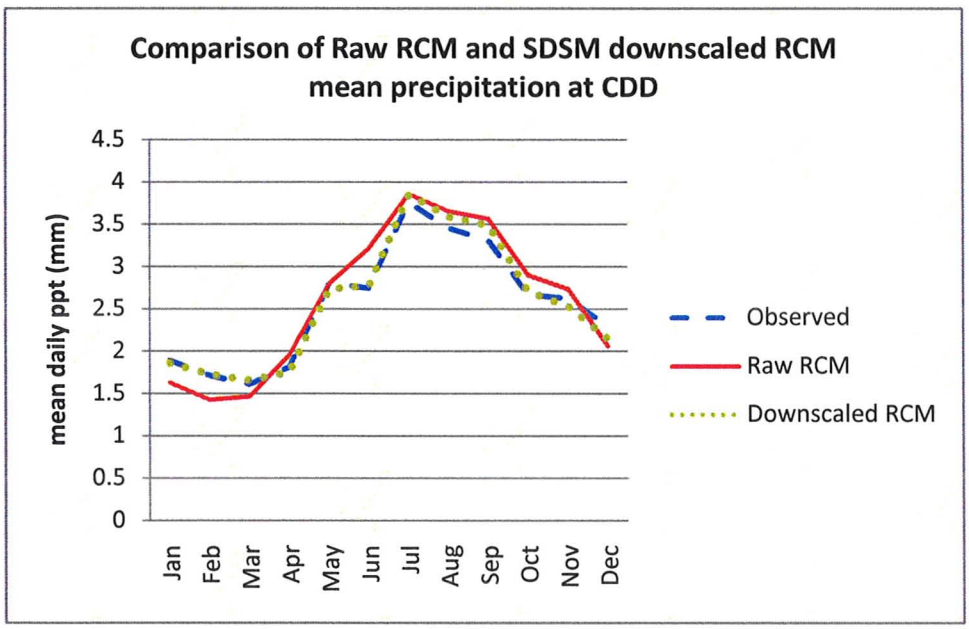

Figure 25: Comparison of Raw RCM and SDSM Downscaled RCM mean ppt. at CDD

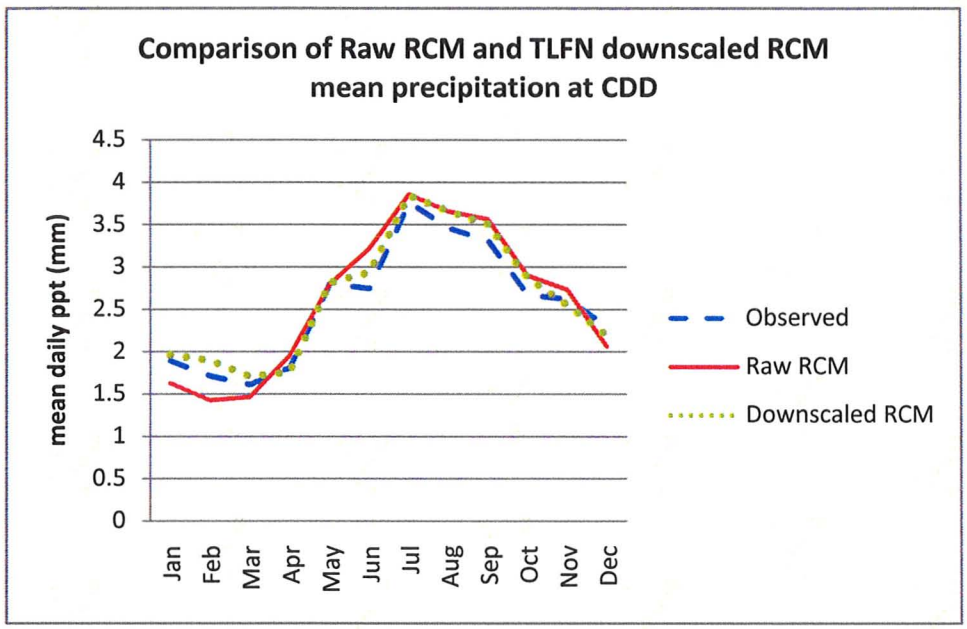

Figure 26: Comparison of Raw RCM and TLFN Downscaled RCM mean ppt. at CDD

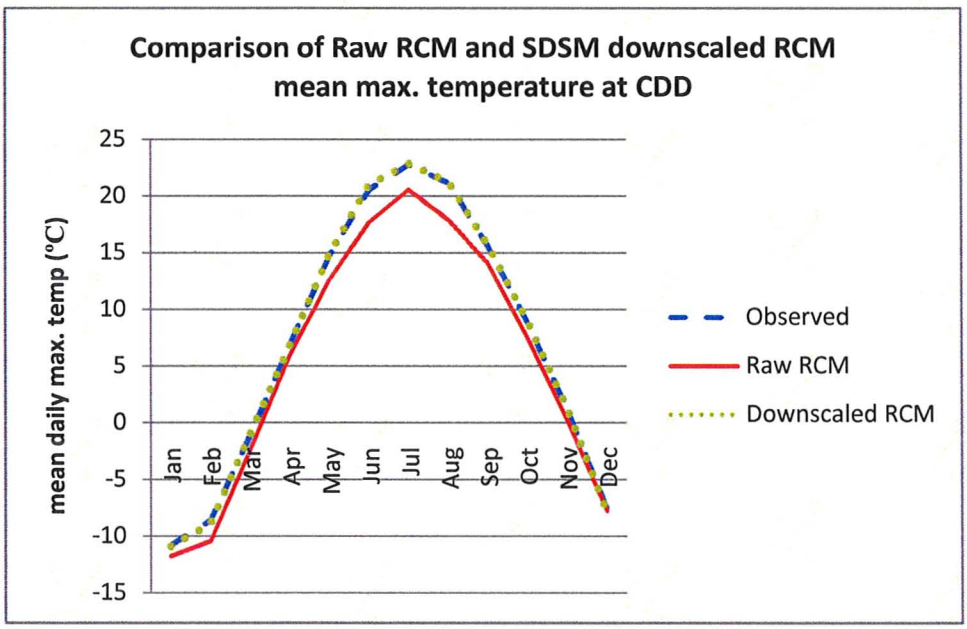

Figure 27: Comparison of Raw RCM and SDSM Downscaled RCM mean max. temp at CDD

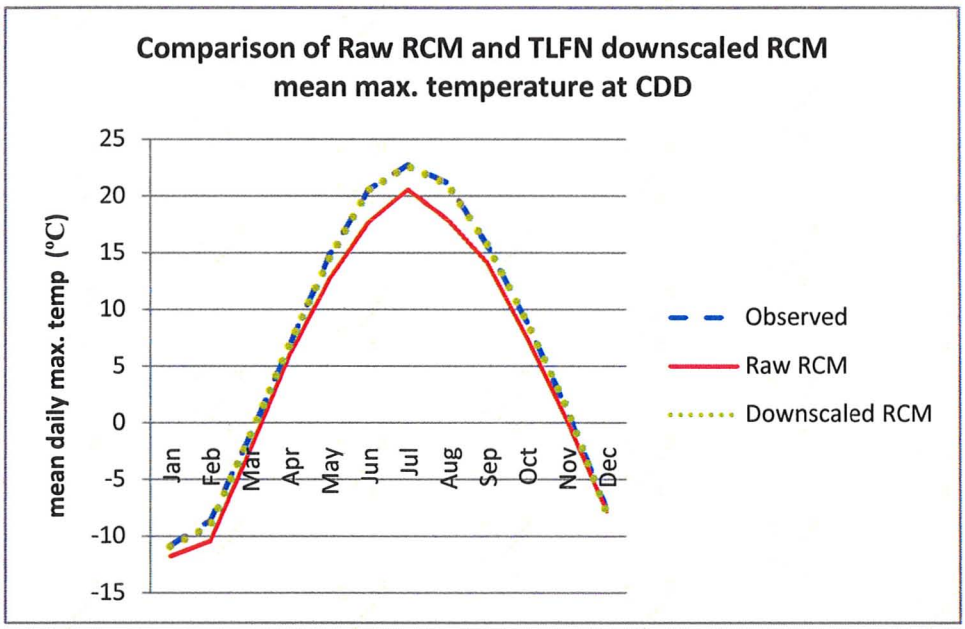

Figure 28: Comparison of Raw RCM and TLFN Downscaled RCM mean max. temp at CDD

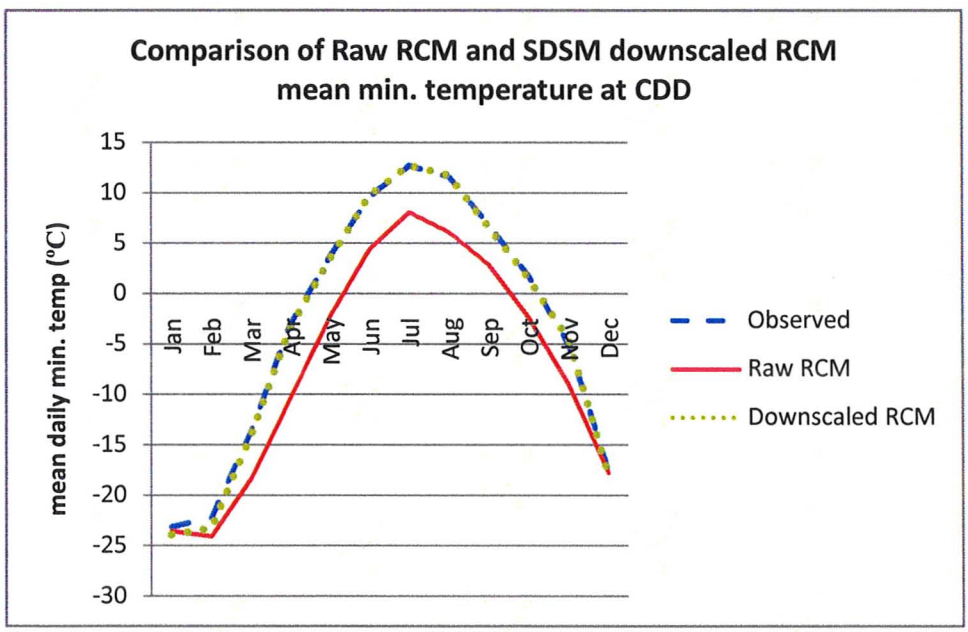

Figure 29: Comparison of Raw RCM and SDSM Downscaled RCM mean min. temp at CDD

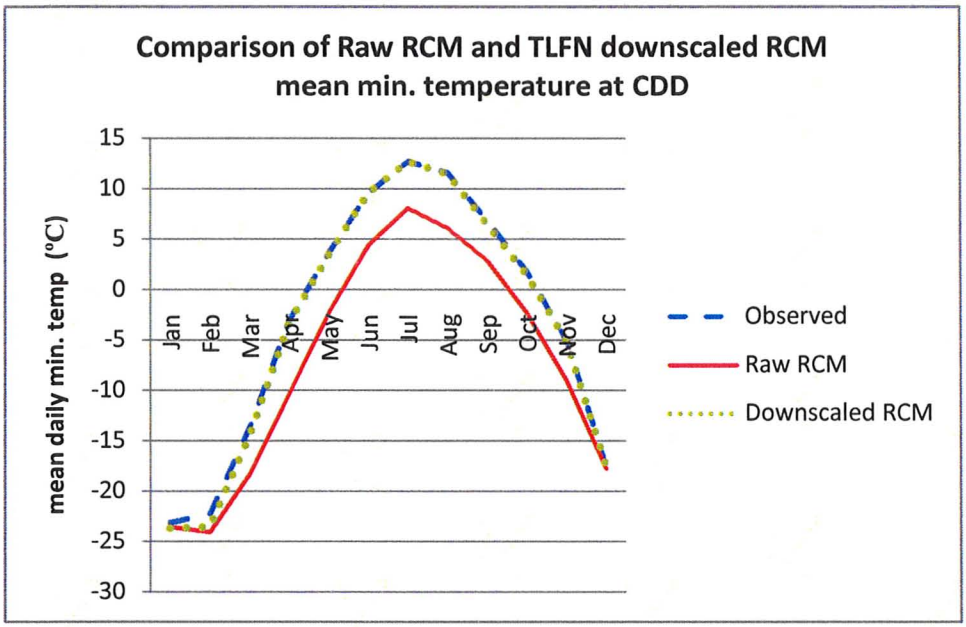

Figure 30: Comparison of Raw RCM and TLFN Downscaled RCM mean min. temp at CDD

	PREC - STATION CDD				TMAX				TMIN			
	SDSM		TLFN		SDSM		TLFN		SDSM		TLFN	
	RCM	GCM	RCM	GCM	RCM	GCM	RCM	GCM	RCM	GCM	RCM	GCM
RMSE	8.3	8.54	9.09	9.12	5.79	5.81	4.47	4.5	5.21	5.24	4.45	4.59
RE	0.12	0.98	1.02	1.41	0.03	0.04	-0.12	-0.17	-0.27	0.36	-0.36	0.36
MAE	1.92	2.35	5.47	6.49	0.17	0.24	0.14	0.22	0.36	0.37	0.36	0.37

	PREC - STATION CDP				TMAX				TMIN			
	SDSM		TLFN		SDSM		TLFN		SDSM		TLFN	
	RCM	GCM	RCM	GCM	RCM	GCM	RCM	GCM	RCM	GCM	RCM	GCM
RMSE	7.76	7.93	9.32	9.88	5.21	5.4	4.08	4.59	5.17	5.86	4.29	4.64
RE	0.14	1.27	1.23	1.31	0.01	-0.02	-0.07	-0.08	-0.19	0.24	-0.18	0.21
MAE	1.46	2.73	6.07	6.77	0.19	0.25	0.12	0.19	0.24	0.21	0.21	0.23

Table 1: Downscaling model validation statistics for the CDD and CDP stations

It is important to assess the validity of the downscaling experiments through an uncertainty assessment. In the case of downscaling daily temperature, because of their nearly normal distribution, the uncertainty can be assessed with comparisons of means and variances of downscaled temperature data with observed readings. In the uncertainty assessment for downscaled precipitation however, comparisons of means and variances is not enough because of the non-normality of precipitation and such is important for some parameter or non-parametric approach to be employed (Khan et al., 2006).

The Levene Test was used to test the equality of variances for precipitation (Levene, 1960). Simply the test assesses the null hypothesis, that the variances of populations from which different samples are drawn are equal; or simply if n samples have equal variance (equality of variance) (Khan et al., 2006). If the resulting p-value of Levene's test is less than some critical value (typically 0.05), the null hypothesis is rejected and it is concluded that there is a difference between the variances of the two populations. The variance test results in Table 2 show the p-values are all above 0.05. This concludes that the observed and simulated daily precipitation variance can be considered statistically equal in all months with a 95% confidence level.

LEVENE TEST RESULTS - CDD				
	SDSM		TLFN	
Month	RCM	GCM	RCM	GCM
Jan	0.783	0.737	0.484	0.932
Feb	0.849	0.733	0.216	0.375
Mar	0.706	0.972	0.654	0.204
Apr	0.458	0.562	0.158	0.599
May	0.512	0.365	0.629	0.326
Jun	0.834	0.353	0.417	0.486
Jul	0.239	0.866	0.341	0.795
Aug	0.769	0.095	0.641	0.276
Sep	0.392	0.148	0.563	0.313
Oct	0.672	0.795	0.690	0.231
Nov	0.835	0.059	0.786	0.439
Dec	0.510	0.717	0.492	0.885

Table 2: Levene Test p-values for precipitation at CDD

The Wilcoxon Rank-Sum Test was used to test the difference of means. This non parametric test tests the hypothesis that two populations have the same population mean, i.e. observations that come from the same distribution. The null hypothesis is that the population means are equal and thus any p-value above a critical value (0.05) will indicate that the observed and generated means are close and come from the same distribution. Further description of the test can be found in Khan et al., 2006b. Table 3 provides the p-values for the precipitation downscaling experiments. As shown, overall the SDSM downscaling method is more effective at capturing the mean as regardless of the climate data type, the p-values are generally larger than 0.05. TLFN on the other hand, is not as good, particularly in August and September. The results also reveal that regardless of the downscaling method employed or the climate data type downscaled the test failed in April. This may be a result of the atmospheric predictors selected for the downscaling. Further both SDSM and TLFN are effective at capturing the mean in the winter months.

WILCOXON RANK SUM TEST - CDD				
	SDSM		TLFN	
Month	RCM	GCM	RCM	GCM
Jan	0.515	0.312	0.180	0.221
Feb	0.322	0.868	0.128	0.018
Mar	0.646	0.447	0.531	0.397
Apr	0.013	0.014	< 0.0001	< 0.0001
May	0.685	0.407	0.055	0.201
Jun	0.476	0.929	0.766	0.445
Jul	0.371	0.476	0.024	0.127
Aug	0.970	0.360	0.004	0.006
Sep	0.133	0.015	0.009	0.028
Oct	0.884	0.783	0.536	0.298
Nov	0.268	0.010	0.966	0.264
Dec	0.283	0.909	0.291	0.391

Table 3: Wilcoxon Rank Sum Test p-values for precipitation at CDD

5.5 Future Climate Change

Once the downscaling models have been calibrated and validated for the current period (1961-1990), the models are used to generate future values of precipitation, maximum & minimum temperature corresponding to the SRES A2 future climate scenario. The goal is to understand and compare what each climate model (CRCM4.2 and CGCM3.1) and downscaling method (TLFN, SDSM) will project for the future period (2046-2065). The monthly mean statistics for the future period (2050s) are compared with current period (1961-1990) results in the following figures. Each figure contains three series – the blue represents the current observed mean value, the red represents the RCM projected mean for the 2050s and the green represents the GCM projected mean for the 2050s future period.

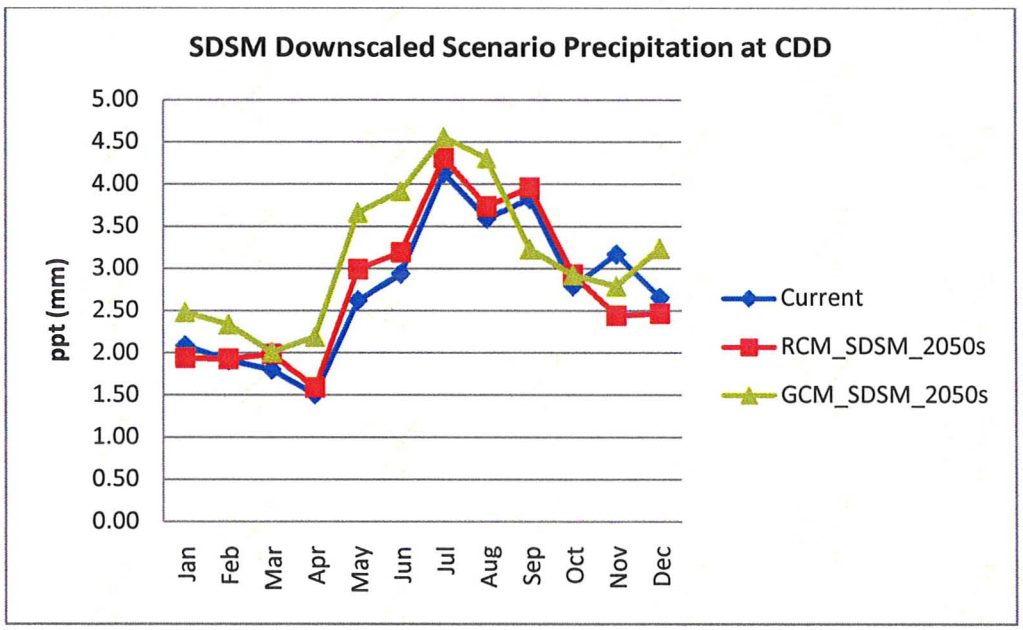

Figure 31: Monthly mean precipitation at CDD for current and future period

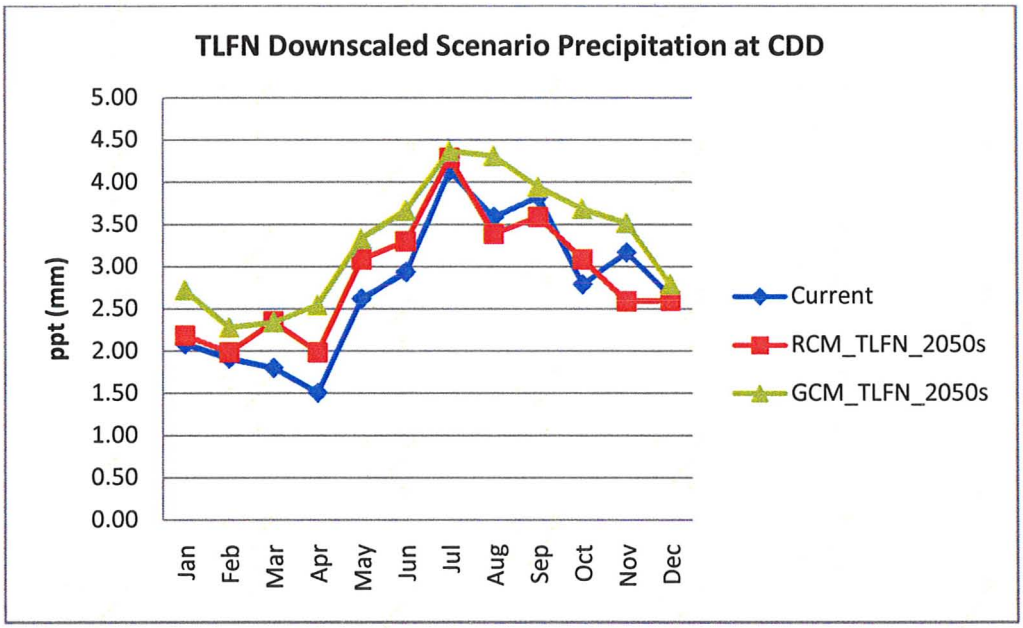

Figure 32: Monthly mean precipitation at CDD for current and future period

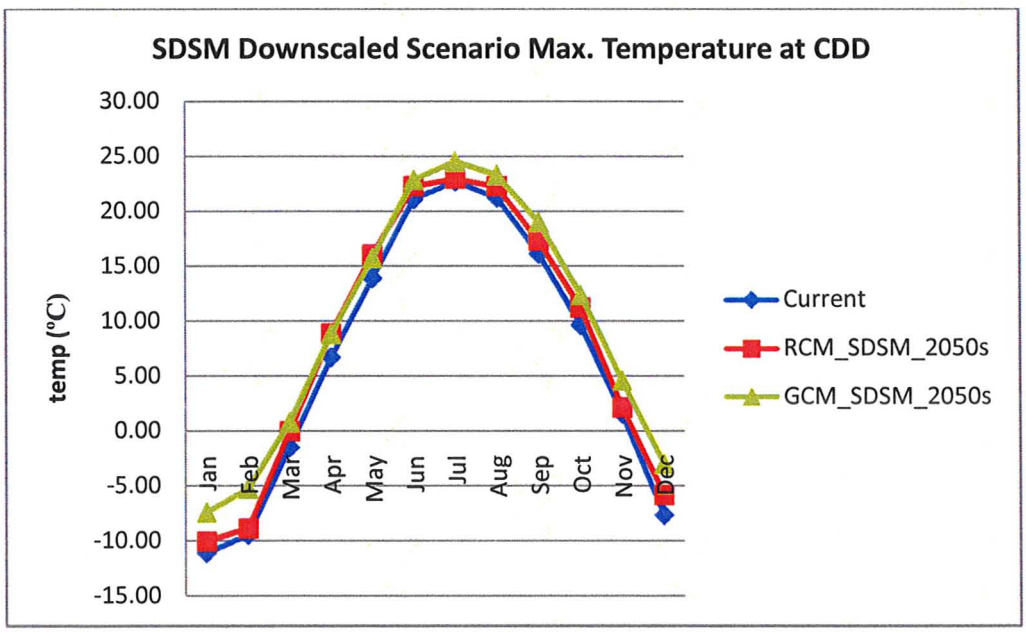

Figure 33: Monthly mean maximum temperature at CDD for current and future period

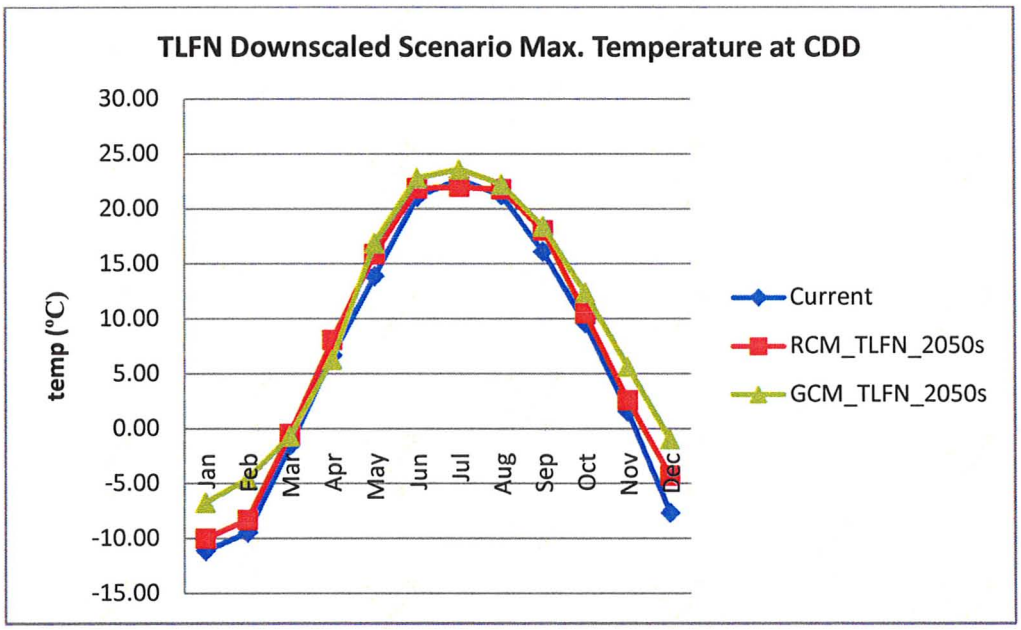

Figure 34: Monthly mean maximum temperature at CDD for current and future period

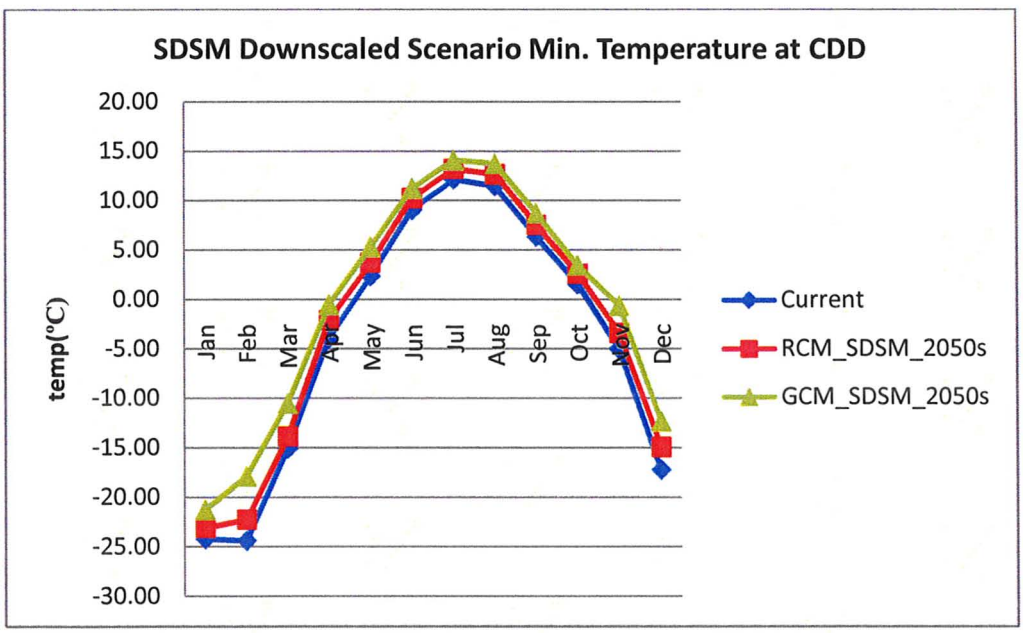

Figure 35: Monthly mean minimum temperature at CDD for current and future period

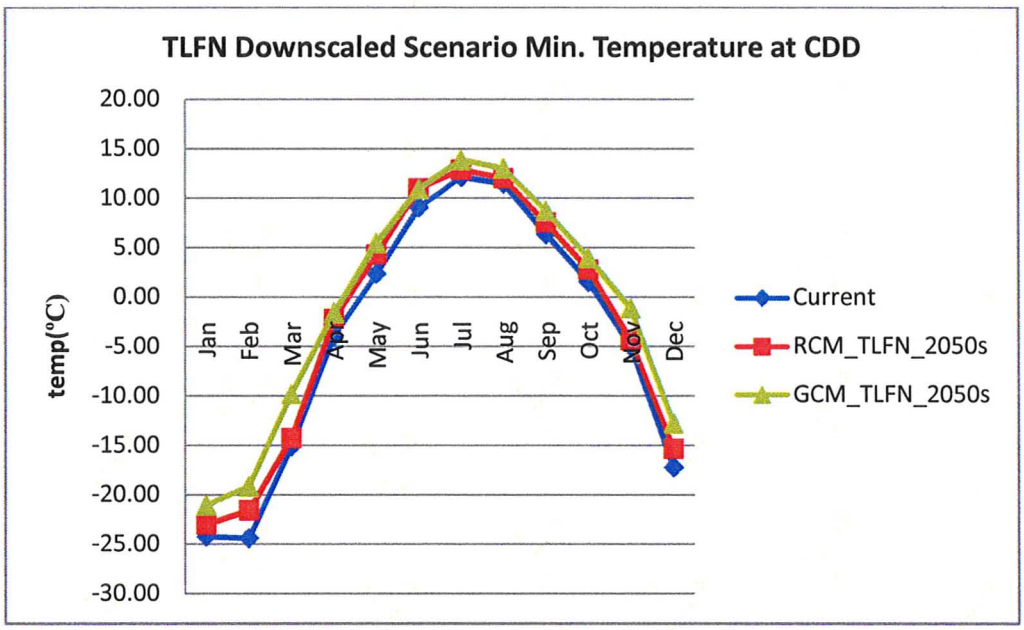

Figure 36: Monthly mean minimum temperature at CDD for current and future period

From Figures 31-36 above and Figures A25-A30 in the Appendix it is clear that at both station CDD and CDP the CGCM3.1 model shows a larger increasing trend in mean precipitation, mean maximum temperature and mean minimum temperature in the 2050s future period than the CRCM4.2 model. For precipitation, regardless of the climate model type, or the downscaling method, the most significant changes in mean occur during the late winter, spring and early summer months. Additionally, regardless of the downscaling method, the CGCM3.1 future monthly mean trend is smoother throughout the year, whereas the CRCM4.2 trend tends to be more sporadic. For maximum temperature, the changes are gradual throughout the entire year for both climate models and downscaling methods with the largest increase in mean maximum temperature occurring during the fall and winter months. For minimum temperature, the most significant changes occur during the winter months with gradual changes throughout the remainder of the seasons. Both CRCM4.2 and CGCM3.1 models provide smooth trends of mean minimum temperature for the future period. Table 5 shows the annual average increase/decrease in mean precipitation, mean maximum temperature and mean minimum

for both stations using both SDSM and TLFN downscaling methods. At both CDD and CDP, for precipitation it is clear the CGCM3.1 shows a much larger increase than the CRCM4.2 model for the 2050s future period. Additionally, the TLFN model shows larger increases in annual mean precipitation than the SDSM model. For maximum and minimum temperature the results are similar as the CGCM3.1 model once again shows a larger increasing trend than the CRCM4.2 model regardless of whatever downscaling method was employed. In these cases however, sometimes the SDSM downscaling model shows a larger increasing trend and in others the TLFN downscaling models does.

Overall, regardless of the climate model or the downscaling method, a 1 to 3˚C increase in annual mean maximum temperature and a 1 to 4˚C increase in annual mean minimum temperature are predicted for the 2050s future period. In the case for precipitation, the CRCM4.2 model shows increases in annual precipitation will vary from 1 to 7% in the 2050s regardless of the downscaling method used. The CGCM3.1 model on the other hand, shows increases in annual precipitation ranging from 15 to 23% regardless of the downscaling method employed. All of these predicted changes will translate into different effects on the catchment scale hydrology.

Average Increase/Decrease												
Station CD	Precipitation (%)				TMAX (°C)				TMIN(°C)			
	SDSM		TLFN		SDSM		TLFN		SDSM		TLFN	
	RCM	GCM	RCM	GCM	RCM	GCM	RCM	GCM	RCM	GCM	RCM	GCM
2050s	1.73	16.76	6.97	23.13	1.27	2.78	1.21	2.68	1.43	3.34	1.41	3.12

Average Increase/Decrease												
Station CDP	Precipitation (%)				TMAX (°C)				TMIN(°C)			
	SDSM		TLFN		SDSM		TLFN		SDSM		TLFN	
	RCM	GCM	RCM	GCM	RCM	GCM	RCM	GCM	RCM	GCM	RCM	GCM
2050s	0.93	14.60	4.30	16.39	1.49	2.58	2.22	2.78	1.40	3.07	1.76	3.07

Table 4: Changes in annual average values at both Stations from current conditions as predicted by the SDSM and TLFN downscaling models

Chapter 6: Hydrological Modeling

Hydrological models are simplified mathematical formulations of a particular phase in the hydrological cycle. At the field scale, models are used for varied purposes, such as planning and designing soil conservation practices, irrigation water management, wetland restoration, stream restoration, and water-table management. On a large scale, models are used for flood protection projects, rehabilitation of aging dams, floodplain management, water-quality evaluation, and water-supply forecasting. Generally, hydrological models can be classified based on (1) process description; (2) timescale; (3) space scale; (4) techniques of solution; (5) land use and (6) model use (Singh et al., 2002). Here a more specific classification will be discussed: fully distributed physical vs. lumped conceptual deterministic models and data driven models.

Physical models are based on the underlying physical equations that represent the physics of the hydrological processes which control the catchment response. These models will solve for processes such as: interception, infiltration, evaporation and transpiration, snow accumulation and ablation, interflow, recharge, baseflow, overland flow, wetland and channel routing throughout the entire catchment (Kouwen, 2009). In these models transfer of mass, momentum and energy are calculated directly from the governing partial differential equations which are solved using numerical methods, for example the St. Venant equations for surface flow, the Richards equation for unsaturated zone flow and the Boussinesq equation for ground water flow (Seth, 2009). Some of the latest most comprehensive models are capable of incorporating radar LANDSAT land cover and radar rainfall data to accurately account for the spatial variability in largely heterogeneous watersheds. Conceptual models on the other hand are based on more simplified representations of the hydrologic processes in a watershed and are normally run with point values of precipitation and temperature as the primary input (Liden & Harlen, 2000). The idea with conceptual modelling is to consider the catchment as a system whose components are precipitation, evapotranspiration, storage and runoff. The water balance equation for a catchment model can be written as

$$P - ET \pm \Delta S = Q \qquad (3)$$

where P is total precipitation on the catchment, ET is the evapotranspiration, ΔS is the change in water storage, and Q the runoff from the catchment (Liden & Harlen, 2000).

The fully distributed nature of a hydrological model refers to its ability to divide the watershed into a square grid system where input is required and output information is produced at all points. These models are capable of incorporating the entire physiography and hydrological variability of a study area accounting for heterogeneities throughout the watershed. Thus, fully distributed physically based models are very data intensive as large amounts of high quality physical, geographical and meteorological data is required to ensure accuracy (Cranmer et. al, 2001).Conventional lumped models on the other hand, simply consider spatial averages of the land surface and are thus less data intensive, but also much less precise.

In the last decade, artificial neural networks (ANNs) have been employed in hydrological modeling as they have the ability to recursively learn from data and are particularly suited for modeling nonlinear systems where traditional parameter estimation techniques are not convenient (Singh et. al 2002). Another benefit stems from the fact that no information on the physics or physiographic nature of the watershed is required as model performance is based on the minimizing of some statistic rather than conceptually representing the hydrologic processes in the study area. A full description of preliminary concepts and applications can be found in (ASCE, 2000 a,b).

Although hydrological models have been around for quite some time, there is yet to be one exclusive model that can stand apart from the rest and be declared best at modeling all aspects of the hydrologic system. The major problem in hydrological modeling is that it is impossible to measure and simulate every single interaction between air, water, and land, whether by limitations in science or in finance (Carlaw, 2000). Thus, models become estimations of real world conditions based on information that is feasible to obtain. With this, models must be comprehensive enough to accurately represent real-

life conditions, but they must also be simple enough to run within a suitable time frame on standard computing resources (Carlaw, 2000). It is this balance between accuracy and simplicity that is hindering the development of a model which simulates all hydrologic processes with perfect accuracy.

6.1 HBV Hydrological Modeling System

Originally developed at the Swedish Meteorological and Hydrological Institute (SMHI) in the early 70's to assist hydropower operations, the Hydrologiska Byrans Vattenbalans-avdeling (HBV) model is a conceptual hydrological model used for continuous calculation of runoff (Linden & Harlin, 2000). The model can be classified as semi-distributed as it uses sub basins, as primary hydrological units in which an area-elevation distribution and a crude classification of land use (forest, open areas, and lakes) are made (Linden & Harlin, 2000). A schematic sketch of the structure and parameters of the HBV model is shown in Figure 37 (Linden & Harlin, 2000). Input data are observations of precipitation, mean temperature, vapour pressure, wind speed and estimates of potential evaporation.

Precipitation calculations are made separately for each elevation/vegetation zone within a basin and a threshold temperature is used to differentiate between snow and rainfall. The snow routine is based on a simple degree day relation and is applied to both snow accumulation and snow melt. Evapotranspiration values are based on long-term monthly averages of potential evaporation as input and a simplified variation of Thornthwaite's equation (Lindstrom et al., 1997). A soil moisture accounting routine is the main part controlling runoff formation. Water not retained in the soil is routed through two stores, an upper one interpreted conceptually as saturated soil and a lower one representing groundwater (Dibike & Coulibaly, 2007). The model parameters are determined through a calibration process, where the parameters are adjusted until simulated and observed flow readings show a good statistical agreement.

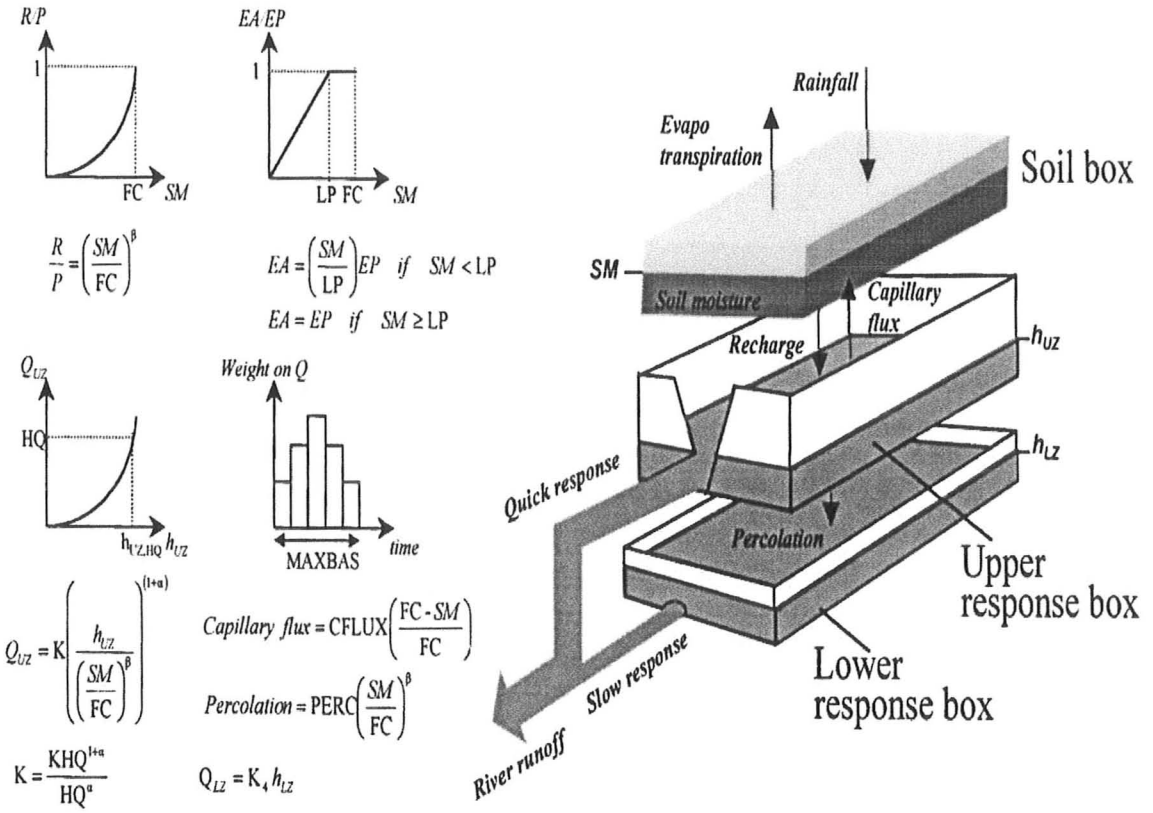

VARIABLES

R	Recharge
P	Rainfall
SM	Soil moisture storage
EP	Potential evapotranspiration
EA	Actual evapotranspiration
h_{UZ}	Storage in upper response box
h_{LZ}	Storage in lower response box
Q_{UZ}	Runoff from upper response box
Q_{LZ}	Runoff from lower response box
Q	River runoff

PARAMETERS

FC	Maximum soil moisture storage
LP	Limit for potential evapotranspiration
β	Soil routine parameter
KHQ	Recession at HQ
HQ	Half of mean annual flood
α,K_4	Recession parameters
$h_{UZ,HQ}$	h_{UZ} level at HQ
PERC	Percolation rate
CFLUX	Capillary flux rate
MAXBAS	Routing parameter

Figure 37: HBV Model schematic (taken from Linden & Harlin, 2000)

To date the HBV model has been applied effectively in over 35 countries encompassing a large variety of climate and geographic locations. See Bergstrom & Forsman, 1973; Brandt, 1990; Liden & Harlin, 2000; Coulibaly et al., 2005. More importantly however, HBV has been used in previous studies in the same study area, the results of which revealed that the HBV model is quite effective in the particular climate and physiography of the study area (Dibike & Coulibaly, 2007 and Dibike & Coulibaly, 2005).

In this study HBV will be used to simulate inflow in the Chute-du-Diable reservoir and flow in the Mistassibi river. The models will first be calibrated with observed data obtained from the CD and CDP weather stations for the years 1961-1980 and then validated for the years 1981-1990. Once a good model has been created, the downscaled CGCM3.1 and CRCM4.2 results will be input in place of the observed data to see how well the downscaled results are able of capturing the observed flows. The root mean square error (RMSE), correlation coefficient (r) and Nash-Sutcliffe model efficiency index (Nash) will be used to judge the accuracy of the models.

6.2 HBV Simulation Results for the Chute-Du-Diable reservoir

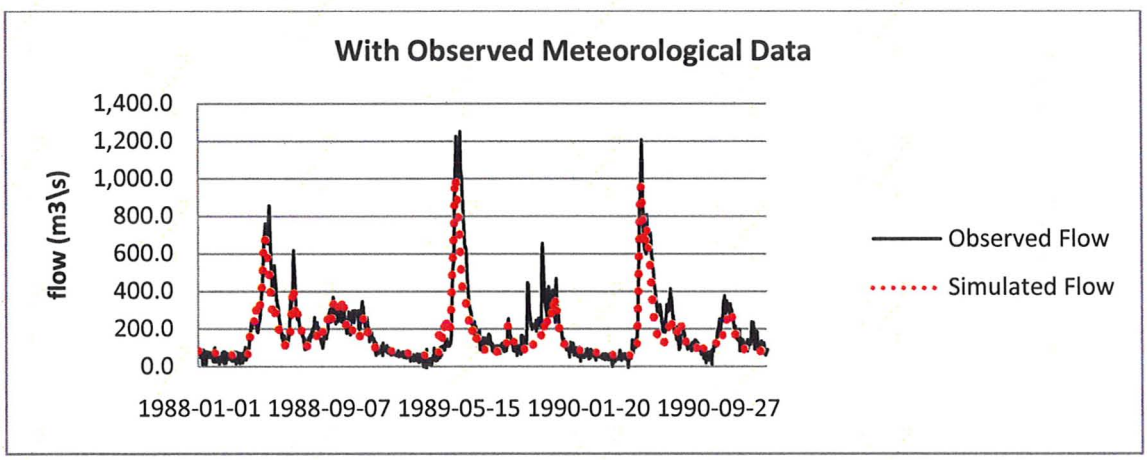

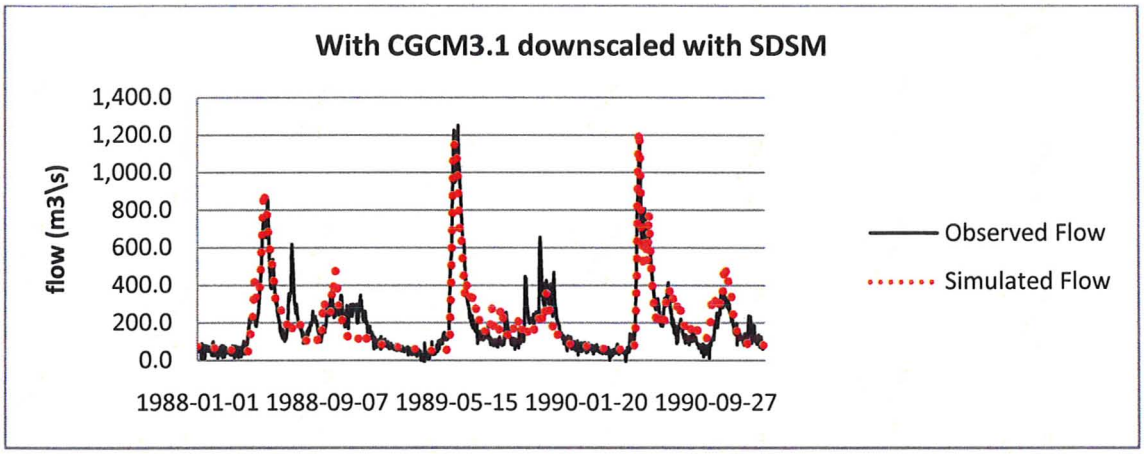
With CGCM3.1 downscaled with SDSM
flow (m3\s)
1,400.0
1,200.0
1,000.0
800.0
600.0
400.0
200.0
0.0
1988-01-01 1988-09-07 1989-05-15 1990-01-20 1990-09-27
Observed Flow
Simulated Flow

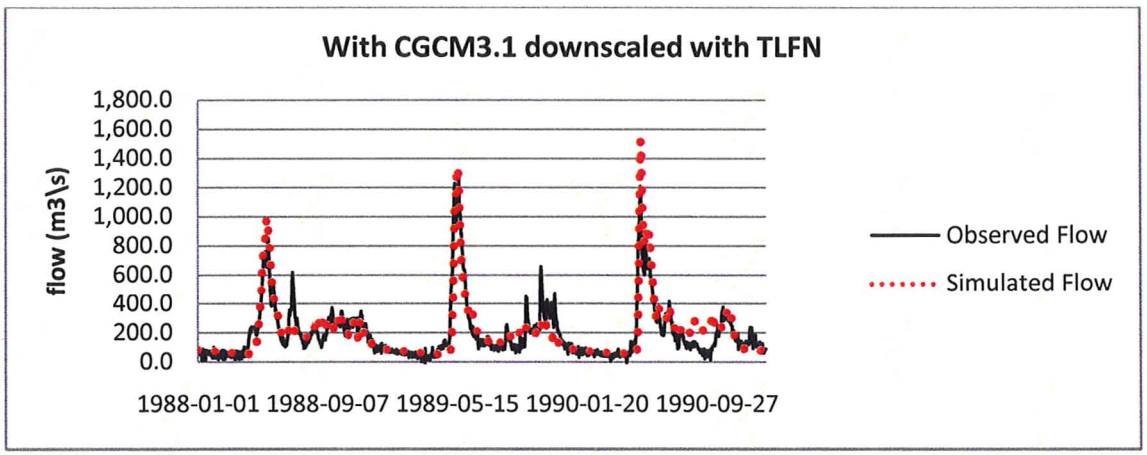
With CGCM3.1 downscaled with TLFN
flow (m3\s)
1,800.0
1,600.0
1,400.0
1,200.0
1,000.0
800.0
600.0
400.0
200.0
0.0
1988-01-01 1988-09-07 1989-05-15 1990-01-20 1990-09-27
Observed Flow
Simulated Flow

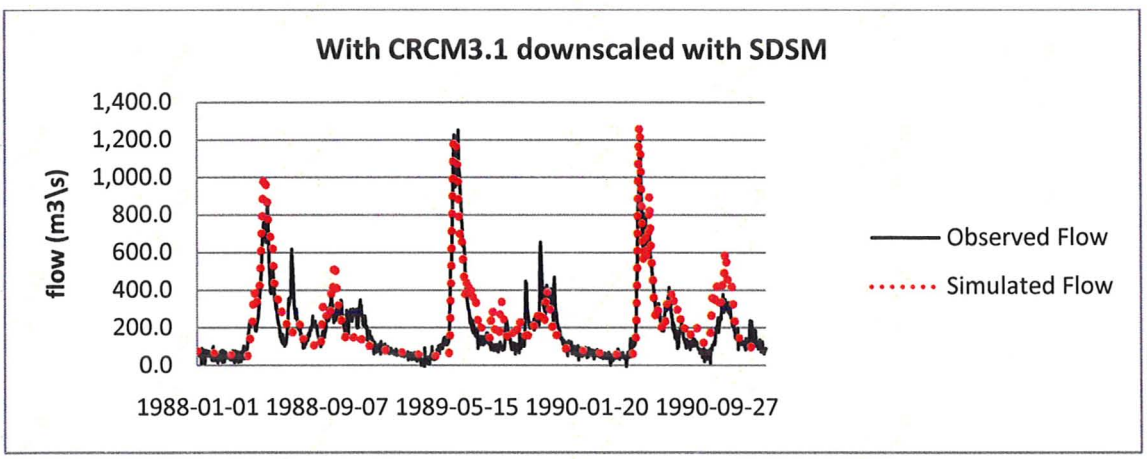
With CRCM3.1 downscaled with SDSM
flow (m3\s)
1,400.0
1,200.0
1,000.0
800.0
600.0
400.0
200.0
0.0
1988-01-01 1988-09-07 1989-05-15 1990-01-20 1990-09-27
Observed Flow
Simulated Flow

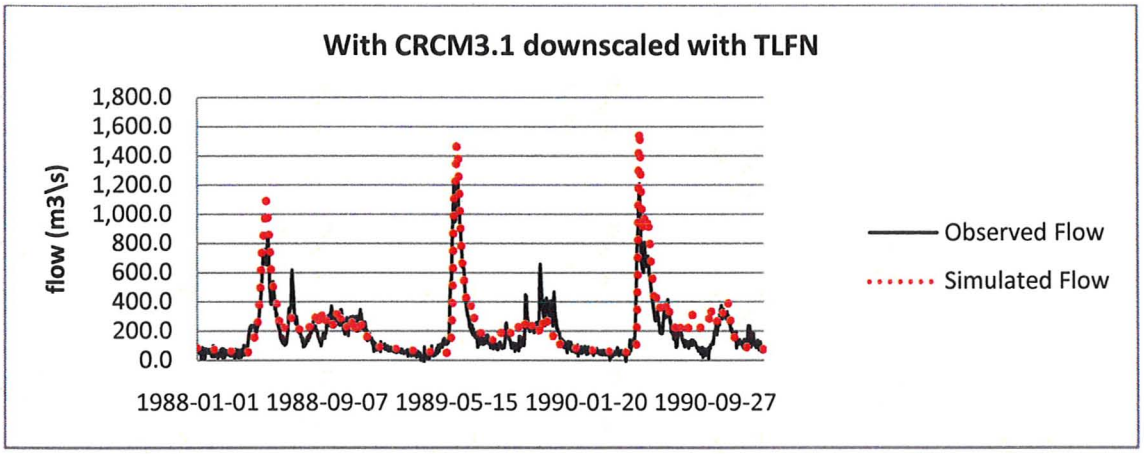

Figure 38: HBV Simulation results for the Chute-du-diable reservoir inflow

6.3 HBV Simulation Results for the Mistassibi River

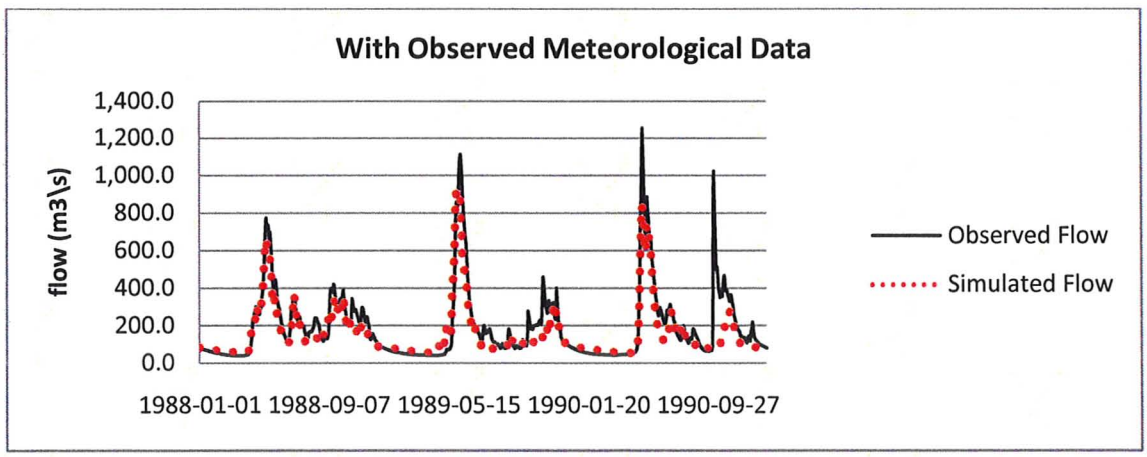

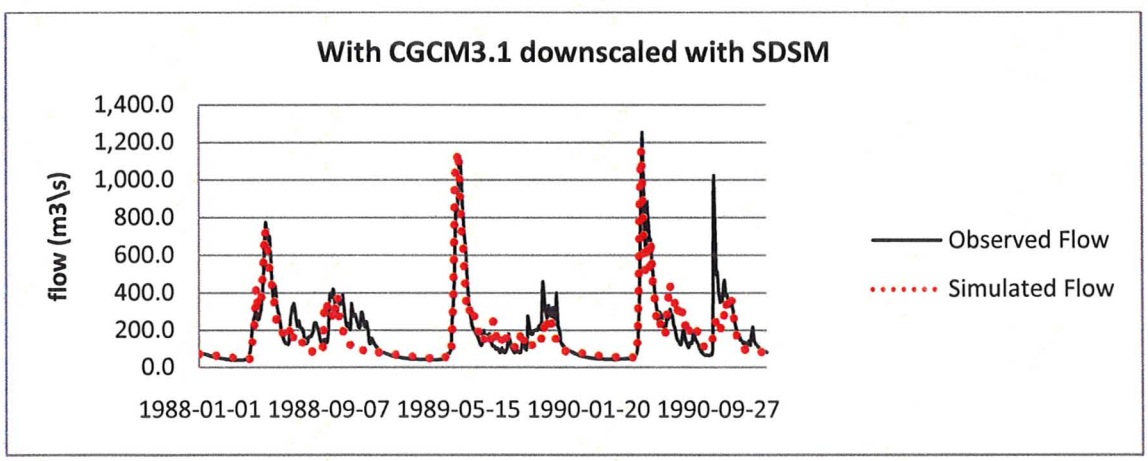

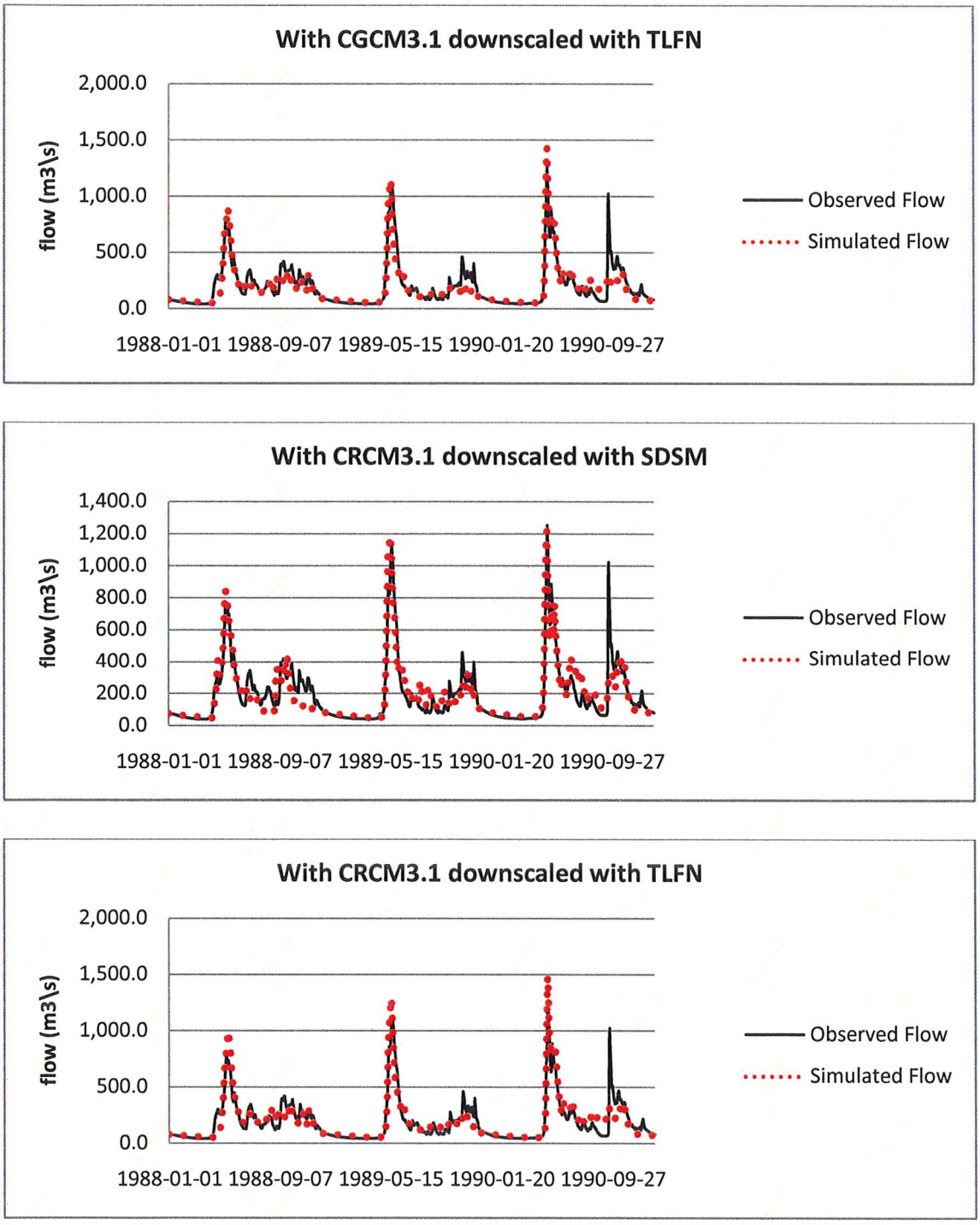

Figure 39: HBV simulation results for the Mistassibi River flow

Figure 38 and Figure 39 provide the HBV simulation results for the Chute-du-diable reservoir and Mistassibi River. The model is calibrated for the years 1961-1980

and validated for 1981-1990 period. The plots provide the simulation results for the last three years for clarity of visualization. As can be seen, each Figure contains 5 plots; the first represents the HBV model setup with observed meteorological data and the remainder plots represent the model setup with the downscaled results as input. The figures reveal that regardless of the climate data type (CRCM4.2 or CGCM3.1) or the downscaling method (SDSM or TLFN) accurate flow simulation results are produced. The overall inflow at the Chute-du-Diable reservoir and river flow in the Mistassibi River are well simulated as the magnitude of flow peaks are generally captured, the base flow values are close and the time and shape of the flow recession curves are almost identical to the observed flow. The scatter plots in Figures B1-B10 in the Appendix also confirm that for the entire validation period, regardless of the input data, overall good performance is achieved.

Table 6 provides the RMSE, r and nash values for inflow simulation at the Chute-du-Diable reservoir with the different input data cases. For the Chute-du-diable inflow simulation with observed data as input, a 0.85 r and 0.70 Nash value is obtained. When the model input is substituted with CRCM4.2 downscaled with SDSM or TLFN an r value of 0.84-0.87 and Nash of 0.68-0.73 are obtained. When the model input is substituted with the downscaled CGCM3.1 data a 0.84-0.87 r value and 0.7-0.75 Nash is obtained. The results reveal that regardless of the climate data type, the TLFN downscaling method provides slightly stronger modeling results than the SDSM downscaling method.

Similarly, Table 6 provides the RMSE, r and Nash values for flow simulation at the Mistassibi River with the different input data cases. For Mistassibi River flow simulation with observed data as input, a 0.84 r and 0.69 Nash is obtained. When the model input is substituted with CRCM4.2 downscaled with SDSM or TLFN an r value of 0.85-0.90 and a Nash of 0.71-0.81 are obtained. When the model input is substituted with the downscaled CGCM3.1 data a 0.84-0.90 r value and 0.69-0.79 Nash is obtained.

Thus, the downscaled CGCM3.1 data once again, the TLFN downscaling procedure provides slightly more accurate Mistassibi River flow simulation results.

	CRCM4.2								
	OBS			SDSM			TLFN		
	RMSE	r	Nash	RMSE	r	Nash	RMSE	r	Nash
Chute-Du-Diable Reservoir	115.95	0.85	0.70	119.73	0.84	0.68	110.61	0.87	0.73
Mistassibi River	109.85	0.84	0.69	106.71	0.85	0.71	86.19	0.90	0.81

	CGCM3.1								
	OBS			SDSM			TLFN		
	RMSE	r	Nash	RMSE	r	Nash	RMSE	r	Nash
Chute-Du-Diable Reservoir	115.95	0.85	0.70	116.52	0.84	0.70	105.39	0.87	0.75
Mistassibi River	109.85	0.84	0.69	109.50	0.84	0.69	89.16	0.90	0.79

Table 5: HBV Model Validation Statistics

6.4 Future Climate Change Flow Simulations

Downscaled meteorological data corresponding to the future 2050s period was input into the HBV modelling system to understand how flow will change in the Chute-du-diable reservoir and Mistassibi River from current conditions. As before, future changes are considered for both climate data types (CRCM4.2 and CGCM3.1) and both downscaling methods (SDSM and TLFN)

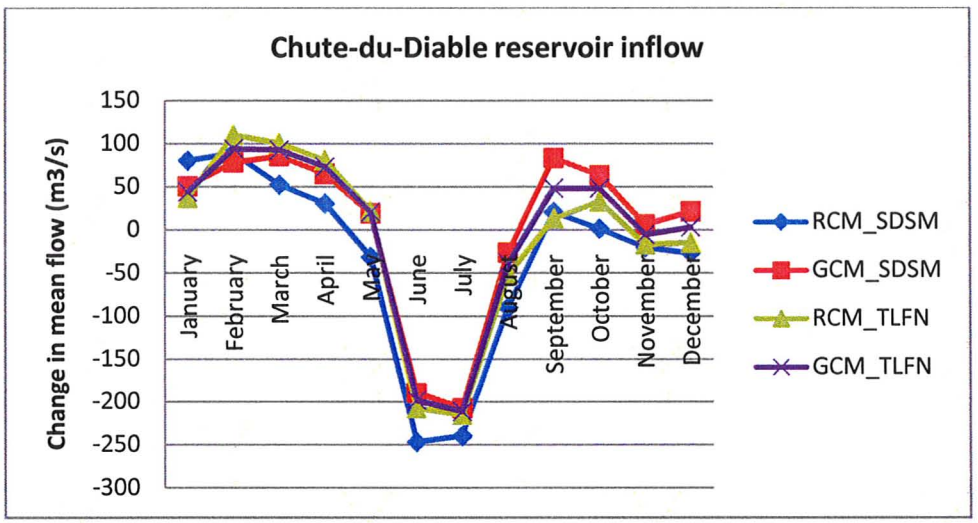

Figure 40: Changes in mean future inflow at Chute-du-Diable reservoir for the 2050s

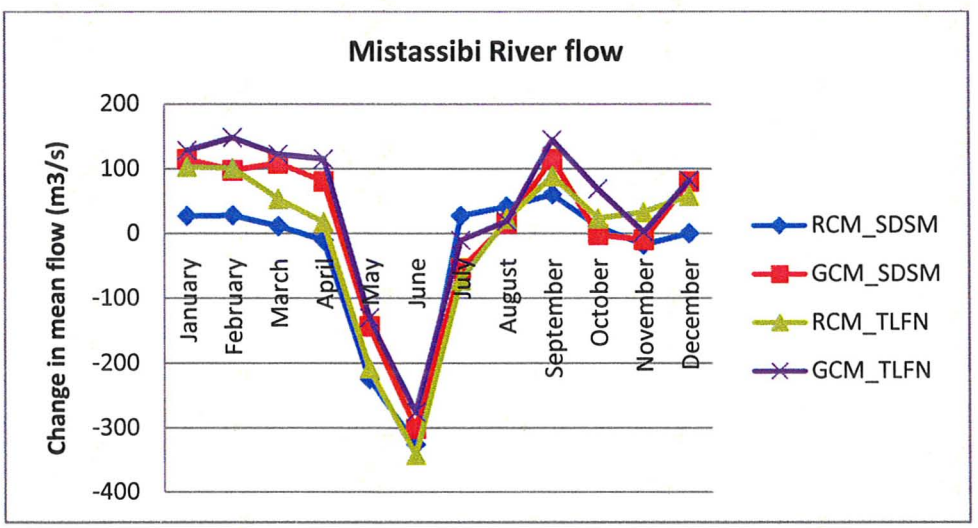

Figure 41: Changes in mean future flow in the Mistassibi River for the 2050s

	% Increase/Decrease in Annual Flow			
	CRCM4.2		CGCM3.1	
	SDSM	TLFN	SDSM	TLFN
Chute-Du-Diable Reservoir	16.90	24.95	28.10	26.52
Mistassibi River	12.36	37.20	58.40	61.74

Table 6: Percentage of Increase/Decrease in annual flow corresponding to the 2050s

	% Increase/Decrease in Seasonal Flow for the Chute-du-diable Reservoir			
	CRCM4.2		CGCM3.1	
	SDSM	TLFN	SDSM	TLFN
Winter	27.36	29.48	34.52	32
Spring	15.4	31.28	51.66	56.65
Summer	-57.72	-47.46	-42.31	-44.89
Fall	0.23	5.68	29.35	17.52

Table 7: Percentage of Increase/Decrease in seasonal flow for the 2050s at the Chute-du-Diable Reservoir

	% Increase/Decrease in Seasonal Flow for the Mistassibi River			
	CRCM4.2		CGCM3.1	
	SDSM	TLFN	SDSM	TLFN
Winter	11.12	58.58	70.17	88.32
Spring	-30.04	-10.92	9.75	23.29
Summer	-27.09	-41.91	-36.28	-28.47
Fall	9.16	24.51	17.42	36.67

Table 8: Percentage of Increase/Decrease in seasonal flow for the 2050s in the Mistassibi River

The results in Figure 40 and Figure 41 show the changes in mean inflow for the Chute-du-diable reservoir and the changes in mean flow in the Mistassibi River. The results reveal that regardless of the climate data type (whether CRCM4.2 or CGCM3.1) or the downscaling procedure the overall trends in the change are similar throughout. At both the Mistassibi River and Chute-du-diable reservoir, significant decreases in flow are observed in the summer months with increases throughout the remainder of the seasons. Further at Chute-du-diable the decrease in flow occurs during May-August, whereas at the Mistassibi River the decrease occurs earlier from April-July. This difference may be a result of their geographical location as the Mistassibi River lies further west than the Chute-du-diable reservoir. Overall, the changes in flow, corresponds well with the predicted increase in temperature found for the 2050s future period in the downscaling experiments. Specifically, higher temperatures in the winter months will have an associated earlier beginning of snow melting which would increase the runoff and bring forth larger flows in the spring. Further, the decrease in flow during the summer months can also be explained partly by the warmer summer temperatures. Higher temperatures during the summer will mean more water will be lost to Evapotranspiration and thus less water will be available to contribute to runoff. Additionally, the downscaling experiments revealed an increase in annual precipitation will occur for the 2050's future period, this can also help explain the increases in flow that occur throughout the remainder of the year.

For the Chute-du-diable reservoir, Table 6 reveals that the CRCM4.2 downscaled with SDSM shows a 17% increase in mean annual flow, whereas the CGCM3.1 downscaled with SDSM shows a 28% increase in mean flow. This trend is similar with the TLFN downscaling procedure and as such the CGCM3.1 downscaled results reveal a larger increase in inflow at the Chute-du-diable reservoir than the CRCM4.2 downscaled results. In terms of comparing the two downscaling methods, TLFN shows larger increases in mean flow with the CRCM4.2 data and SDSM shows larger changes with the CGCM3.1 data. Table 8 shows the seasonal increase/decrease in reservoir inflows. As shown, regardless of the climate data or the downscaling method, significant decreases in

mean flow occur during the summer seasons and smaller changes occur during the fall. Further in all seasons, the CGCM3.1 reveals larger changes in mean flow than the CRCM4.2.

For the Mistassibi River we see once again the CGCM3.1 data shows larger increases in mean annual river flow than the CRCM4.2 data. This time however, the difference between the CRCM4.2 and CGCM3.1 results is much larger as shown in Table 7. For example, the CRCM4.2 data downscaled with TLFN reveals a 37% increase in mean annual river flow, whereas the downscaled CGCM3.1 with TLFN reveals a 62% increase in mean flow. Table 8 shows that the CRCM4.2 model suggests a reduction in flow for both the spring and summer seasons, whereas the CGCM3.1 model shows a reduction in flow for only the summer. In comparing the two downscaling methods, regardless of the climate data type, TLFN once again produce larger changes in flow than SDSM.

Chapter 7: Conclusions

To date, climate change impact studies have generally involved the downscaling of large-scale atmospheric predictors with the result then being input into a hydrological model to see how flow in a river/basin will change under various future climate change scenarios. Although many studies have been completed using large scale global climate model (GCM) data, few studies have shown the strength of regional climate models (RCM). In this work, a comparison between the effectiveness of using CRCM4.2 vs. CGCM3.1 data in a climate change impact study (climate forcing under the SRES A2 climate scenario) is considered. The study area is the Chute-du-Diable sub-basin located within the Saguenay-Lac-Saint-Jean Watershed in Quebec (Canada). Downscaled results are compared with observed meteorological data for the years 1961-1990 at the Chute-des-Passes (CDP) and Chute-du-Diable (CDD) weather stations; and flow is simulated for the Mistassibi River and the Chute-du-Diable reservoir. A multivariate regression technique (SDSM) and a dynamic artificial neural network model (Time lagged feed-forward neural network (TLFN)) are used for downscaling the CRCM4.2 and CGCM3.1 data, and the HBV2005 hydrological modeling system is used for simulating flows in the watershed.

For the current period (1961-1990), downscaling results reveal that downscaled CRCM4.2 is closer to observed meteorological data at both CDD and CDP stations than downscaled CGCM3.1 is. More importantly however, the downscaling results reveal that regardless of the predictand, the downscaled CRCM4.2 results are much closer to the observed data than the raw CRCM4.2 data is. Statistical results reveal that regardless of the climate model, TLFN is best for downscaling temperature and SDSM is best for downscaling precipitation. The Levene Test and Wilicoxon Rank-Sum Test were carried out to determine the uncertainty of the downscaling results. The results revealed that regardless of the climate model, or the downscaling method employed, overall both the mean and variance was captured quite well. With respect to the future "business as usual climate scenario", regardless of the climate model or the station or the downscaling

method, a 1 to 3˚C increase in annual mean maximum temperature and a 1 to 4˚C increase in annual mean minimum temperature are predicted for the 2050s future period. In the case for precipitation, the CRCM4.2 model shows increases in annual precipitation will vary from 1 to 7% in the 2050s regardless of the downscaling method used. The CGCM3.1 model on the other hand, shows increases in annual precipitation ranging from 15 to 23%. Further, whether simulating future mean precipitation, mean maximum temperature or mean minimum temperature, the CGCM3.1 model consistently shows a larger increasing trend than the CRCM4.2 model.

The hydrographs and statistical results of the hydrologic model HBV shows that good flow simulation results were obtained for the Chute-du-diable Reservoir inflows and Mistassibi River flows - Nash values range from 0.69-0.81 and correlation coefficient values range from 0.84-0.90. Simulations of future river flows and reservoir inflows reveal that significant seasonal changes in mean flow will occur as a result of the warming trend and the increased precipitation predicted in the downscaling experiments for the 2050s. For the Chute-du-Diable reservoir, the results show that for TLFN and SDSM, the CRCM4.2 and CGCM3.1 model shows decreases in mean annual flow during the summer season and increases during the remaining seasons for the 2050s. For the Mistassibi River, the CRCM4.2 model shows that decreases in mean flow will occur during the spring and summer seasons with increases in flow during the remaining two seasons. The CGCM3.1 model consistently shows larger increases in mean flow for the 2050s when compared with the CRCM4.2 model, but it also indicates significant decreases in the summer season regardless of the downscaling method used. Further in all cases, the TLFN downscaling procedure shows larger changes in mean flow than SDSM.

Incorporation of downscaled RCM data in a hydrologic impact study can help to provide a broader picture for decision making, as the GCM consistently gives large estimates of changes for the 2050s, whereas the RCM consistently gives smaller estimates.

References

Arora, V.K., 2002. Studying Climate Change Impact on Rivers within the Framework of Global Climate Models, Newsletter of the Canadian Water Resources Association.

Arora V.K., 2001. The potential impact of climate change on the Mackenzie River basin hydrology, CWRA BC Branch 2001 Conference – Changing Water Environments: Research and Practice.

American Society of Civil Engineers, 2000a. Artificial neural networks in hydrology, 1: Preliminary concepts, Journal of Hydrologic Engineering, 5-2, 115–123.

American Society of Civil Engineers, 2000b, Artificial neural networks in hydrology, 2: Hydrology applications, Journal of Hydrologic Engineering, 5-2, 124–137.

Barrow EM, Hulme M, Semenov M., 1996. Effect of using different methods in the construction of climate change scenarios: examples for Europe, Climate Research, **7**, 195–211.

Bergeron G., Laprise L., and Caya D., 1994: Formulation of the Mesoscale Compressible Community (MC2) Model. Internal Report from Cooperative Centre for Research in Mesometeorology, Montréal, Canada, 165 pp. [Available from D. Paquin Ouranos 550 Sherbrooke West Montreal H3A 1B9]

Bergstrom S, Forsman A., 1973. Development of a conceptual deterministic rainfall–runoff model, Nordic Hydrology 4, 147–170.

Brandt M. 1990. Simulation of runoff and nitrate transport from mixed basins in Sweden, Nordic Hydrology, 21, 13–34.

Brissette F., Leconte R., Minville M. and Roy R., 2006. Can we adequately quantify the increase/decrease in flooding due to climate change?, EIC Climate Change Technology,1-6.

Canadian Centre for Climate Modeling and Analysis. Environment Canada. http://www.cccma.ec.gc.ca/eng_index.shtml. Date Accessed: 2007-2009.

Canadian Climate Impacts and Scenarios. Canadian Institute for Climate Studies. http://www.cics.uvic.ca/scenarios/index.cgi Date Accessed: 2007-2009.

Carlaw S., 2000. Soil Moisture Accounting in Distributed Hydrologic Modelling: A Thesis. University of Waterloo, Waterloo Ontario.

Caya D., and R. Laprise, 1999. A Semi-Implicit Semi-Lagrangian Regional Climate Model: The Canadian RCM, Mon. Wea. Rev., 127, 341-362.

Cranmer AJ, Kouwen N., Mousavi S.F. 2001. Proving WATFLOOD: modeling the nonlinearities of hydrologic response to storm intensities, Canadian Journal of Civil Engineering, 28, 837-855.

Coulibaly P., Dibike Y.B, Anctil F., 2005. Downscaling Precipitation and Temperature with Temporal Neural Networks, Journal of Hydrometeorology, 6, 483-496.

Coulibaly, P. and Dibike, Y.B., 2004. Downscaling of Global Climate Model Outputs for Flood Frequency Analysis in the Saguenay River System. Project Report prepared for the Canadian Climate Change Action Fund, Environment Canada, 84p.

Coulibaly P., Anctil F., Bobee B., 2001. Multivariate Reservoir Inflow Forecasting using Temporal Neural Networks, Journal of Hydrologic Engineering, 6(5), 367-376.

Cubash U, von Storch H, Waszkewitz J, Zorita E. 1996. Estimates of climate change in Southern Europe derived from dynamical climate model output. Climate Research, **7**, 129–149.

Diaz-Nieto J, Wilby R L, 2005. A comparison of statistical downscaling and climate change factor methods: impacts on low flows in the River Thames, United Kingdom, Climate Change, 69, 245 – 268.

Dibike Y. B. and Coulibaly P. (2005) Hydrologic Impact of Climate Change in the Saguenay Watershed: Comparison of Downscaling Methods and Hydrologic Models, *Journal of Hydrology*, 307, 145-163.

Dibike Y.B. and Coulibaly P., 2006. Temporal neural networks for downscaling climate variability and extremes, Neural Networks, 19, 135-144.

Dibike Y.B. and Coulibaly P., 2007.Validation of hydrological models for climate scenario simulation: the case of the Saguenay watershed in Quebec, Hydrological Processes, 21, 3123-3135.

Easterling D. R., 1999. Development of regional climate scenarios using a downscaling approach, Climatic Change, 41, 615–634.

Flato G.M. and G.J. Boer, 2001. Warming Asymmetry in Climate Change Simulations, Geophys. Res. Lett., 28, 195-198.

Giorgi F., Mearns L.O.,1991. Approaches to the simulation of regional climate change - A review, Reviews of Geophysics 29, 191–216.

Grotch S.L. and MacCracken M.C. 1991. The use of general circulation models to predict regional climate change. Journal of Climate 4, 286–303.

Haykin, S.,1999. Neural Networks – A Comprehensive Foundation (2nd Edition). Prentice Hall. New Jersey.

Hay, L.E. and Clark M.P, 2003.Use of statistically and dynamically downscaled atmospheric model output for hydrologic simulations in three mountainous basins in the western United States, Journal of Hydrology, 282, 56-75.

Haylock M. R., Cawley G. C., Harpham C, Wilby R. L., Goodess C. M., 2006. Downscaling heavy precipitation over the United Kingdom: A comparison of dynamical and statistical methods and their future scenarios, International Journal of Climatology, 26, 1397-1415.

Hewitson BC. and Crane RG. 1996. Climate downscaling: techniques and application, Climate Research, 7, 85–95.

Intergovernmental Panel on Climate Change, Fourth Assessment Report: Climate Change 2007. Core Writing Team, Pachauri, R.K. and Reisinger, A. 104 pp.

Jyrkama M. and Sykes J.F., 2007. The impact of climate change on spatially varying groundwater recharge in the Grand River watershed (Ontario), Journal of Hydrology,338,237-250.

Karl T.R., Wang W.C., Schlesinger M.E., Knight R.W., Portman D., 1990. A method of relating General Circulation Model simulated climate to the observed local climate. Part I: seasonal statistics, Journal of Climate, 3, 1053–1079.

Kattenberg A., Giorgi F., Grassl H., Meehl G.A., Mitchell J.F.B., Stouffer R.J., Tokioka T., Weaver A.J. and Wigley T.M.L. 1996. Climate models—projections of the future' in Houghton, J.T., Meiro Filho, L.G., Callendar, B.A., Harris, N., Kattenberg, A. and Maskell, K. (eds), The Science of Climate Change. The Second Assessment of the Intergo6ernmental Panel on Climate Change, Cambridge University Press, Cambridge, 285–357.

Khan M.S., Coulibaly P., Dibike,Y., 2006a. Uncertainty Analysis of Statistical Downscaling Methods, Journal of Hydrology, 319, 357-382.

Khan M.S., Coulibaly P., Dibike Y., 2006b. Uncertainty Analysis of Statistical Downscaling Methods using Canadian Global Climate Model Predictors, Hydrological Processes, 20, 3085-3104.

Kim S.J., G.M. Flato, G.J. Boer and N.A. McFarlane, 2002: A coupled climate model simulation of the Last Glacial Maximum, Part 1: transient multi-decadal response. Climate Dynamics, 19, 515-537.

Kim S.-J., G.M. Flato, G.J. Boer, 2003: A coupled climate model simulation of the Last Glacial Maximum, Part 2: approach to equilibrium Climate Dynamics, 20, 635-661.

Kouwen N., 2009. WATFLOOD/SPL9 Hydrological Model & Flood Forecasting System Manual. Department of Civil Engineering, University of Waterloo. Waterloo Ontario, Canada.

Laprise R., Caya D., Bergeron G. and Giguère M., 1997: The formulation of André Robert MC2 (Mesoscale Compressible Community) model. Atmos.-Ocean, 35(1), 195-220.

Levene H. 1960. *Contributions to Probability and Statistics*. Stanford University Press.

Liden R, Harlin J. 2000. Analysis of conceptual rainfall–runoff modelling performance in different climates. Journal of Hydrology 238: 231–247.

Lindstrom G, Johansson B, Persson M, Gardelin M, Bergstrom S. 1997. Development and test of the distributed HBV-96 hydrological model, Journal of Hydrology 201: 272–288.

Liu, X., 2007. Downscaling Meteorological Predictions for Short Term Hydrologic Forecasting. McMaster University. Thesis.

Mareiul A., Leconte R., Brissette F. and Minville M., Impacts of climate change on the frequency and severity of floods in the Chateauguay River basin, Canada. Canadian Journal of Civil Engineering, Vol. 34 2007 1048-1060

McFarlane, N.A., J. F. Scinocca, M. Lazare, R. Harvey, D. Verseghy, and J. Li, 2005. The CCCma third generation atmospheric general circulation model. CCCma Internal Rep., 25.

Mearns LO, Bogardi I, Giorgi F, Matyasovzky I, Palecki M. 1999. Comparison of climate change scenarios generated from regional climate model experiments and statistical downscaling, Journal of Geophysical Research 104(D6): 6603–6621

Minville M., Brissette F., Leconte R., 2008. Uncertainty of the impact of climate change on the hydrology of a Nordic watershed. Journal of Hydrology, 358, 70-83.

Murphy, J.M. (2000), Predictions of climate change over Europe using statistical and dynamical downscaling techniques, Int. J. Climatol., 20, 489– 501

Music B., and Caya D, 2007: Evaluation of the Hydrological Cycle over the Mississippi River Basin as Simulated by the Canadian Regional Climate Model (CRCM). J. Hydromet., 8(5), 969-988.

Osborn, T.J. and Hulme, M. 1997. Development of a relationship between station and grid-box rainday frequencies for climate model evaluation, Journal of Climatology, 10, 1885–1908.

Prudhomme C., Reynard N. and Crooks S., 2002. Downscaling of global climate models for flood frequency analysis: where are we now? Hydrological processes. 16, 1137-1150.

Prudhomme C. and Davies H., 2009. Assessing uncertainties in climate change impact analyses on the river flow regimes in the UK. Part 1: baseline climate, Climate Change, 93, 177-195

Salathe E. P., 2005. Downscaling Simulations of Future Global Climate with application to hydrologic modeling, International Journal of Climatology, 25, 419-436.

Schoof, J.T and Pryor, S.C., 2001. Downscaling temperature and precipitation: A comparison of regression-based method and artificial neural networks, International Journal of Climatology, 21, 773-790.

Scinocca, J. F., N. A. McFarlane, M. Lazare, J. Li, and D. Plummer, 2008: The CCCma third generation AGCM and its extension into the middle atmosphere. Atmos. Chem. and Phys., submitted.

Simonovic S. and Lanhai L., 2004. Sensitivity of the Red River Basin Flood Protection System to Climate Variability and Change. Water Resources Management 18, 89-110.

Singh V.P., ASCE F., and Woolhiser D.A., 2002. Mathematical Modeling of Watershed Hydrology, Journal of Hydrologic Engineering, 7 (4), 270-292.

Tolika K., Anagnostopoulou C., Maheras P., Vafiadis M., 2008. Simulation of future changes in extreme rainfall and temperature conditions over the Greek area: a comparison of two statistical downscaling approaches. Global and Planetary Change, 63, 132-51.

Tripathi, S, Srinivas, V.V., Nanjundiah, R. S., 2006. Downscaling of precipitation for climate change scenarios: A support vector machine approach Journal of Hydrology, 330, 621-640.

Von Storch H., Zorita E. and Cubash U. 1993. Downscaling of global climate change
estimates to regional scales: an application to Iberian rainfall in wintertime, Journal of Climate
6, 1161–71.

Von Storch, H., Hewitson, B., Mearns, L., 2000. Review of empirical downscaling techniques. In: Regional Climate Development under Global Warming. General Technical Report No. 4. Conference Proceedings, Torbjornrud, Norway.

Wilby R.L., Wigley T.M.L., 1997. Downscaling General Circulation Model output: a review of methods and limitations. Progress in Physical Geography 21, 530–548.

Wilby R.L., 1994. Stochastic weather type simulation for regional climate change impact assessment, Water Resources Research, 30, 3395-3403.

Wilby R.L., 1997. Non-stationarity in daily precipitation series: implications for GCM downscaling using atmospheric circulation indices, International Journal of Climatology, 17,
439-454.

Wilby R.L. and Wigley T.M.L., 1997. Downscaling General Circulation Mode[output: a review of methods and limitations, Progress in Physical Geography, 21,530 548.

Wilby R.L., Charles S.P., Zorita E., Timbal B., Whetton P. and Meanrns LO, 2004. Guidelines for use of climate scenarios developed from statistical downscaling methods. 27.

Wilby R.L, Hay L.E and Leavesley G.H.,1999. A comparison of downscaled and raw GCM output: implications for climate change scenarios in the San Juan River basin, Colorado, Journal of Hydrology, 225, 67-91.

Wilby RL. and Dawson CW., 2007. SDSM–a decision support tool for the assessment of regional climate change impacts. Software Manual.

Wilby RL., Dawson C.W. and Barrow E.M., 2002. SDSM- a decision support tool for the assessment of regional climate change impacts, Environmental Modeling and Software, 17, 145-157.

Wilby R. L., Hay L, E., Gutowski Jr, W. J., Arritt, R. W., Takle E. S., Pan, Z., Leavesley G, H. and Clark M. P., 1999. Hydrological responses to dynamically and statistically downscaled climate model output, Geophysical Research Letters, 27, 1199-1202

Winkler, J.A., Palutikof, J.P., Andresen, J.A. and Goodess, C.M., 1997. The simulation of daily temperature series from GCM output. Part II: sensitivity analysis of an empirical transfer function methodology, Journal of Climate 10, 2514–2532.

Xu CY. 1999. From GCMs to river flow: a review of downscaling methods and hydrologic modelling approaches, Progress in Physical Geography 23(2), 229–249.

APPENDIX A

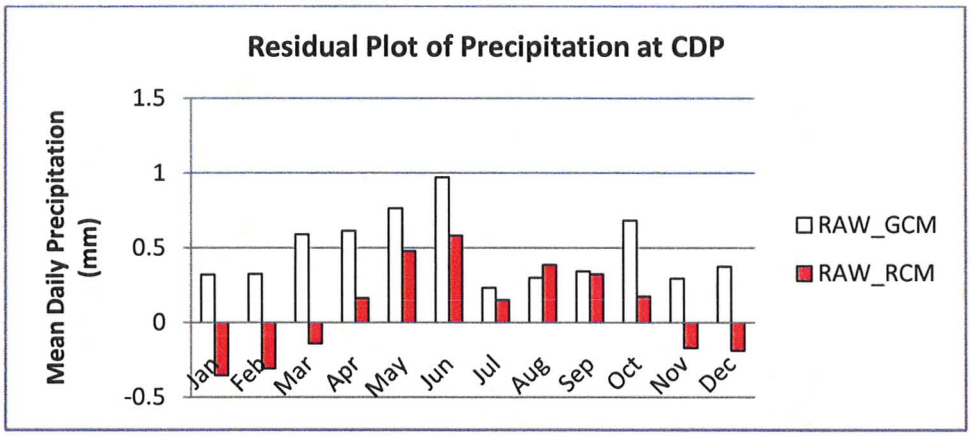

Figure A1: Residual plot of mean precipitation at CDP: Raw GCM & Raw RCM output

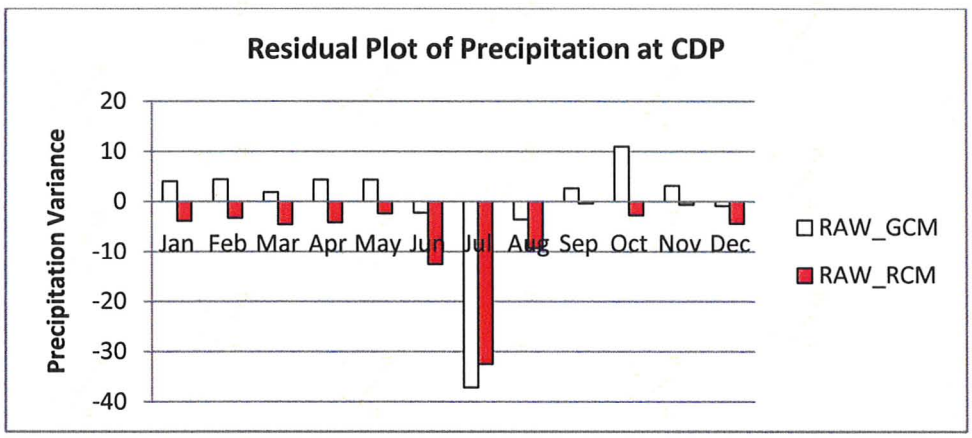

Figure A2: Residual plot of precipitation variability at CDP: Raw GCM & Raw RCM

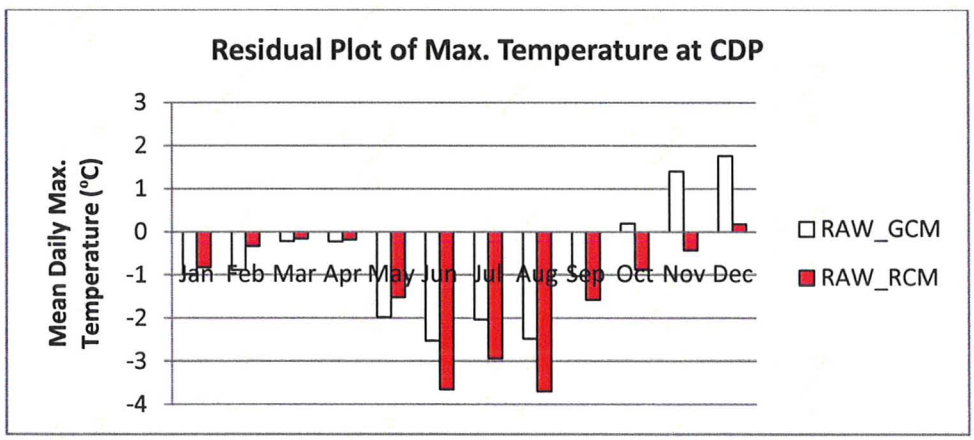

Figure A3: Residual plot of mean max. temp. at CDP: Raw GCM & Raw RCM output

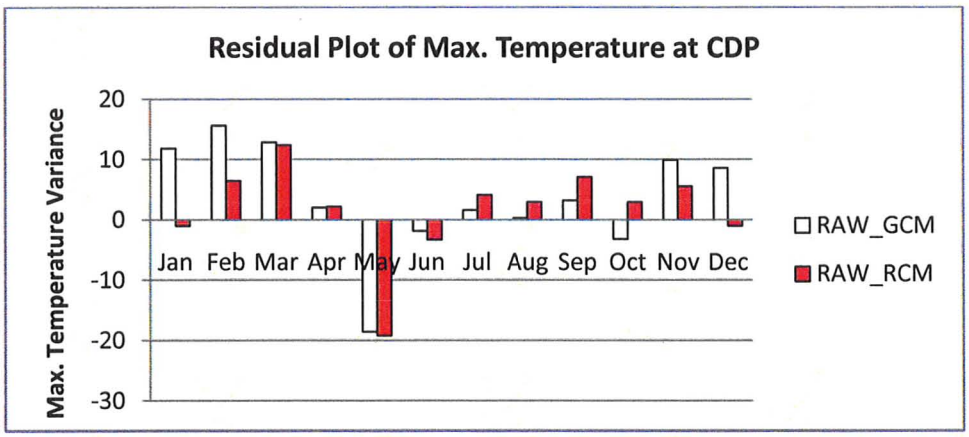

Figure A4: Residual plot of max. temp variability at CDP: Raw GCM & Raw RCM output

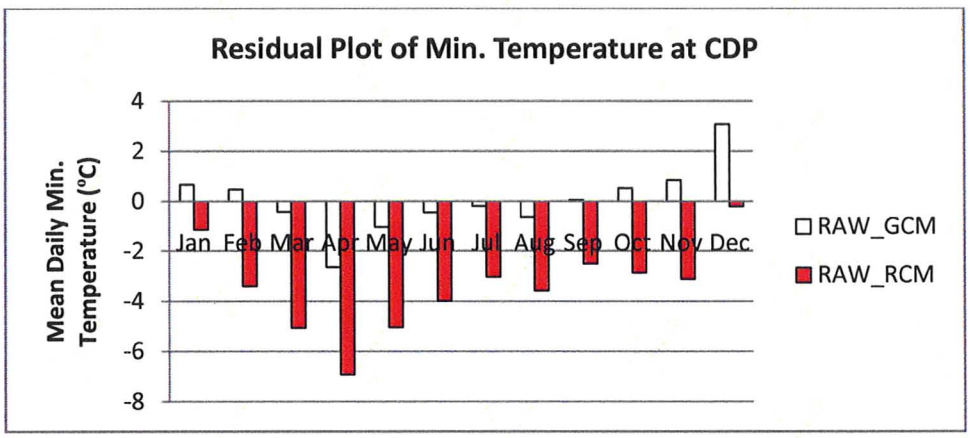

Figure A5: Residual plot of mean min. temp. at CDP: Raw GCM & Raw RCM output

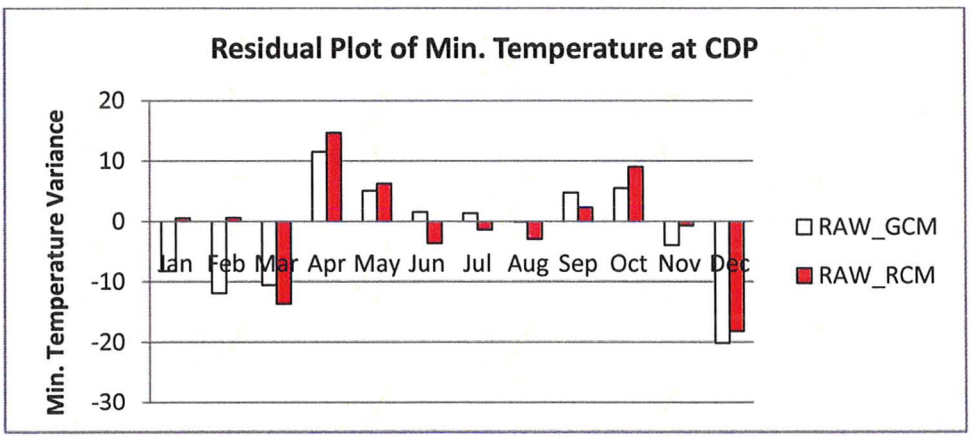

Figure A6: Residual plot of min. temp variability at CDP: Raw GCM & Raw RCM output

SDSM Predictors					
Precipitation		Max. Temperature		Min. Temperature	
CRCM4.2	CGCM3.1	CRCM4.2	CGCM3.1	CRCM4.2	CGCM3.1
hsf	hfss	hsf	hfss	hfs	hfss
pcp	Pr	pcp	pr	pcp	pr
phi850	Psl	pmsl	psl	phi850	psl
pmsl	tas	stmxd	tas	pmsl	tas
sq	uas	su	uas	stmnd	uas
stmnd	vas	sv	vas	su	vas
stmxd		swmx		sv	
Su				swmxx	
Sv					

Table A1: GCM and RCM predictors used in SDSM downscaling

TLFN Predictors					
Precipitation		Max. Temperature		Min. Temperature	
CRCM4.2	CGCM3.1	CRCM4.2	CGCM3.1	CRCM4.2	CGCM3.1
Hsf	evspsbl	Hsf	Hfss	hsf	prsn
Pcp	Hfls	Pcp	Rlds	pcp	ps
phi850	hus_850	phi850	Rsds	phi850	psl
Pmsl	Pr	Pmsl	ta_850	pmsl	ta_850
Sq	Psl	Sq	Vas	sq	vas
Stmnd	Rlus	stmnd	zg_500	stmnd	zg_500
Stmxd	Tas	stmxd	Rlus	stmxd	
Su	Uas	Su	Ps	su	
Sv	Vas	Sv		sv	
Swmx	zg_850	Swmx		swmx	

Table A2: GCM and RCM predictors used in TLFN downscaling

	CRCM4.2 Predictors
hsf	surface upward sensible heat flux (W/m2)
pcp	Precipitation(mm)
phi850	geopotential height at 850 hPa (m2/s2)
pmsl	mean sea level pressure (Pa)
sq	screen specific humidity at 2m (kg/kg)
stmnd	minimum temperature ©
stmxd	maxmimum temperature ©
su	eastward surface wind (m/s)
sv	northward surface wind (m/s)
swmx	mean amplitude of sustained wind at 10 m (m/s)
	CGCM3.1 Predictors
evspsbl	surface water evaporation flux (kg m-2 s-1)
hfls	surface upward latent heat flux (W m-2)
hus_850	specific humidity at 850 m(dimensionless fraction)
pr	precipitation flux (kg m-2 s-1)
psl	air pressure at sea level (Pa)
rlus	surface upwelling longwave flux in the air (W m-2)
tas	near surface daily mean temperature (K)
uas	near-surface eastward wind (m s-1)
vas	near-surface northward wind (m s-1)
zg_850	geopotential height at 850 (m)
hfss	surface upward sensible heat flux (W m-2)
rlus	surface upwelling longwave flux in the air (W m-2)
rlus	surface upwelling longwave flux in the air (W m-2)
rlds	surface downwelling longwave flux in the air (W m-2)
rsds	surface downwelling shortwave flux in the air (W m-2)
ps	surface air pressure (Pa)
zg_500	geopotential height at 500 (m)
ta_850	mean air temperature at 850 m (K)

Table A3: Description of CRCM4.2 and CGCM3.1 predictors.

Figure A7 shows an example of the correlation matrix produced in SDSM and the bar plot produced in TLFN during the sensitivity analysis procedure to determine the best predictors for downscaling. The case for downscaling precipitation at station CDD with GCM data is shown here. In SDSM the correlation matrix helps investigate the inter-variable correlations and the partial correlations identify which predictors have the

strongest association with the predictand. In TLFN the sensitivity about the mean of the predictand and predictors is carried out.

CC Closes this window

Analysis Period: 01/01/1961 - 31/12/1990 (Annual)

Missing values: 0
Missing rows: 0
Values less than or equal to threshold: 5173

		1	2	3	4	5	6	7
1	obs_cd_precip.dat	1	0.044	0.004	0.009	0.111	0.000	0.001
2	gcm3hfssxx.dat	0.044	1	-0.340	0.085	0.222	0.153	-0.419
3	gcm3prxx.dat	0.004	-0.340	1	-0.202	0.183	-0.275	0.198
4	gcm3pslxx.dat	0.009	0.085	-0.202	1	-0.207	-0.313	-0.006
5	gcm3tasxx.dat	0.111	0.222	0.183	-0.207	1	0.053	0.196
6	gcm3uasxx.dat	0.000	0.153	-0.275	-0.313	0.053	1	-0.122
7	gcm3vasxx.dat	0.001	-0.419	0.198	-0.006	0.196	-0.122	1

PARTIAL CORRELATIONS WITH obs_cd_precip.dat

	Partial r	P value
gcm3hfssxx.dat	0.002	0.5559
gcm3prxx.dat	-0.007	0.4929
gcm3pslxx.dat	0.028	0.0556
gcm3tasxx.dat	0.106	0.0000
gcm3uasxx.dat	-0.002	0.5595
gcm3vasxx.dat	-0.018	0.2306

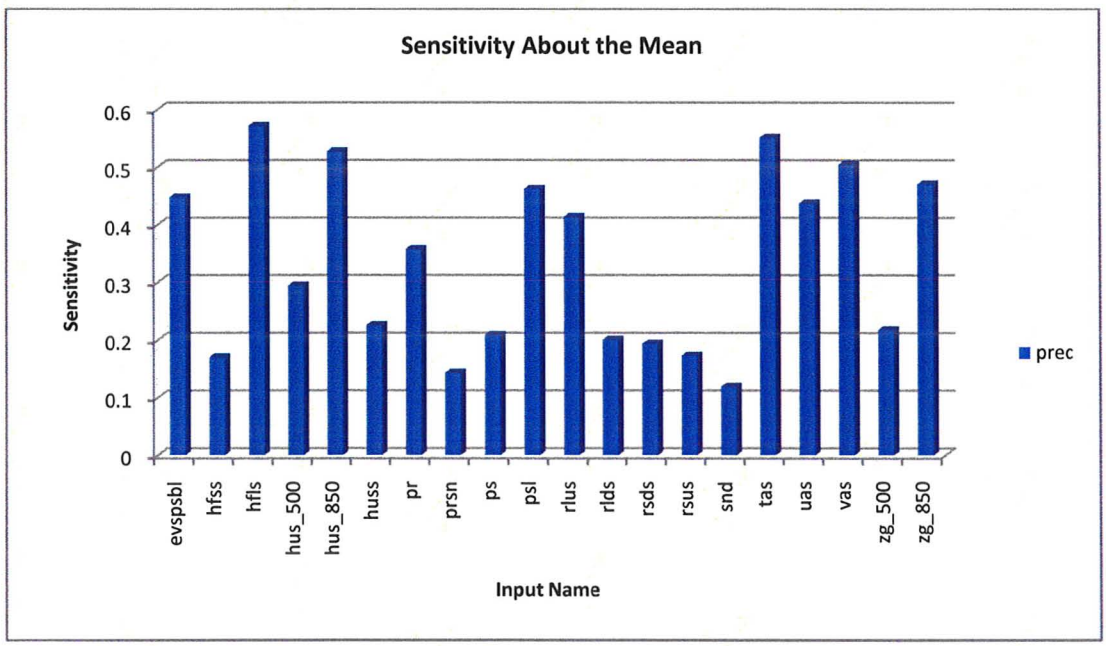

Figure A7: Example of Sensitivity Analysis results for SDSM and TLFN downscaling

Example of SDSM and TLFN Model Setup

	SDSM	
	RCM	GCM
Prec	Natural log, 13 V.I., 0.8 Bias, Ordinary Simplex	Natural log, 11 V.I.,0.9 Bias, Ordinary Simplex
Tmax	No transformation, 12 V.I. 1 Bias, Ordinary Simplex	No transformation, 12 V.I. 1 Bias, Ordinary Simplex
	TLFN	
	RCM	GCM
Prec	TDNNAxon, 9 PE, delta-bar-delta, 3000 epochs	TDNNAxon, 11 PE, delta-bar-delta, 3000 epochs
Tmax	TDNNAxon, 7 PE, delta-bar-delta, 2000 epochs	TDNNAxon, 9 PE, delta-bar-delta, 2000 epochs

Table A4: SDSM and TLFN model setup for the case of downscaling precipitation at CDD

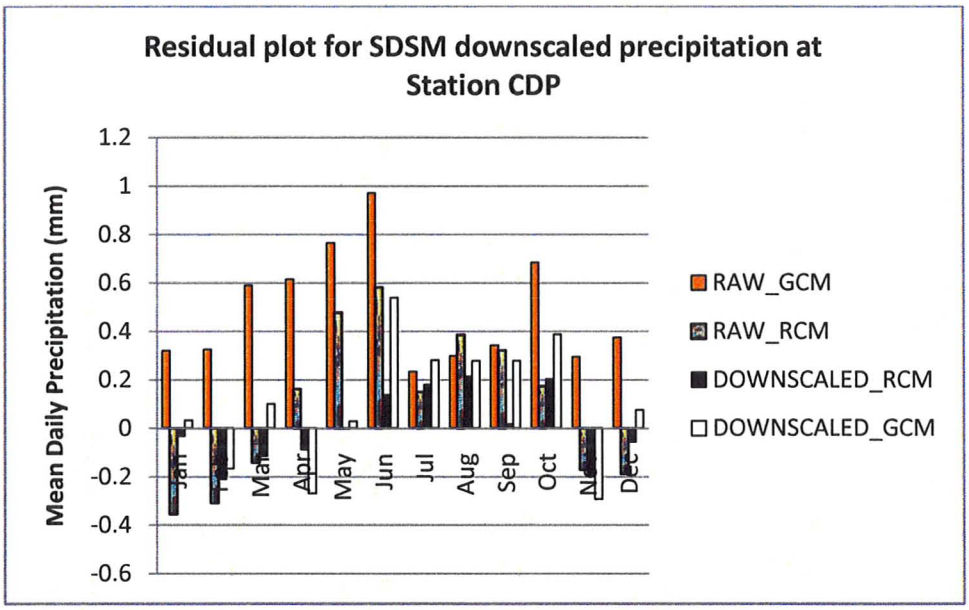

Figure A8: Residual plot for SDSM downscaled precipitation (comparing mean) at CDP

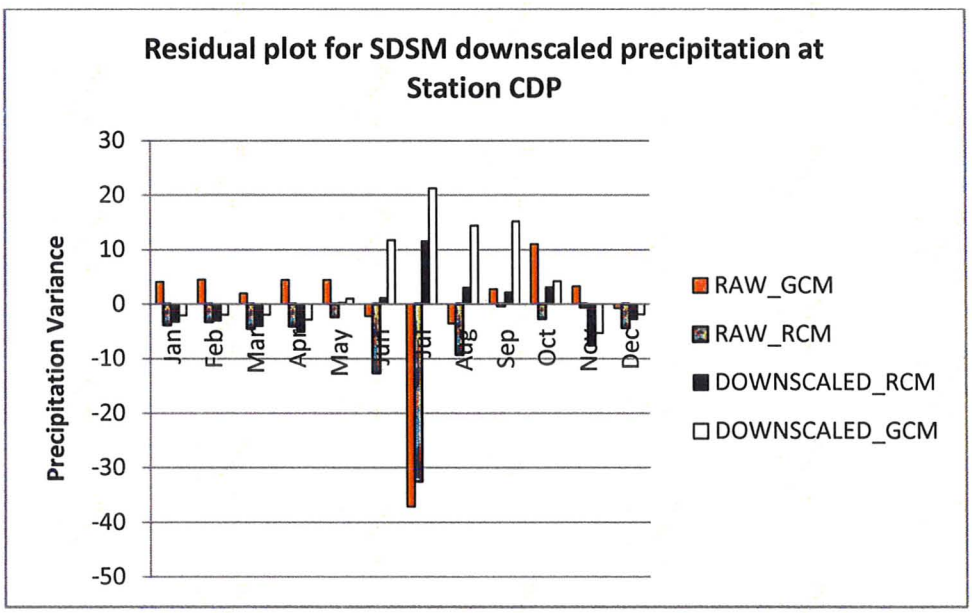

Figure A9: Residual plot for SDSM downscaled precipitation (comparing variance) at CDP

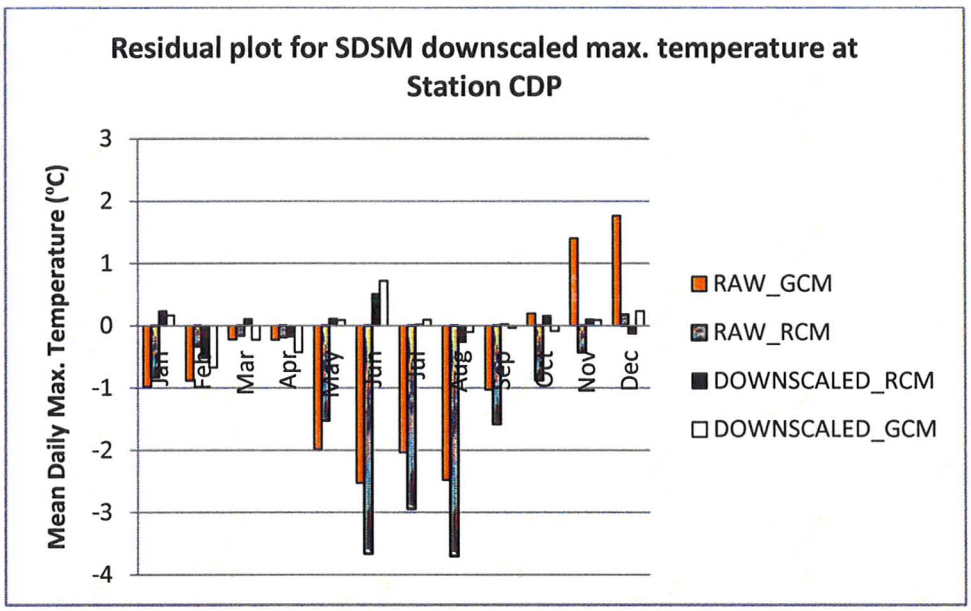

Figure A10: Residual plot for SDSM downscaled maximum temperature (comparing mean) at CDP

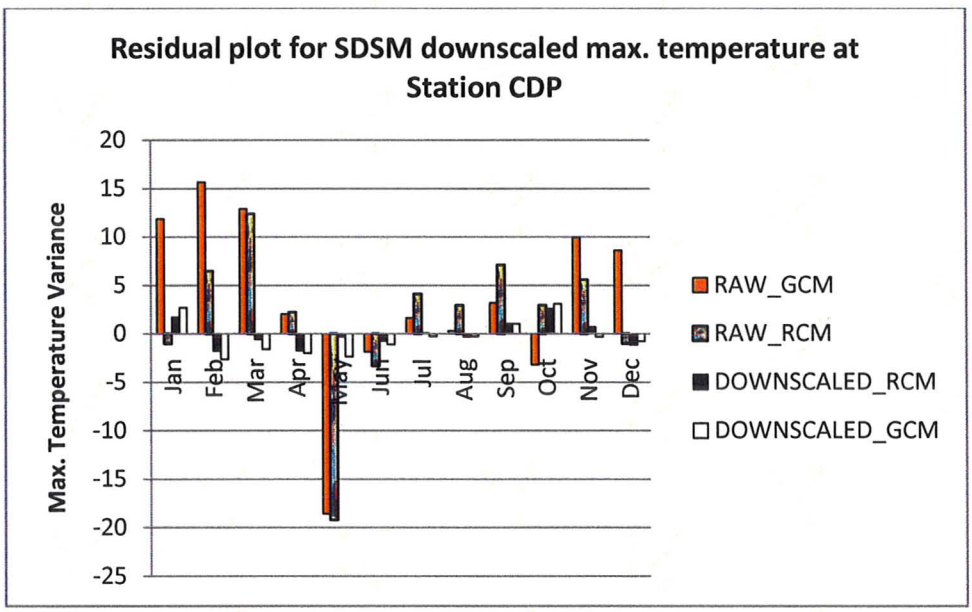

Figure A11: Residual plot for SDSM downscaled maximum temperature (comparing variance) at CDP

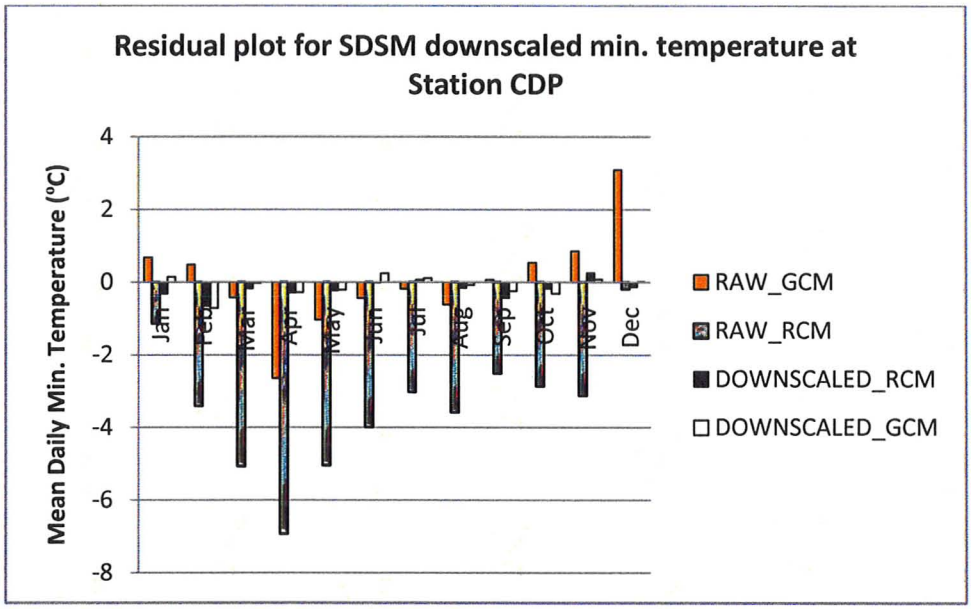

Figure A12: Residual plot for SDSM downscaled minimum temperature (comparing mean) at CDP

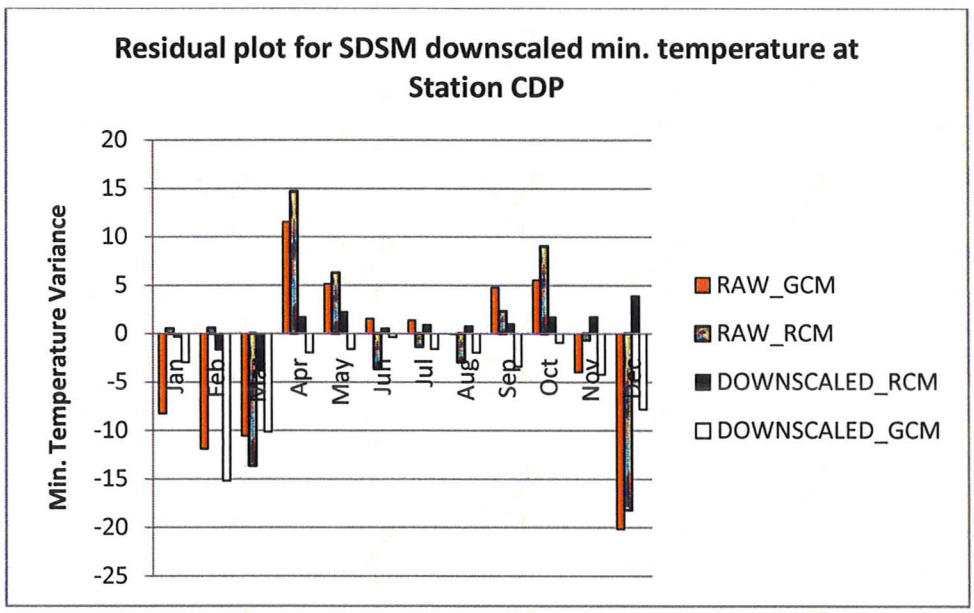

Figure A13: Residual plot for SDSM downscaled minimum temperature (comparing variance) at CDP

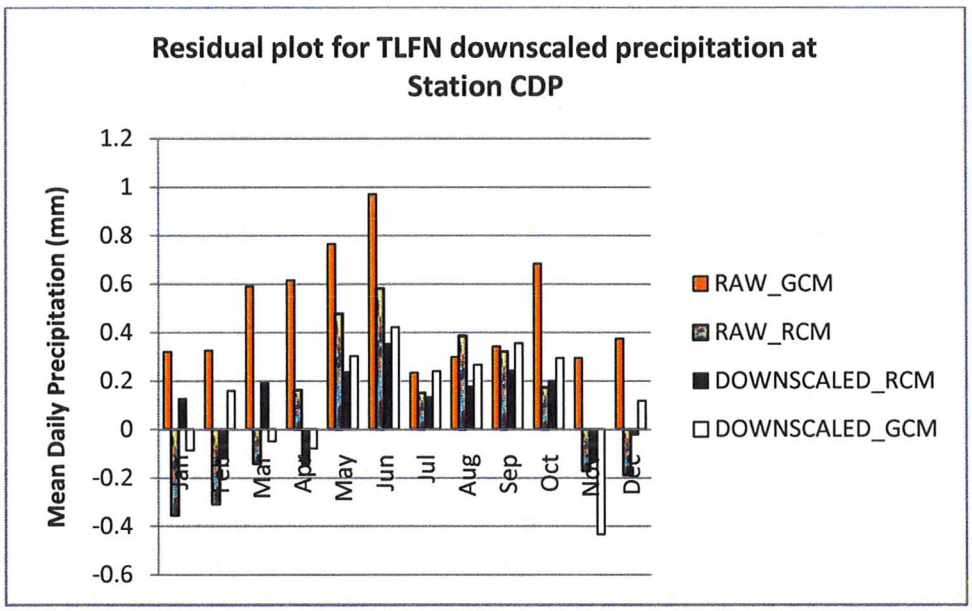

Figure A14: Residual plot for TLFN downscaled precipitation (comparing mean) at CDP

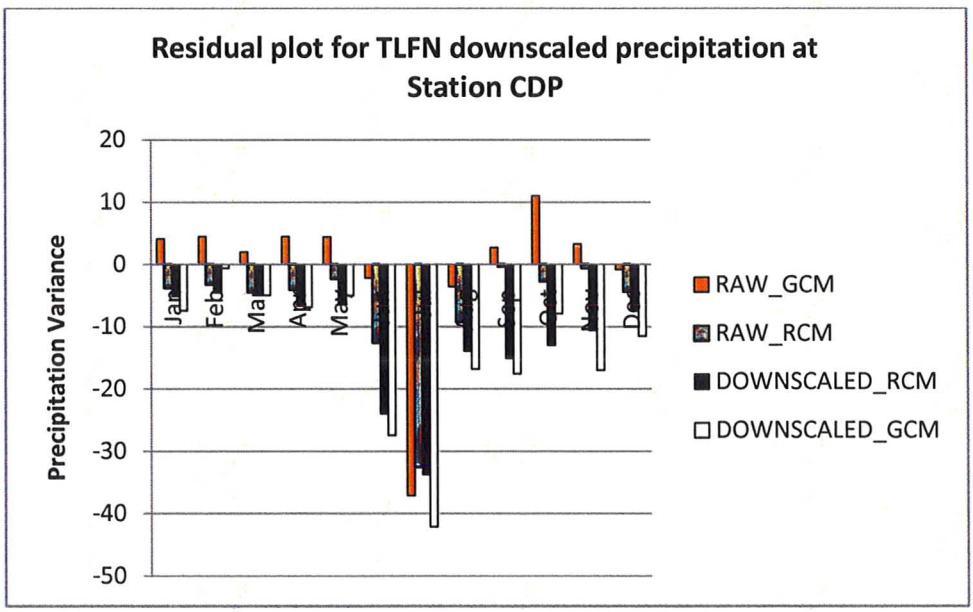

Figure A15: Residual plot for TLFN downscaled precipitation (comparing variance) at CDP

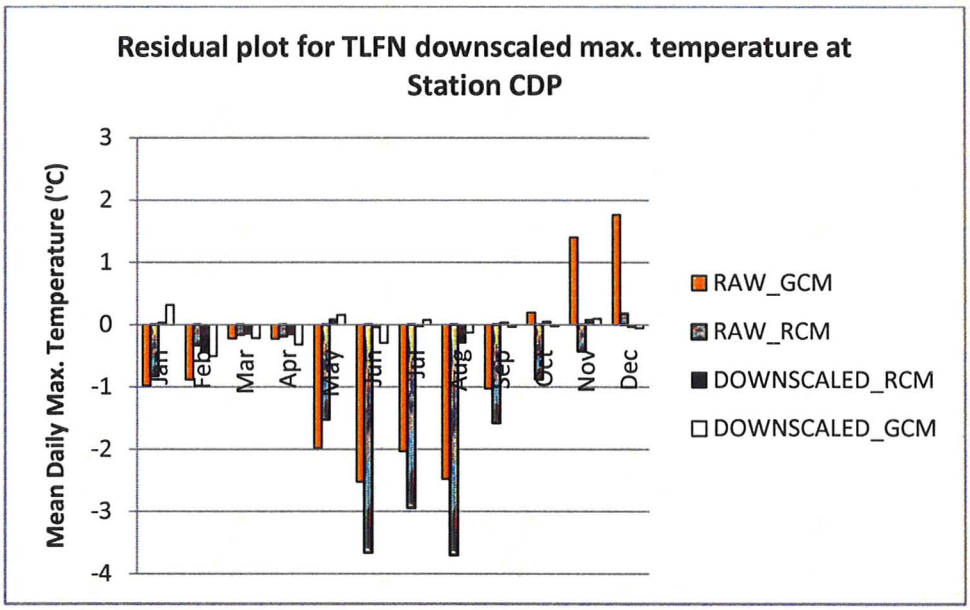

Figure A16: Residual plot for TLFN downscaled maximum temperature (comparing mean) at CDP

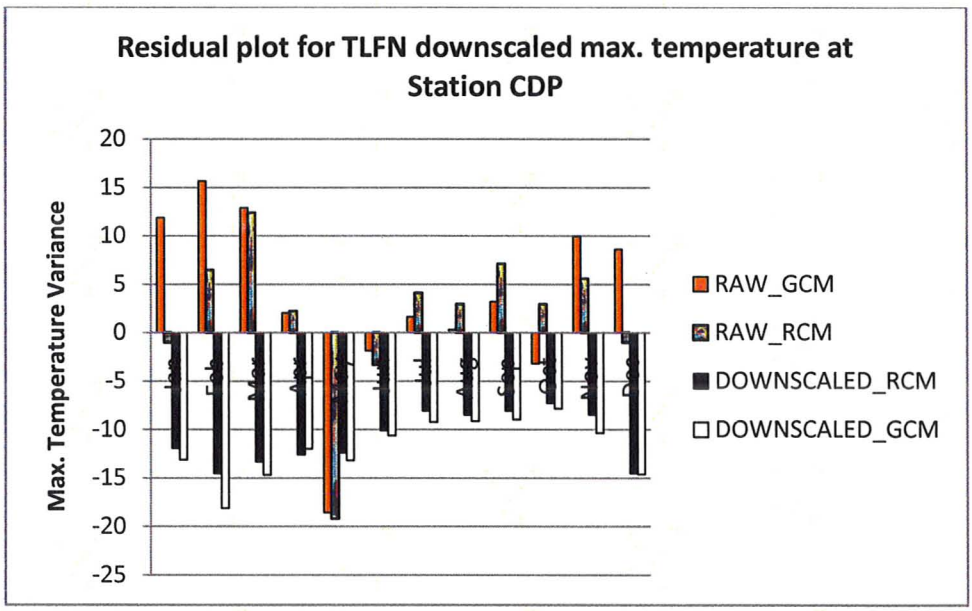

Figure A17: Residual plot for TLFN downscaled maximum temperature (comparing variance) at CDP

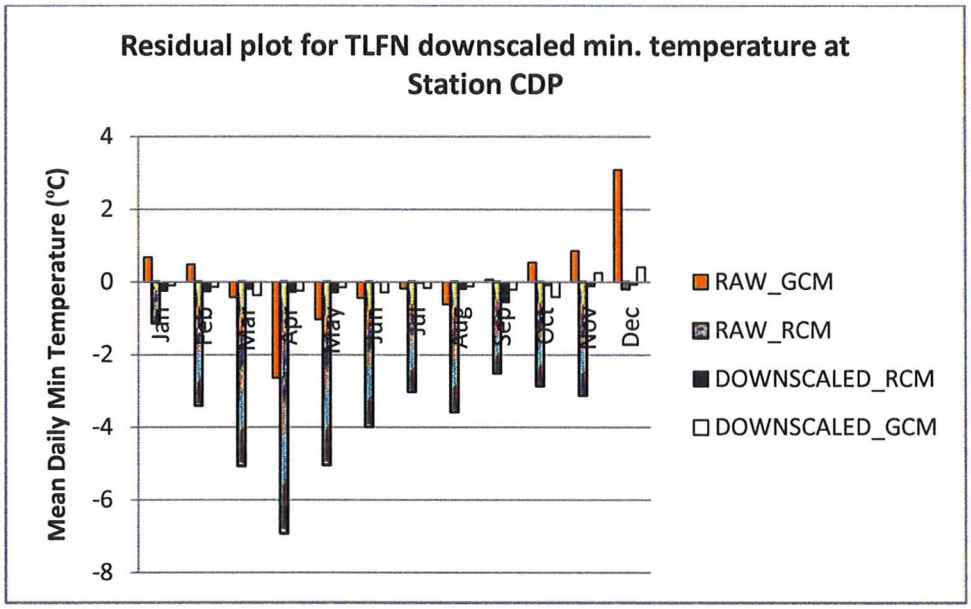

Figure A18: Residual plot for TLFN downscaled minimum temperature (comparing mean) at CDP

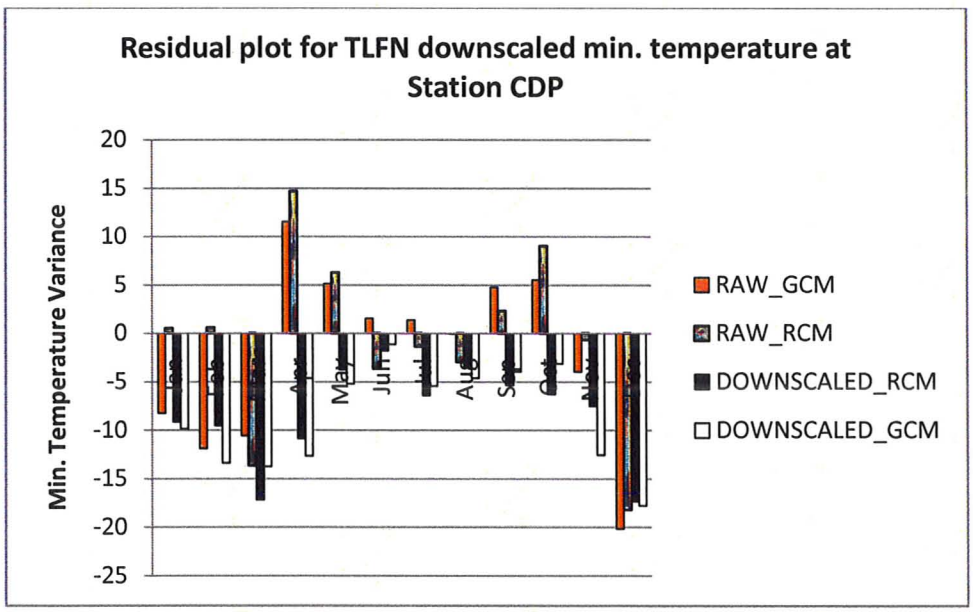

Figure A19: Residual plot for TLFN downscaled minimum temperature (comparing variance) at CDP

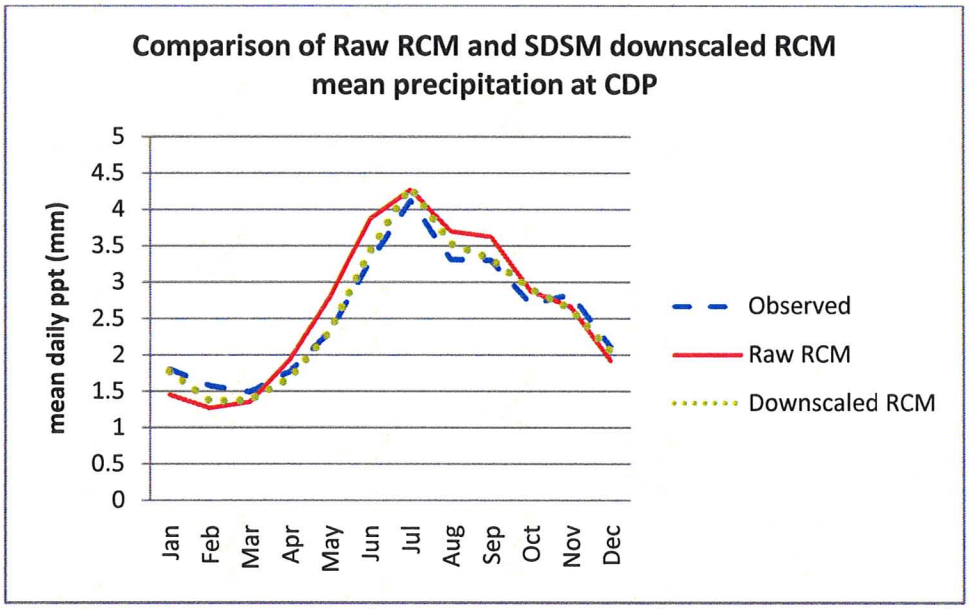

Figure A20: Comparison of Raw RCM and SDSM Downscaled RCM mean ppt. at CDP

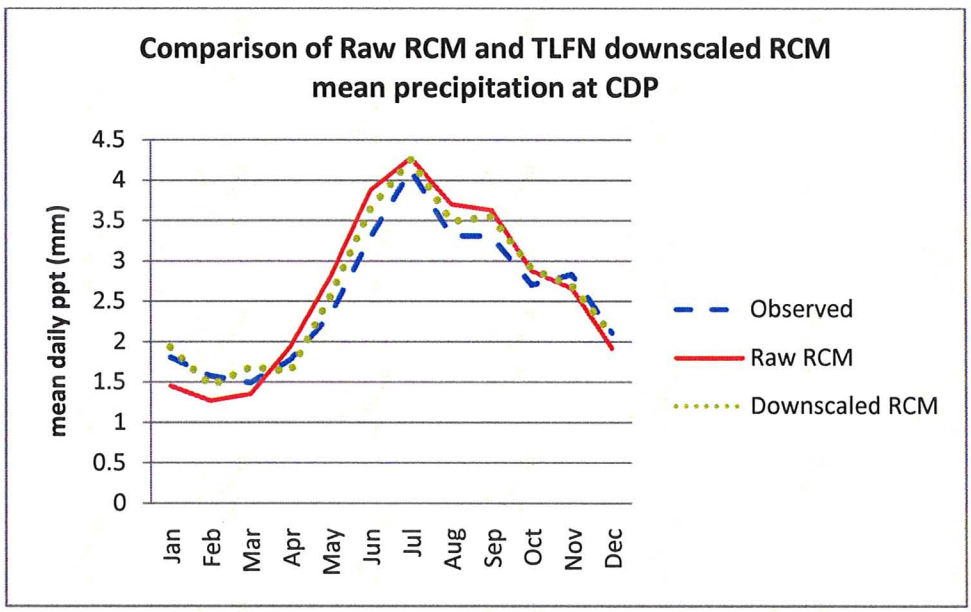

Figure A21: Comparison of Raw RCM and TLFN Downscaled RCM mean ppt. at CDP

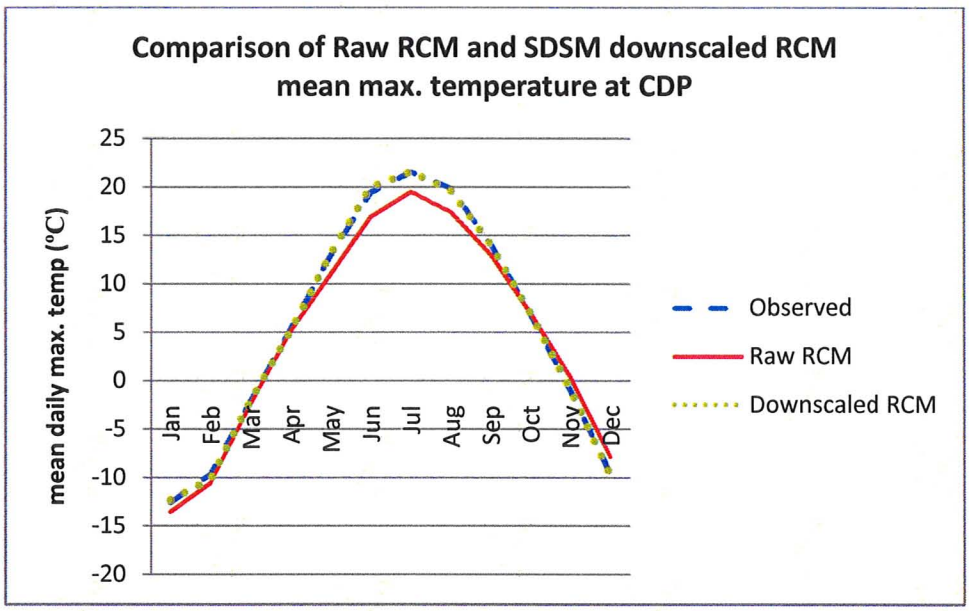

Figure A22: Comparison of Raw RCM and SDSM Downscaled RCM mean max. temp at CDP

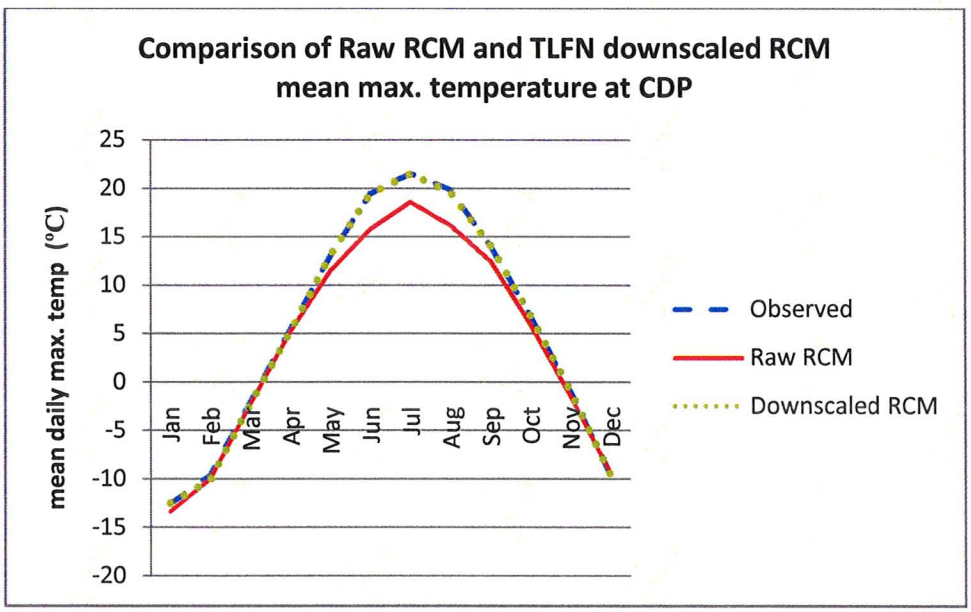

Figure A23: Comparison of Raw RCM and TLFN Downscaled RCM mean max. temp at CDP

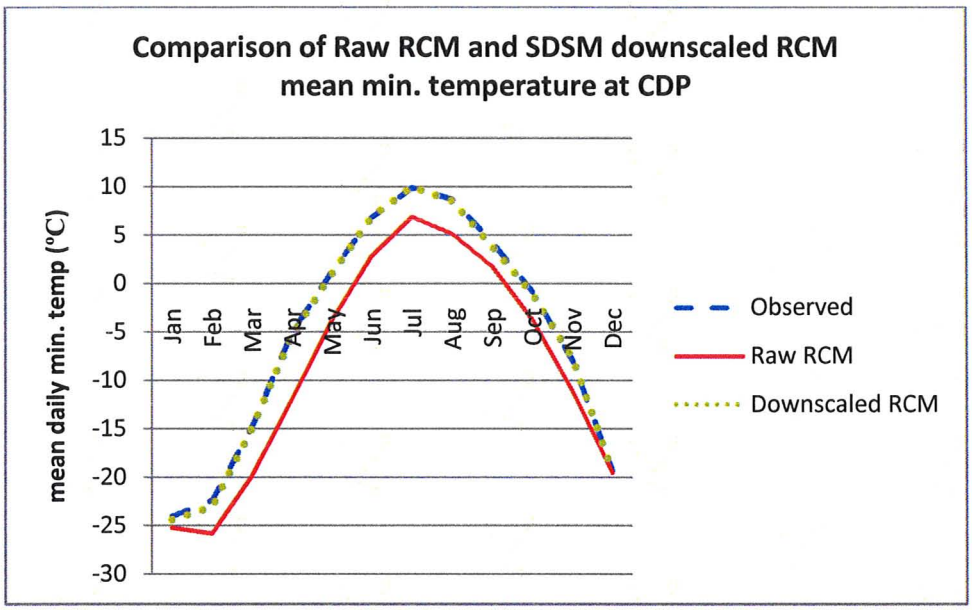

Figure A24: Comparison of Raw RCM and SDSM Downscaled RCM mean min. temp at CDP

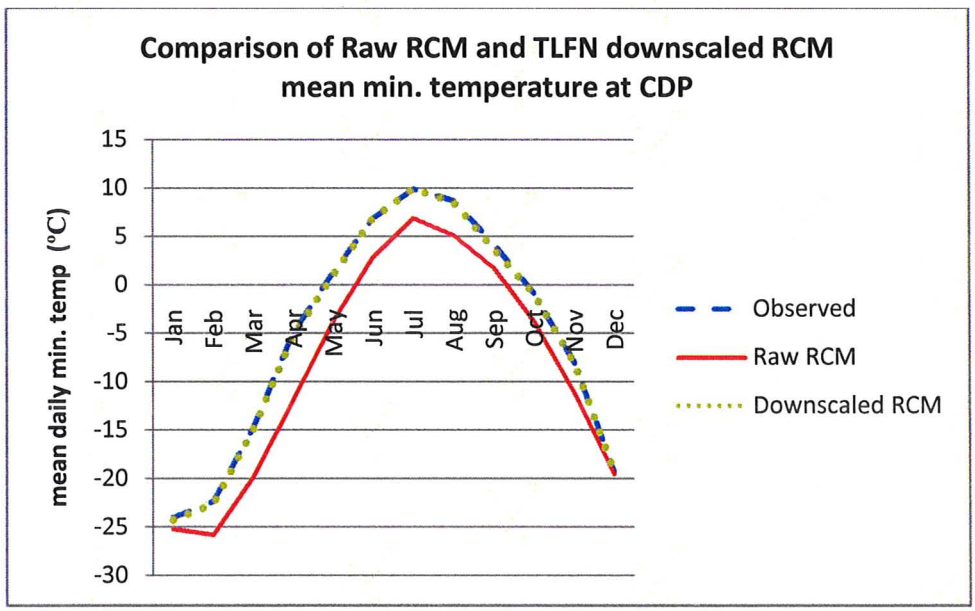

Figure A25: Comparison of Raw RCM and TLFN Downscaled RCM mean min. temp at CDP

Bias Table - PPT Monthly Mean - STATION CDD						
Month	SDSM			TLFN		
	Raw_RCM	RCM	GCM	Raw_RCM	RCM	GCM
J	-0.257	-0.032	0.040	-0.257	0.072	-0.345
F	-0.283	0.014	0.172	-0.283	0.184	-0.116
M	-0.143	0.044	0.132	-0.143	0.098	-0.267
A	0.145	-0.058	-0.191	0.145	-0.050	-0.050
M	0.001	-0.066	-0.010	0.001	0.017	0.188
J	0.469	0.025	0.136	0.469	0.188	0.537
J	0.097	0.092	0.435	0.097	0.086	0.396
A	0.202	0.134	0.267	0.202	0.202	0.213
S	0.255	0.175	0.346	0.255	0.195	0.300
O	0.229	0.036	0.136	0.229	0.202	0.316
N	0.116	-0.091	-0.297	0.116	-0.065	-0.328
D	-0.235	-0.149	-0.188	-0.235	-0.106	-0.436

Bias Table - PPT Monthly Variance - STATION CDD						
Month	SDSM			TLFN		
	Raw_RCM	RCM	GCM	Raw_RCM	RCM	GCM
J	-2.917	-0.565	-2.524	-2.917	-6.364	-6.663
F	-5.243	1.785	-1.342	-5.243	-5.311	-7.733
M	-5.876	-1.526	-4.322	-5.876	-5.240	-6.711
A	-1.742	-2.583	-4.083	-1.742	-5.175	-6.298
M	-2.762	-0.562	-2.081	-2.762	-8.235	-10.171
J	-0.888	-6.083	-9.558	-0.888	-12.929	-15.846
J	-24.288	9.882	-4.260	-24.288	-21.402	-21.757
A	-15.516	0.483	3.477	-15.516	-12.716	-13.995
S	-11.240	0.092	-2.412	-11.240	-11.146	-20.408
O	-5.373	2.728	0.271	-5.373	-6.136	-3.350
N	-0.019	-2.149	-4.321	-0.019	-10.763	-15.508
D	-5.137	-3.167	-4.490	-5.137	-9.321	-11.797

Table A5: Bias Statistics of monthly mean and variance of precipitation at Station CDD

Bias Table - PPT Monthly Mean - STATION CDP						
Month	SDSM			TLFN		
	Raw_RCM	RCM	GCM	Raw_RCM	RCM	GCM
J	-0.354	-0.033	0.032	-0.354	0.126	-0.087
F	-0.308	-0.211	-0.167	-0.308	-0.120	0.158
M	-0.141	-0.116	0.100	-0.141	0.190	-0.050
A	0.162	-0.089	-0.269	0.162	-0.145	-0.079
M	0.477	-0.002	0.028	0.477	0.235	0.302
J	0.582	0.137	0.538	0.582	0.352	0.422
J	0.150	0.180	0.281	0.150	0.133	0.240
A	0.386	0.212	0.279	0.386	0.176	0.267
S	0.322	0.016	0.278	0.322	0.243	0.356
O	0.173	0.203	0.387	0.173	0.200	0.294
N	-0.171	-0.198	-0.293	-0.171	-0.132	-0.434
D	-0.188	-0.057	0.075	-0.188	-0.022	-0.083

Bias Table - PPT Monthly Variance - STATION CDP						
Month	SDSM			TLFN		
	Raw_RCM	RCM	GCM	Raw_RCM	RCM	GCM
J	-3.840	-3.309	-2.090	-3.840	-5.170	-7.466
F	-3.267	-3.045	-2.025	-3.267	-4.584	-0.673
M	-4.514	-4.084	-1.993	-4.514	-4.879	-5.025
A	-4.110	-5.122	-2.896	-4.110	-6.722	-6.923
M	-2.349	0.211	0.960	-2.349	-6.288	-5.077
J	-12.625	1.055	11.720	-12.625	-24.029	-27.500
J	-32.528	11.464	21.175	-32.528	-33.798	-42.165
A	-9.253	2.944	14.330	-9.253	-13.927	-16.854
S	-0.380	2.099	15.098	-0.380	-15.123	-17.610
O	-2.747	3.026	4.148	-2.747	-13.035	-7.938
N	-0.633	-7.648	-5.357	-0.633	-10.614	-17.052
D	-4.407	-2.831	-1.928	-4.407	-7.285	-11.584

Table A6: Bias Statistics of monthly mean and variance of precipitation at Station CDP

Bias Table - TMAX Monthly Mean - STATION CDD						
Month	SDSM			TLFN		
	Raw_RCM	RCM	GCM	Raw_RCM	RCM	GCM
J	-0.934	-0.101	0.049	-0.934	-0.079	0.105
F	-1.840	-0.338	-0.622	-1.840	-0.550	-0.597
M	-1.273	0.122	-0.286	-1.273	-0.094	-0.189
A	-0.901	-0.057	-0.297	-0.901	-0.016	0.042
M	-2.080	0.149	0.265	-2.080	-0.357	-0.692
J	-2.860	0.448	0.702	-2.860	-0.067	-0.378
J	-2.168	0.112	0.231	-2.168	-0.123	-0.173
A	-3.237	0.098	0.142	-3.237	-0.137	-0.361
S	-1.481	0.107	0.124	-1.481	0.097	0.193
O	-1.362	0.075	0.065	-1.362	0.022	-0.064
N	-0.907	0.091	0.117	-0.907	0.142	0.195
D	-0.155	-0.309	-0.032	-0.155	-0.311	-0.113

Bias Table - TMAX Monthly Variance - STATION CDD						
Month	SDSM			TLFN		
	Raw_RCM	RCM	GCM	Raw_RCM	RCM	GCM
J	-1.640	-3.325	-4.669	-1.640	-11.649	-12.576
F	9.680	-7.436	-7.483	9.680	-14.563	-17.093
M	15.418	-4.540	-5.973	15.418	-13.620	-14.250
A	5.387	-5.057	-4.413	5.387	-12.086	-11.196
M	-12.185	-3.946	-3.205	-12.185	-10.358	-11.048
J	2.372	-2.758	-2.372	2.372	-8.778	-9.147
J	7.110	-3.969	-3.472	7.110	-9.294	-9.901
A	6.154	-2.533	-2.101	6.154	-8.699	-8.311
S	13.145	-1.684	-2.821	13.145	-8.769	-9.522
O	8.394	-0.270	0.654	8.394	-7.056	-7.217
N	6.971	-1.864	-2.308	6.971	-9.110	-9.162
D	3.183	-3.976	-6.304	3.183	-13.153	-14.666

Table A7: Bias Statistics of monthly mean and variance of maximum temperature at Station CDD

Bias Table - TMAX Monthly Mean - STATION CDP						
Month	SDSM			TLFN		
	Raw_RCM	RCM	GCM	Raw_RCM	RCM	GCM
J	-0.822	0.233	0.166	-0.822	0.030	0.313
F	-0.330	-0.517	-0.672	-0.330	-0.434	-0.506
M	-0.159	0.104	-0.230	-0.159	-0.144	-0.216
A	-0.183	-0.180	-0.431	-0.183	-0.154	-0.324
M	-1.521	0.109	0.085	-1.521	0.083	0.156
J	-3.660	0.504	0.719	-3.660	-0.041	-0.294
J	-2.939	0.011	0.089	-2.939	-0.028	0.070
A	-3.699	-0.267	-0.105	-3.699	-0.290	-0.131
S	-1.578	0.021	-0.040	-1.578	0.032	-0.040
O	-0.876	0.154	-0.091	-0.876	0.045	-0.025
N	-0.426	0.098	0.088	-0.426	0.076	0.092
D	0.175	-0.130	0.229	0.175	-0.039	-0.059

Bias Table - TMAX Monthly Variance - STATION CDP						
Month	SDSM			TLFN		
	Raw_RCM	RCM	GCM	Raw_RCM	RCM	GCM
J	-1.042	1.681	2.659	-1.042	-11.942	-13.141
F	6.441	-1.784	-2.645	6.441	-14.550	-18.122
M	12.355	-0.588	-1.635	12.355	-13.340	-14.709
A	2.199	-1.741	-2.031	2.199	-12.607	-12.014
M	-19.211	-0.332	-2.386	-19.211	-12.403	-13.195
J	-3.332	-0.742	-1.117	-3.332	-10.110	-10.646
J	4.082	0.028	-0.277	4.082	-8.109	-9.250
A	2.913	-0.337	-0.308	2.913	-8.536	-9.173
S	7.089	0.990	1.009	7.089	-8.081	-8.983
O	2.913	2.571	3.067	2.913	-7.301	-7.853
N	5.546	0.668	-0.319	5.546	-8.482	-10.380
D	-1.038	-1.147	-0.778	-1.038	-14.537	-14.636

Table A8: Bias Statistics of monthly mean and variance of maximum temperature at Station CDP

Bias Table - TMIN Monthly Mean - STATION CDD						
Month	SDSM			TLFN		
	Raw_RCM	RCM	GCM	Raw_RCM	RCM	GCM
J	-0.436	-0.770	-0.364	-0.436	-0.572	-0.736
F	-1.822	-1.018	-1.116	-1.822	-1.315	-0.928
M	-4.676	-0.380	-0.480	-4.676	-0.835	-0.544
A	-7.312	-0.319	-0.709	-7.312	-0.340	-0.608
M	-5.960	-0.286	-0.310	-5.960	-0.256	-0.346
J	-5.197	0.078	0.259	-5.197	-0.058	-0.129
J	-4.648	0.000	0.120	-4.648	-0.049	-0.100
A	-5.527	0.099	0.099	-5.527	-0.115	-0.202
S	-3.979	-0.273	-0.308	-3.979	-0.371	-0.212
O	-4.100	-0.234	-0.345	-4.100	-0.317	-0.361
N	-4.005	0.418	-0.263	-4.005	-0.123	-0.142
D	-0.171	-0.494	0.036	-0.171	0.013	0.122

Bias Table - TMIN Monthly Variance - STATION CDD						
Month	SDSM			TLFN		
	Raw_RCM	RCM	GCM	Raw_RCM	RCM	GCM
J	-10.706	1.316	0.018	-10.706	-12.327	-15.678
F	-26.761	-14.734	-16.781	-26.761	-23.643	-22.642
M	-21.432	-7.068	-10.038	-21.432	-19.575	-17.960
A	20.824	1.120	1.342	20.824	-9.812	-8.088
M	4.739	0.197	-1.165	4.739	-10.647	-10.669
J	1.453	0.463	1.449	1.453	-9.284	-10.735
J	1.893	0.194	0.629	1.893	-7.401	-7.859
A	-0.133	-0.933	-1.383	-0.133	-8.619	-9.716
S	5.628	-0.884	-1.438	5.628	-7.769	-5.770
O	8.794	-0.658	-0.080	8.794	-9.372	-6.014
N	5.874	-0.569	-2.187	5.874	-13.290	-13.751
D	-23.829	-3.216	-4.477	-23.829	-14.041	-15.924

Table A9: Bias Statistics of monthly mean and variance of minimum temperature at Station CDD

Bias Table - TMIN Monthly Mean - STATION CDP						
Month	SDSM			TLFN		
	Raw_RCM	RCM	GCM	Raw_RCM	RCM	GCM
J	-1.142	-0.255	-0.101	-1.142	-0.255	-0.101
F	-3.408	-0.270	-0.143	-3.408	-0.270	-0.143
M	-5.066	-0.195	-0.378	-5.066	-0.195	-0.378
A	-6.925	-0.290	-0.247	-6.925	-0.290	-0.247
M	-5.041	-0.292	-0.151	-5.041	-0.292	-0.151
J	-3.989	0.084	0.207	-3.989	0.084	0.207
J	-3.026	0.072	0.145	-3.026	0.072	0.145
A	-3.586	-0.197	-0.126	-3.586	-0.197	-0.126
S	-2.511	-0.560	-0.218	-2.511	-0.560	-0.218
O	-2.866	-0.095	-0.419	-2.866	-0.095	-0.419
N	-3.126	-0.117	0.244	-3.126	-0.117	0.244
D	-0.197	-0.073	0.407	-0.197	-0.073	0.407

Bias Table - TMIN Monthly Variance - STATION CDP						
Month	SDSM			TLFN		
	Raw_RCM	RCM	GCM	Raw_RCM	RCM	GCM
J	0.513	-9.144	-9.887	0.513	-15.144	-12.887
F	0.568	-9.561	-13.415	0.568	-13.561	-17.415
M	-13.645	-17.189	-13.789	-13.645	-17.189	-13.789
A	14.638	-10.871	-12.668	14.638	-10.871	-12.668
M	6.257	-3.787	-5.234	6.257	-8.787	-7.234
J	-3.654	-1.821	-1.165	-3.654	-10.821	-10.165
J	-1.384	-6.421	-5.471	-1.384	-6.421	-5.471
A	-2.961	-3.551	-4.635	-2.961	-7.551	-6.635
S	2.287	-5.374	-3.973	2.287	-5.374	-3.973
O	8.991	-6.302	-3.138	8.991	-6.302	-3.138
N	-0.694	-7.544	-12.590	-0.694	-7.544	-12.590
D	-18.211	-17.362	-17.808	-18.211	-17.362	-17.808

Table A10: Bias Statistics of monthly mean and variance of minimum temperature at Station CDP

LEVENE TEST RESULTS - CDP				
	SDSM		TLFN	
Month	RCM	GCM	RCM	GCM
Jan	0.294	0.174	0.578	0.806
Feb	0.056	0.066	0.107	0.759
Mar	0.963	0.827	0.122	0.639
Apr	0.294	0.173	0.962	0.799
May	0.723	0.158	0.715	0.734
Jun	0.963	0.827	0.203	0.142
Jul	0.056	0.041	0.746	0.605
Aug	0.068	0.009	0.472	0.204
Sep	0.723	0.158	0.492	0.253
Oct	0.808	0.273	0.261	0.202
Nov	0.156	0.022	0.786	0.708
Dec	0.959	0.372	0.800	0.978

Table A11: Levene Test p-values for precipitation at CDP

WILCOXON RANK SUM TEST -CDP				
	SDSM		TLFN	
Month	RCM	GCM	RCM	GCM
Jan	0.575	0.300	0.024	0.209
Feb	0.336	0.223	0.006	0.008
Mar	0.437	0.588	0.940	0.649
Apr	0.050	0.003	< 0.0001	< 0.0001
May	0.669	0.197	0.312	0.984
Jun	0.979	0.050	0.495	0.057
Jul	0.296	0.100	0.017	0.040
Aug	0.003	0.003	0.001	0.006
Sep	0.155	0.103	0.067	0.024
Oct	0.787	0.350	0.135	0.433
Nov	0.008	0.007	0.367	0.550
Dec	0.314	0.329	0.612	0.339

Table A12: Wilcoxon Rank Sum Test p-values for precipitation at CDP

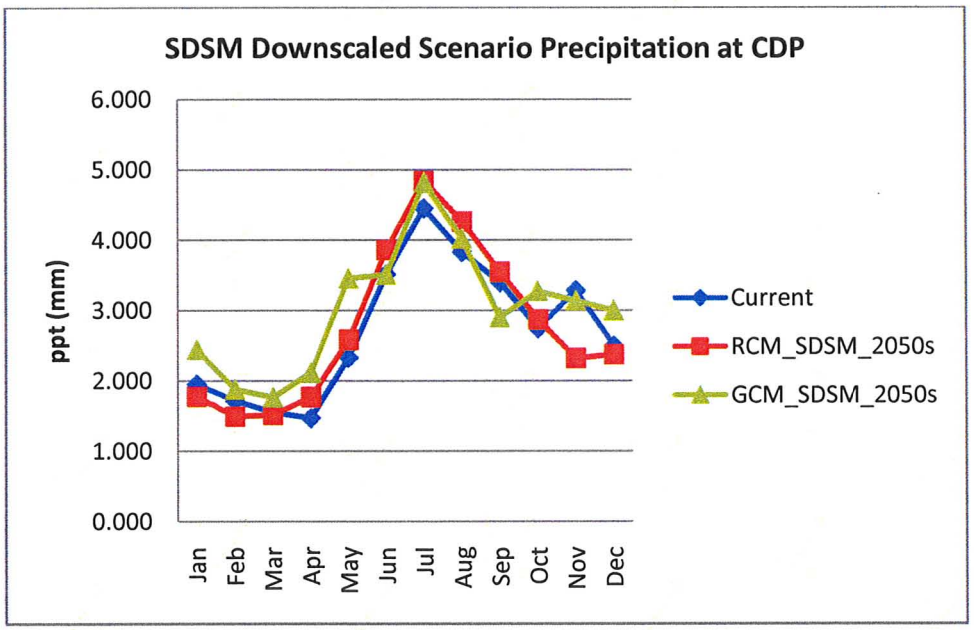

Figure A26: Monthly mean trend in precipitation at CDP using SDSM

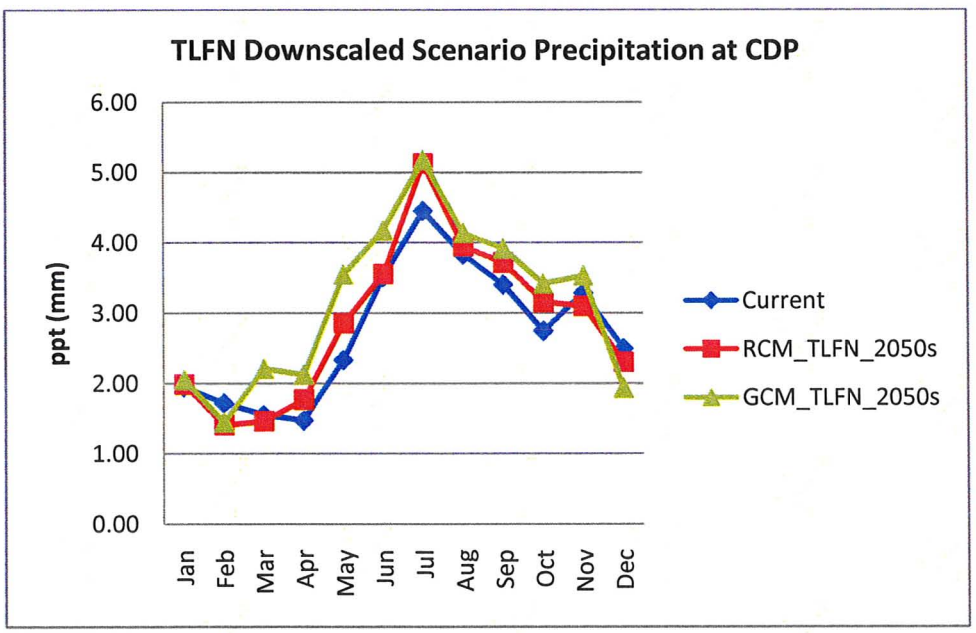

Figure A27: Monthly mean trend in precipitation at CDP using TLFN

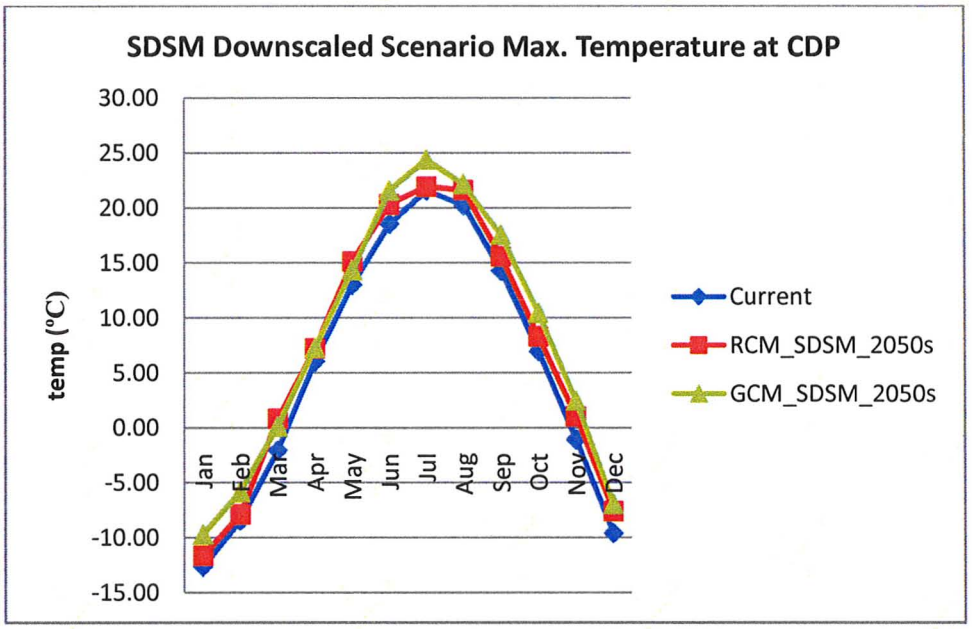

Figure A28: Monthly mean trend in maximum temperature at CDP using SDSM

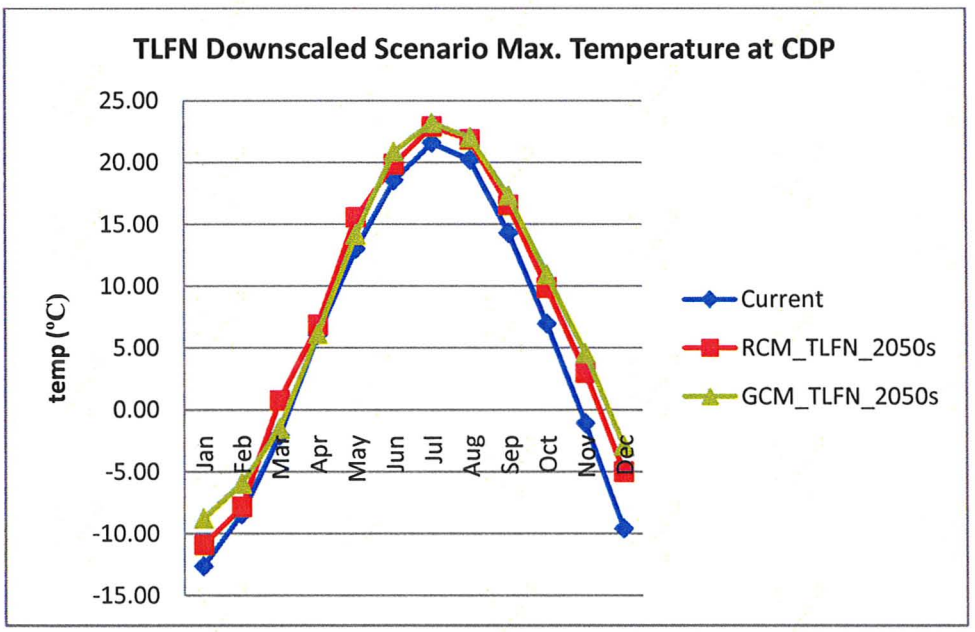

Figure A29: Monthly mean trend in maximum temperature at CDP using TLFN

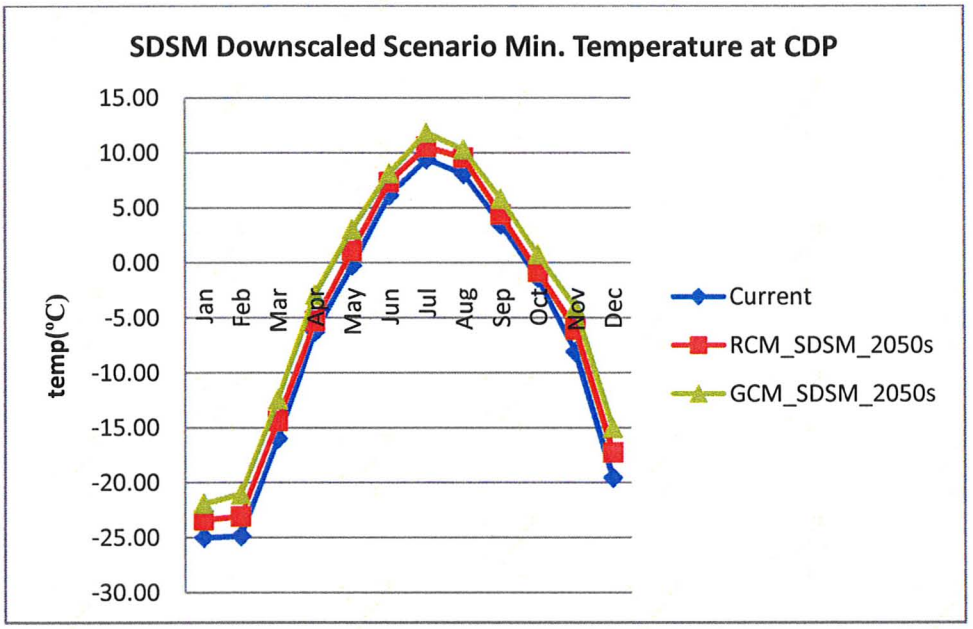

Figure A30: Monthly mean trend in minimum temperature at CDP using SDSM

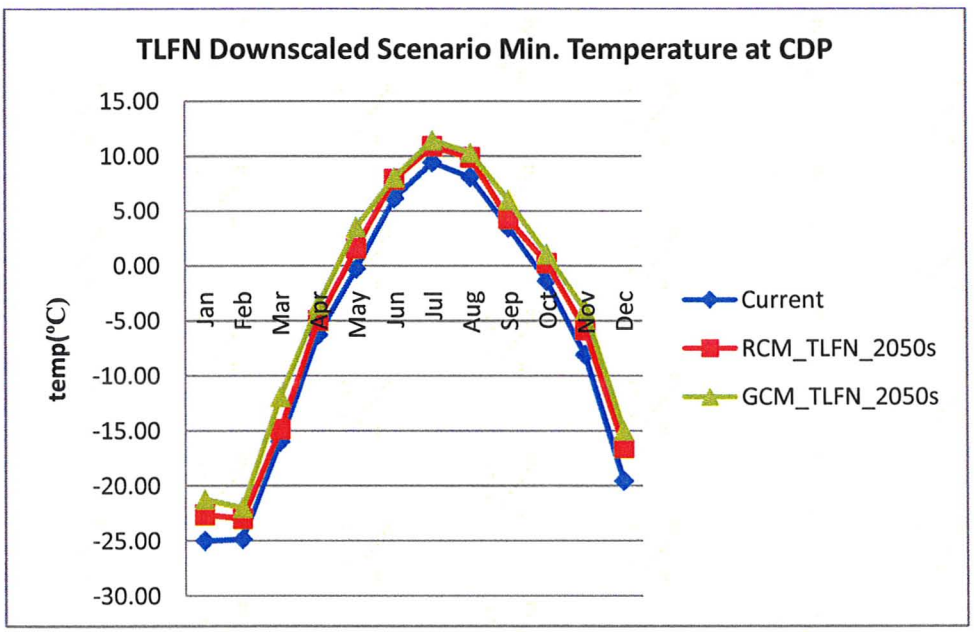

Figure A31: Monthly mean trend in minimum temperature at CDP using TLFN

APPENDIX B

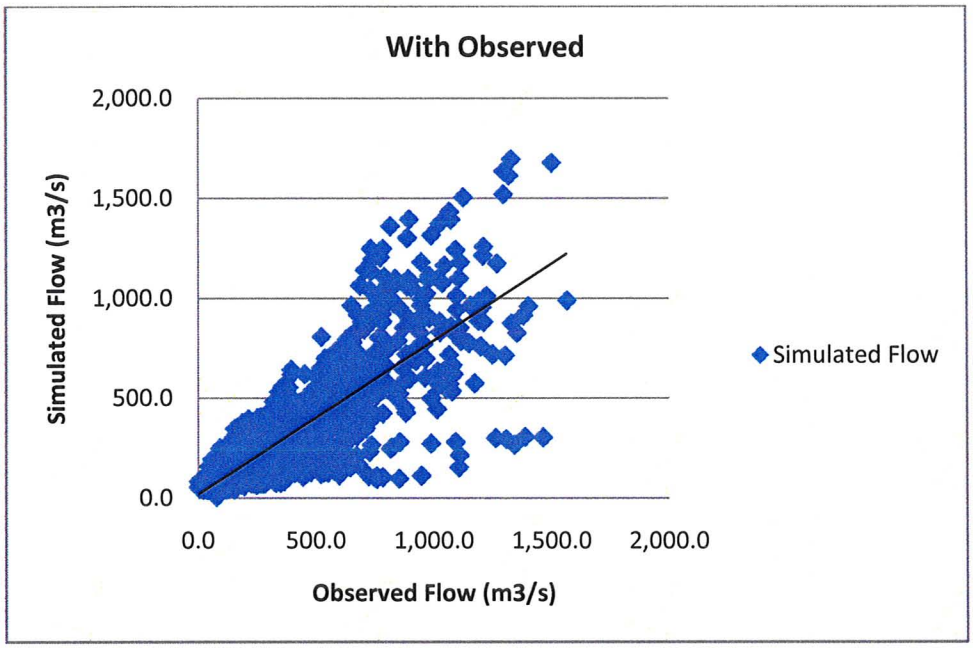

Figure B1: Scatter plot of Simulation Results for (1981-1990) for Chute-du-Diable inflows

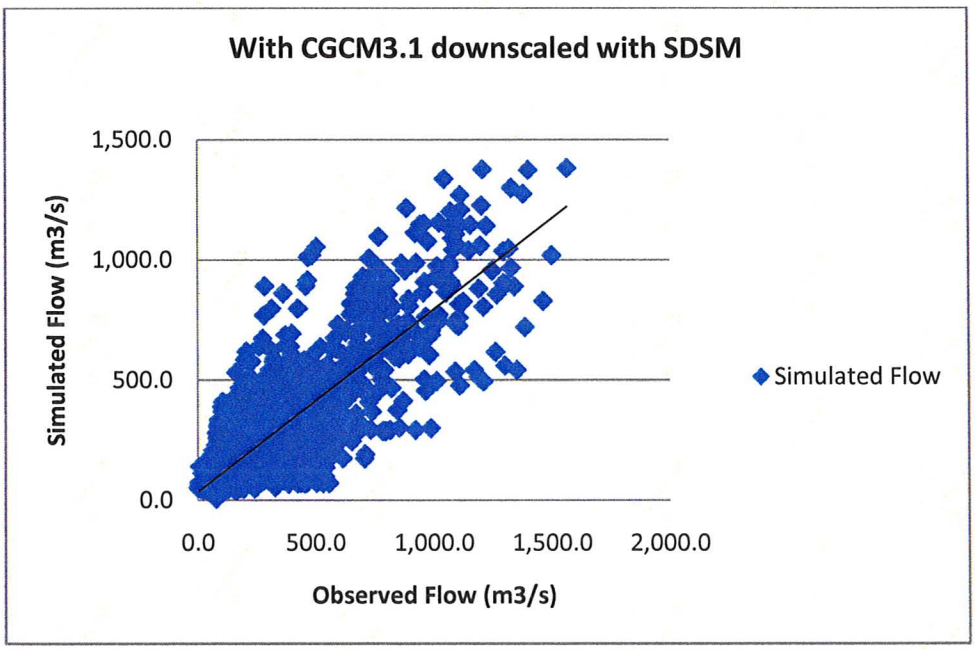

Figure B2: Scatter plot of Simulation Results for (1981-1990) for Chute-du-Diable inflows

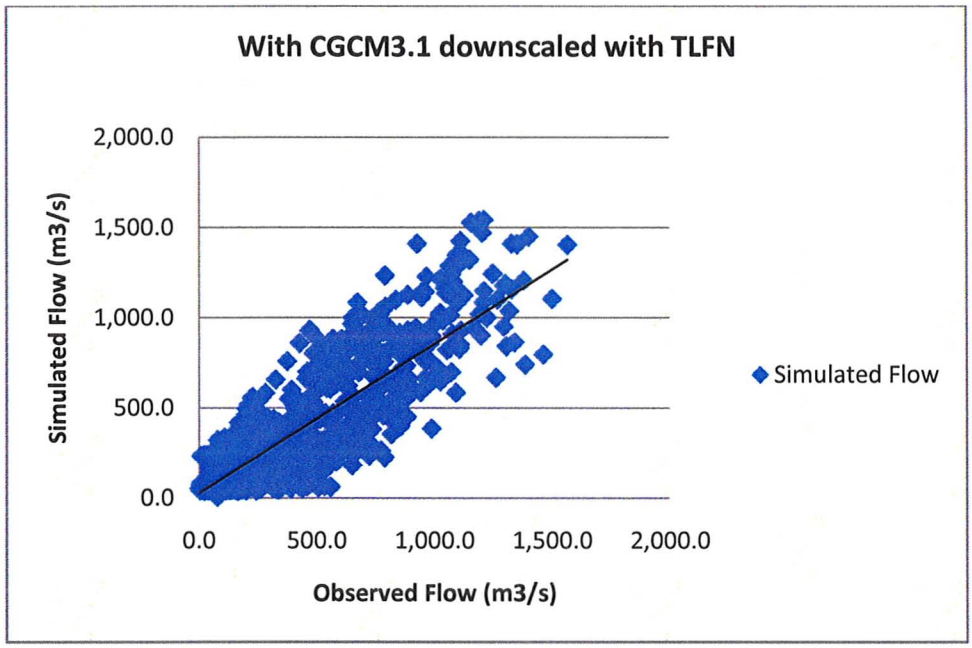

Figure B3: Scatter plot of Simulation Results for (1981-1990) for Chute-du-Diable inflows

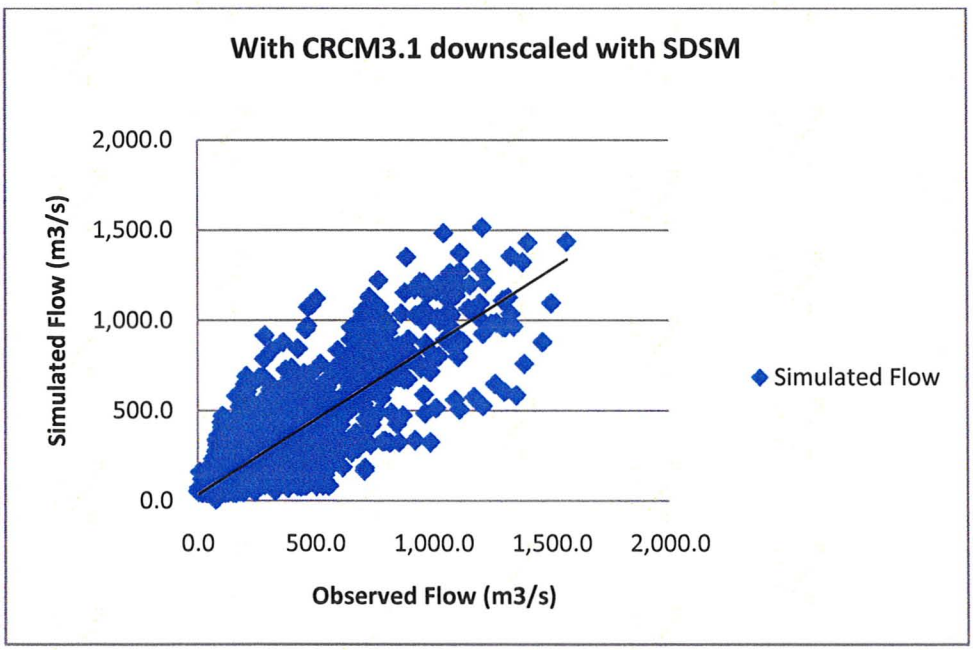

Figure B4: Scatter plot of Simulation Results for (1981-1990) for Chute-du-Diable inflows

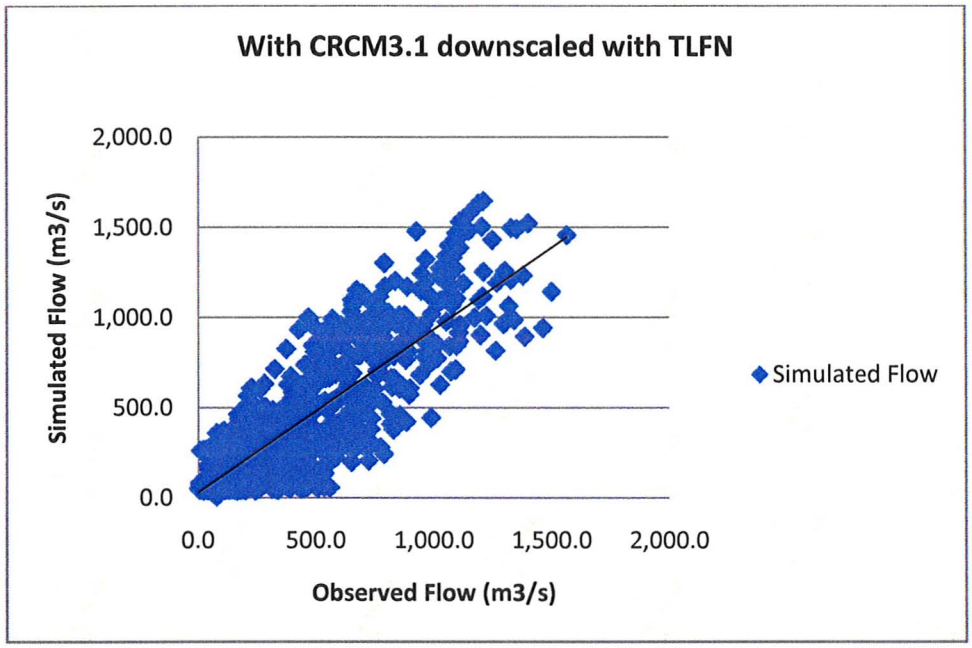

Figure B5: Scatter plot of Simulation Results for (1981-1990) for Chute-du-Diable inflows

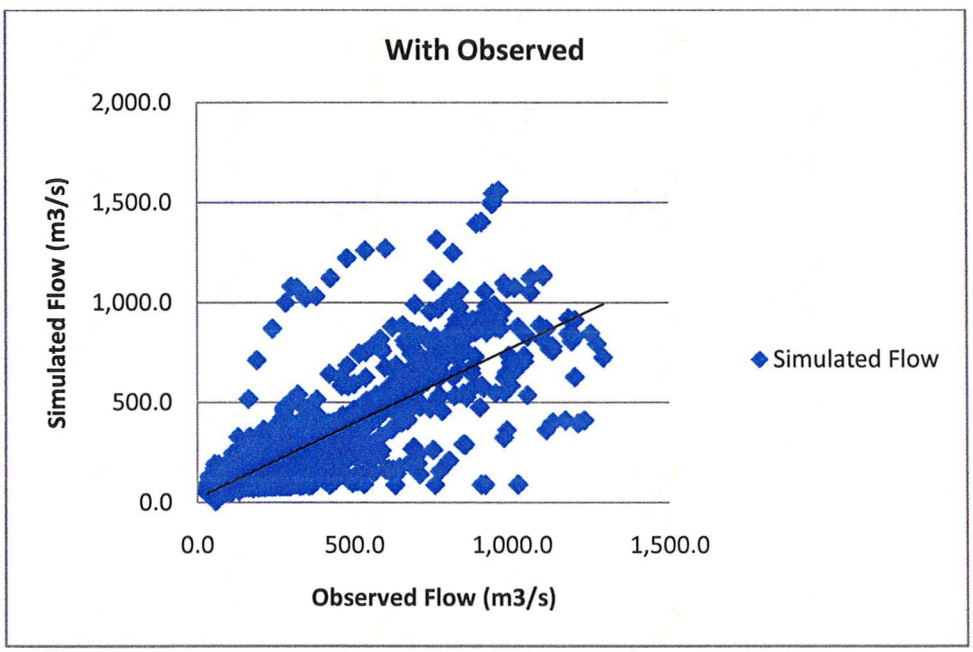

Figure B6: Scatter plot of Simulation Results for (1981-1990) for Mistassibi River flow

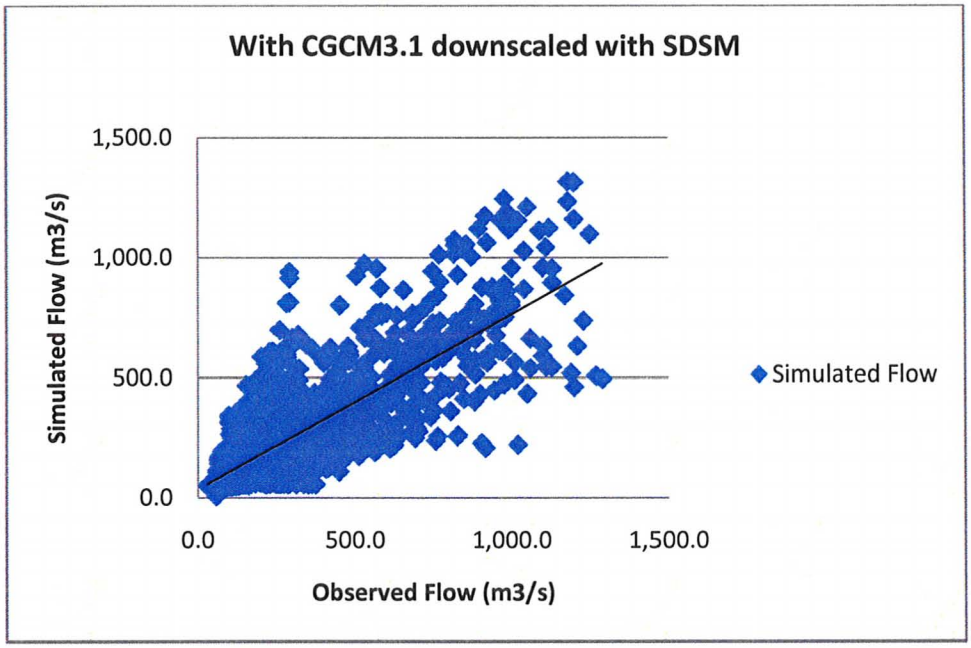

Figure B7: Scatter plot of Simulation Results for (1981-1990) for Mistassibi River flow

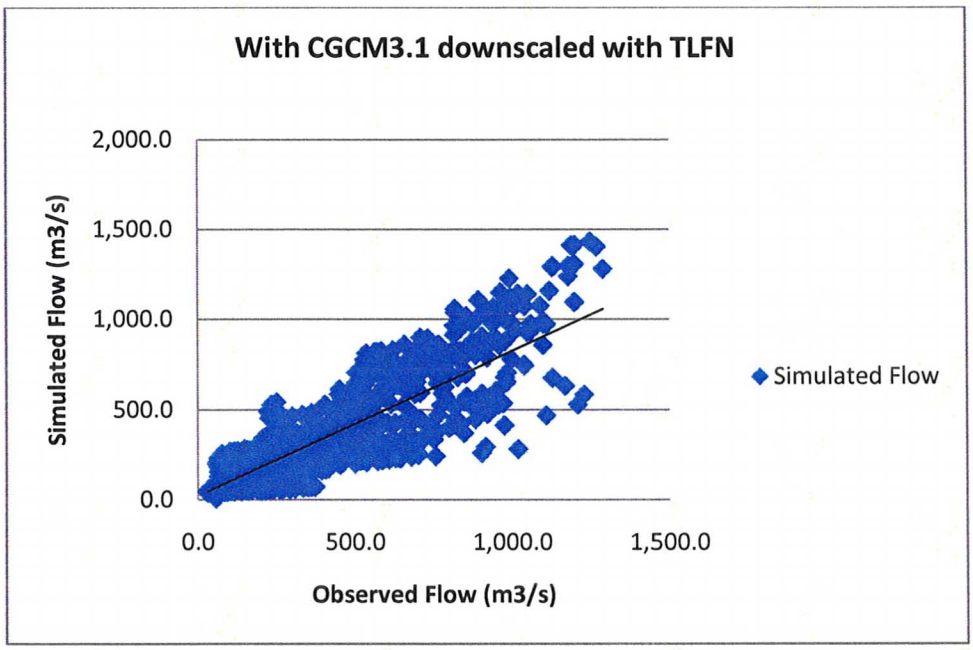

Figure B8: Scatter plot of Simulation Results for (1981-1990) for Mistassibi River flow

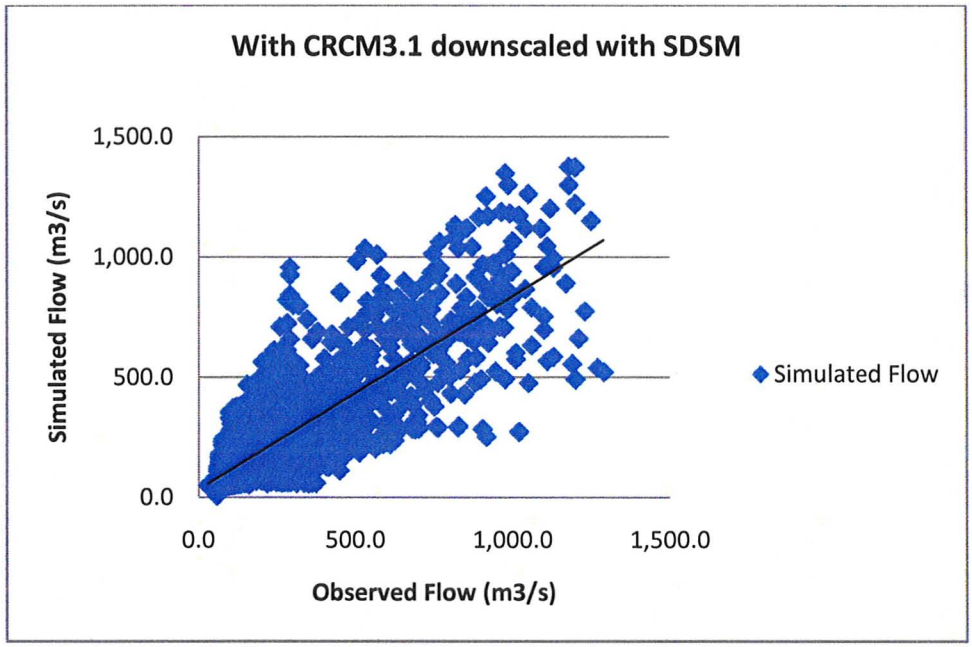

Figure B9: Scatter plot of Simulation Results for (1981-1990) for Mistassibi River flow

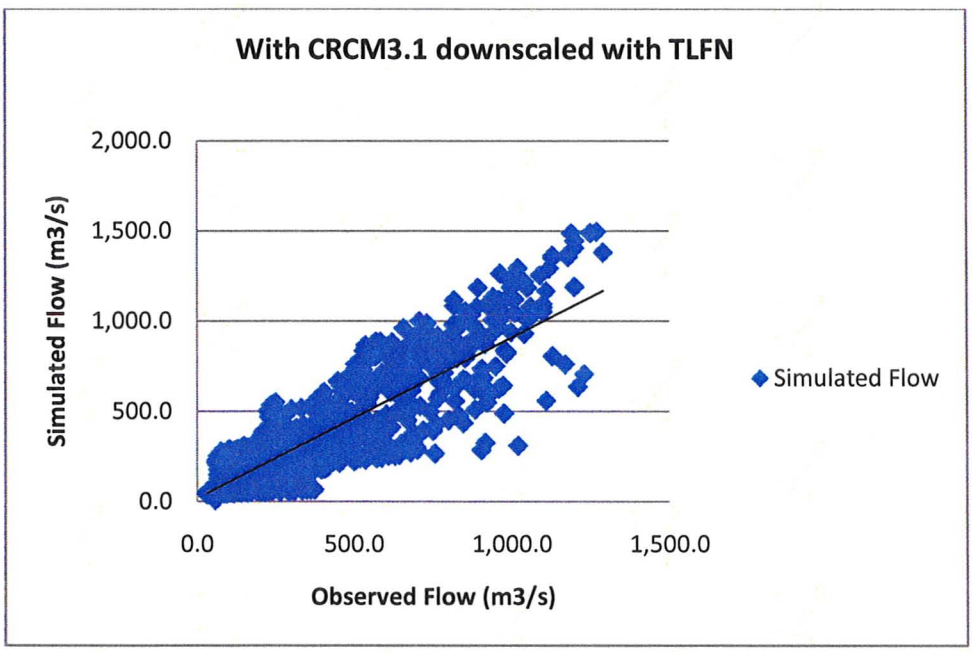

Figure B10: Scatter plot of Simulation Results for (1981-1990) for Mistassibi River flow